STEADY STATE AND TRANSIENT PHOTOCONDUCTIVITY IN n-TYPE AMORPHOUS SILICON

A thesis presented by
Amar Merazga (M.Sc)
to the CNAA
in partial fulfilment of the requirements
for the degree of Doctor of Philosophy
Sponsoring Establishment: Dundee Institute of Technology
December 1990

To my brothers. Sajid, Zubeir,
Abid and Zakir.

DECLARATION

I declare that while registered as a candidate for the degree for which this thesis is presented I have not been a candidate for any other award. I further declare that except where stated the work contained in this thesis is original and was performed by the author.

Signed [redacted]

Amar Merazga

ADVANCED STUDIES

In addition to the original research reported in this thesis, the author followed a programme of postgraduate study. This programme included attendence of the 1988 and 1990 Chelsea meetings on Liquid and Amorphous Semiconductors and contribution to paper presentations at the 1987 Chelsea meeting on Liquid and Amorphous Semiconductors and the 12th International Conference on Amorphous and Liquid semiconductors.

ACKNOWLEDGEMENTS

The author is greatly indebted to Dr. C. Main and Dr. S. Reynolds under whose supervision the research was conducted. The author especially wishes to record his sincere thanks for the continued encouragement, help and constructive criticism he received from Dr. C. Main.

The author also wishes to express his gratitude to Dr.I K. Kristensen for his critical comments and discussions during his visit to D.I.T and to Dr. J. Berkin for his assistance with computer simulations.

Sincere thanks are due to the following who helped in bringing this work to a successful end.

Dr. B. Jefferies, Head of the department for his kindness and support.

Members of the technical staff for their help during this study.

D. P. Webb, C. Soutar and R. Bruggemann for their helpful comments during the preparation of this thesis.

Finally, the author would like to express his appreciation to the Algerian ministry of higher education without whose support this work would have never been started.

STEADY STATE AND TRANSIENT PHOTOCONDUCTIVITY IN
n-TYPE AMORPHOUS SILICON
AMAR MERAZGA

Comprehensive measurements of secondary photoconductivity with steady optical excitation (SSPC), transient excitation (TPC), and steady state optical bias plus transient excitation (OB) were carried out on samples of glow-discharge produced n-type a-Si:H from two sources, lightly doped with phosphorus and arsenic respectively.

The data from the short time TPC, measured as a function of excitation density are consistent with multiple trapping and saturation of the trap states above the electron quasi-Fermi level, which allows determination of the distribution of conduction band tail (CBT) states, and hence comparison of the quality of the two materials. A broad exponential tail of high state density was found for the As-doped material while the CBT in the P-doped material was found to be characterised by a shallow shoulder ($\approx$0.17eV below the conduction mobility edge) below which the density of states falls sharply.

Both the SSPC and the long time TPC results from the P-doped sample were interpreted in terms of a recombination model in which the recombination centres are exclusively dangling bond defects mainly in the D^- state. The band tail states trap most of the charge, act as carrier reservoirs and manifest themselves only in the charge neutrality relation. The recombination rate limiting step is hole release and subsequent monomolecular recombination via D^- states.

In addition, the model explains the SSPC maximum observed in annealed n-type a-Si:H at relatively high temperatures and predicts the thermal quenching caused by light soaking of such material. It is of interest to note that the independence of the SSPC with temperature at very low temperatures, coupled with a linear response to excitation can also be explained by the model in terms of a changeover to *hole* conduction.

TABLE OF CONTENTS

CHAPTER.1
INTRODUCTION

Over the last decade, hydrogenated amorphous silicon (a-Si:H) has been widely used as the basic material in a large variety of electronic and photoconductive devices. For example, the use of a-Si:H in junction form in solar cells, in electrophotography as a photoreceptor, or as a photosensor in image sensors ; Amongst electronic uses are included its incorporation in arrays of thin film transistors for liquid crystal displays and televisions, and in memory junctions. In these and many other applications (see Le Comber, 1989), a-Si:H has come to replace crystalline semiconductors because of its low fabrication cost and suitability for large area integration on one hand, and its photosensitive properties on the other. However, its performance in many areas is inferior to that of conventional crystalline semiconductors.

From this latter point of view, fundamental studies are necessary to understand the photoresponse behaviour and to investigate the electronic structure of this material. For this purpose, techniques of photoconductivity are probably the most powerful means.

In the present study, samples of this semiconductor material are investigated by the use of steady state and transient photoconductivity (applied separately and in the form of steady state bias + transient) in a coplanar structure. The samples are n-type, doped with Phosphorus and alternatively with Arsenic in the gas phase during deposition by the glow discharge method . The work aims at the following points:

i) Understanding the photocarrier transport, trapping and recombination in the samples through investigation of their photoresponse behaviour over ranges of excitation intensities and temperatures.

ii) Trying to develop a physical model of recombination which satisfies both steady state and transient regimes of photoconductivity for the particular case of n-type a-Si:H treated here.

iii) Comparing the two sample types with regard to the electronic structure described in the model .

The present work will be reported along with the necessary background to its subject in the following order:

Chapter.2 will present the basic electronic properties and photoconductivity concepts in amorphous semiconductors in general. In Chapter.3, recombination models previously put forward to explain the different SSPC and TPC responses observed in different amorphous semiconductors will be reviewed in the form of a historical background with emphasis on a-Si:H. The fourth chapter will present in detail the experimental methods and procedures employed throughout the work. Chapter.5 will be concerned with the theory of the photocarrier transport and the model of recombination developed in this work. The experimental results will be interpreted and discussed in chapter.6 in accordance with the theory given in chapter.5, together with some details about the model physics. In Chapter 7, the results will be briefly summarised and some points on further research will be suggested.

CHAPTER 2
ELECTRONIC AND PHOTOCONDUCTIVE PROPERTIES OF AMORPHOUS SEMICONDUCTORS

2.1 Energy bands in a perfect crystal.

With the assumption of perfect structural periodicity (long range order), the atoms in crystalline solids are arranged in similar unit cells which repeat spatially in a periodic manner to form the whole crystal lattice. The electron is subject to a potential with the periodicity of the lattice, and may therefore be described by a "Bloch wavefunction", a free electron plane wave modulated by a spatial function which has, similarly to the potential, the lattice periodicity. The resulting solutions of the Schrödinger equation (McKelvey, 1966) form a quasi-continuous spectrum of states, or allowed energy bands, separated by forbidden bands (or gaps) where no allowed states exist (Fig.2.1). The Bloch wavefunctions extend in the allowed bands throughout the infinite lattice, and thus describe delocalised states. Theoretically, the mean free path L in an ideal crystal is infinite.

2.2 Effect of disorder.

The structural disorder in an amorphous solid causes scattering (changes Δk in the wave vector, k, direction) by randomly positioned atoms and thereby limits the electron mean free path L. In an amorphous material, where the disorder is strong, k is not a good quantum number since $\Delta k/k \simeq 1$ and the wavefunction gains a local extention describing a localised electron (Fig.2.3.c).

2.3 Localisation criterion of Anderson

The Anderson model is based on the narrow tight binding approximation (McKelvey,1966) which is appropriate to weakly overlapping wavefunctions in narrow bands (eg the s-states in crystalline material) (Fig.2.2.a). The model, as presented by Mott (Mott and Davis 1979, p15) has the following features.

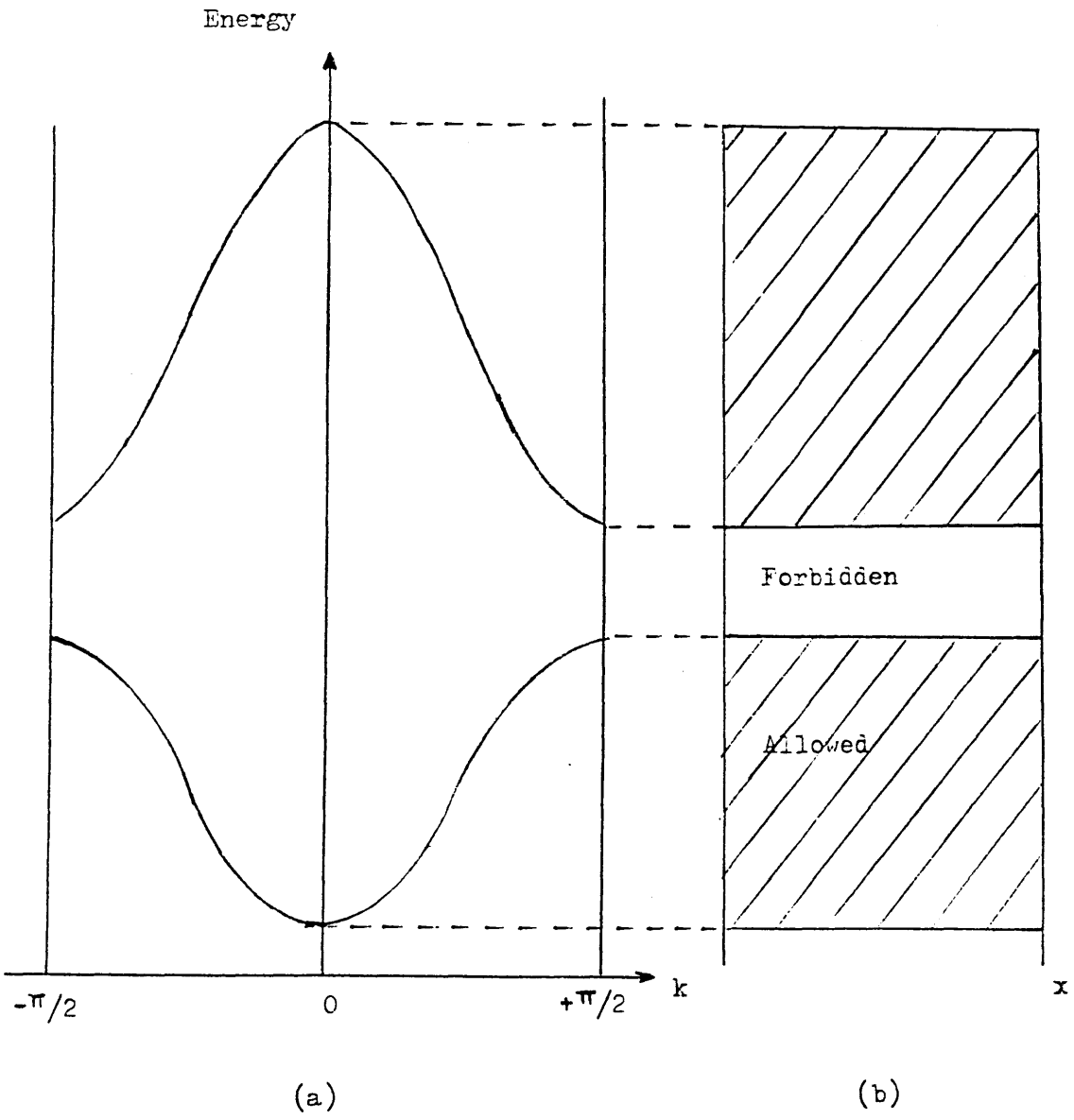

Figure.2.1. Unidimensional representation of the electron energy spectrum in an ideal crystal.
(a) in k space, limited to the first Brillouin zone
(b) in x space, showing the allowed and forbidden energy bands.

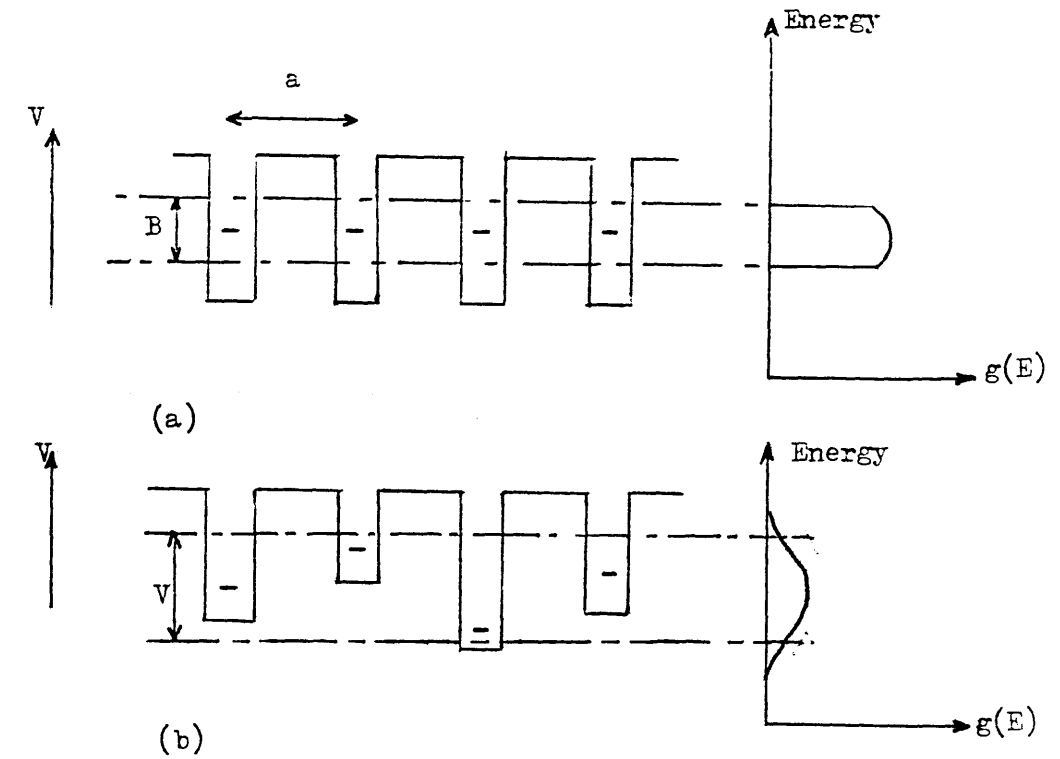

Figure.2.2. (a) Potential wells for an ideal crystal.
(b) Potential wells with fluctuations due to disorder.
The density of states is shown on the right.

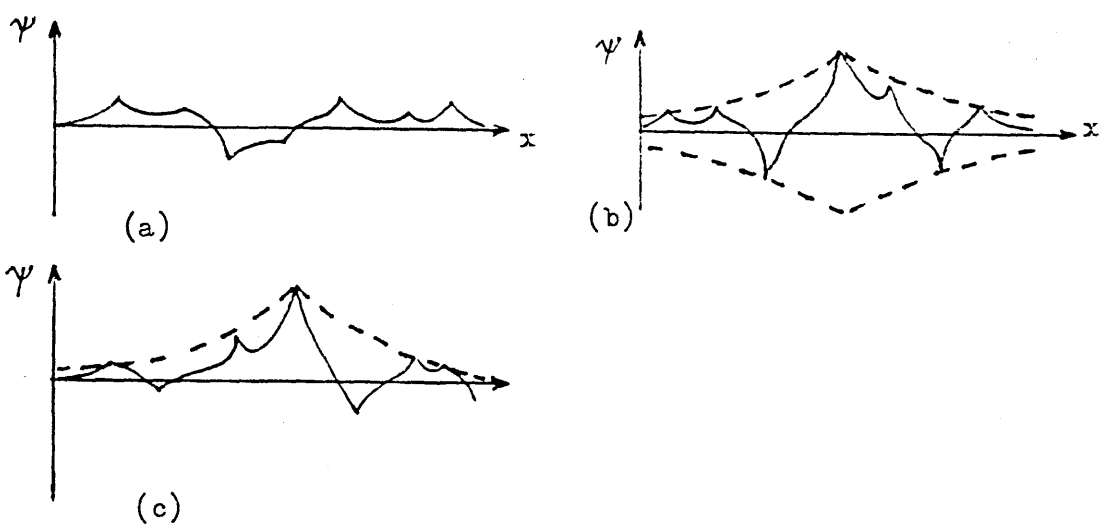

Figure.2.3. The wavefunction form in the Anderson model of Fig.2.2
(a) delocalisation just above E_c, (b) weak localisation $E \leq E_c$, and (c) strong localisation.

The bandwidth B is related to the overlapping by

$$B = 2.z.J \qquad (2.3.1)$$

where z is a coordination number and J the exchange integral which measures the wavefunction overlap on neighbouring sites. The Anderson model deals only with vertical disorder (ie fluctuations in potential depths over the width V_0) (Fig.2.2.b). The use of scattering theory with the results of the tight binding approximation gives the important relation,

$$a/L = (1/32.\pi).(V_0/I)^2 = (z^2/8.\pi).(V_0/B)^2 \quad L \geq a, \qquad (2.3.2)$$

An increase in V_0 (as a measure of disorder) is accompanied by a decrease in L, and the limiting condition $L \simeq a$ results in the criterion,

$$V_0/B \geq (8.\pi/z^2)^{(1/2)} \quad (\simeq 0.6 \quad \text{for } z = 6) \qquad (2.3.3)$$

In fact, this first criterion denotes the point at which the wavefunction loses its phase coherence (Figure.2.3.a), rather than a transition from a delocalised to a localised wavefunction. The Anderson transition (from delocalisation to localisation) occurs with further disorder when the parameter V_0/B attains a critical value $\simeq 2$ (Fig.2.3.b,c), above which the average conductivity $\langle\sigma\rangle$ at zero absolute temperature falls to zero. This means that the electron states become far apart on an energy scale, and consequently the probability of tunneling without thermal assistance becomes negligibly small.

2.4 The band tail of localised states

In broad conduction bands, as in the amorphous case, the onset of localisation appears in the band tail states. This is because, even at constant V_0 throughout the whole band, the exchange integral J decreases with increasing inter-state distance as a result of decreasing the state density g(E). Thus the low density levels in the band tail are more localised; The transition from localised to extended states for a given degree of disorder is known as the mobility edge E_c (Fig.2.4). In physical terms, the band-tail states

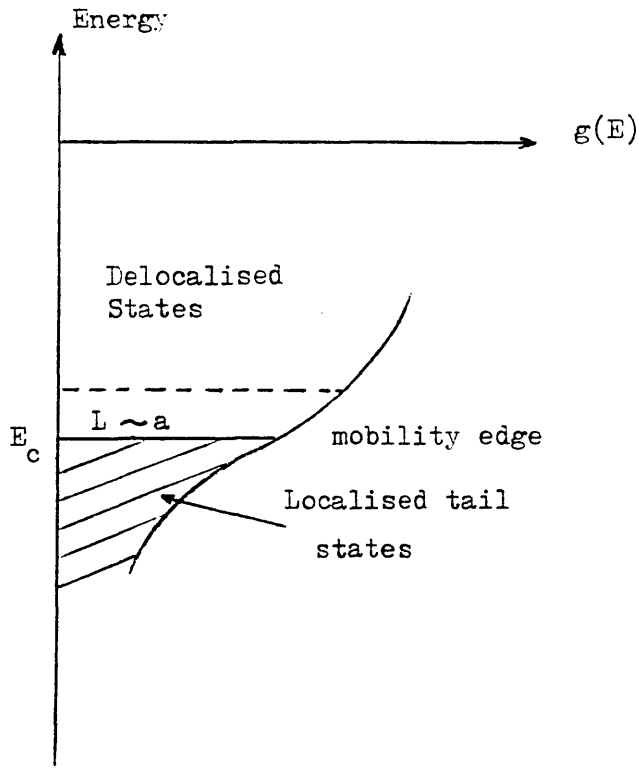

Figure.2.4. Density of states in a broad band of an a-semiconductor showing localised tail states.

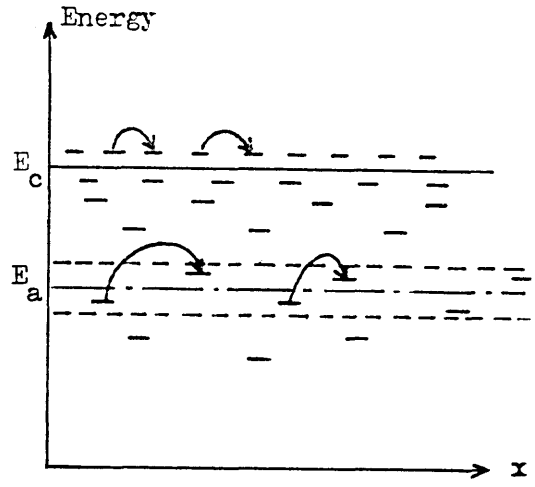

Figure.2.5. Electronic transport: Diffusion without thermal assistance just above E_c and hopping with thermal assistance through localised states.

result from the lack of long-range order arising from variations in bond lengths and bond angles.

2.5 Electrical transport

Depending on the distribution of the density of states g(E) and the carrier mobility $\mu(E)$, the major contribution to the conductivity σ can take place, under certain conditions of temperature, via a conduction path involving extended states near E_c or via localised states in the band tail at, say, E_a (Fig.2.5). The conduction process determines the mobility μ.

In the following, the n-type case will be adopted, where majority carriers are electrons.

2.5.1 Extended state conduction

Just above E_c, the effect of potential fluctuations begin to dominate since the mean free path is comparable to the inter-atomic distance. Therefore, the free electron picture with occasional scattering is no longer valid. Cohen (1970) suggested diffusive or Brownian motion without thermal activation and obtained the mobility at E_c as

$$\mu_c = (e.a^2/6.k.T).\nu_{el} \qquad (2.5.1)$$

where ν_{el} is the electron frequency of diffusive hopping near E_c.

The random phase model describing the ideal case of the amorphous state has been used (Hindley, N, K, 1970) to give more exact estimate of μ_c ($\mu_c \simeq$ 1-10 $cm^2.V^{-1}.sec^{-1}$) (cf review by Nagels, P. 1985). In the non degenerate case, the conductivity σ_c at E_c is

$$\sigma_c = e.\mu_c.g(E_c).k.T.\exp(\delta/K).\exp(-E_0/k.T) \qquad (2.5.2)$$

where $\exp(\delta/K)$ is a constant associated with the gap reduction as the temperature increases, appearing in the relation $E_c - E_f = E_0 - \delta.T$, and E_0 is the extrapolation of $E_c - E_f$ to T=0.

2.5.2 Conduction in the band tail

The transport process, when the conduction path energy E_a lies in the band tail below E_c, is electron hopping to neighbour states with phonon assistance. The hopping mobility is given by

$$\mu_H = (e.R_0^2/6.k.T).\nu_{ph}.\exp(-2.\alpha.R_0).\exp(-w/k.T)$$
$$= \mu_{H0}.\exp(-w/k.T) \qquad (2.5.3)$$

which differs from μ_c by the electron hopping rate $\nu_{ph}.\exp(-w/k.T)$, ν_{ph} being the phonon frequency and w the energy distance between two neighbours, and the overlapping term $\exp(-2.\alpha.R_0)$ between two wavefunctions centered at a separating distance R_0 with a spatial decay α^{-1}. The associated conductivity is

$$\sigma_H = \mu_{H0}.\exp\{-[(E_a-E_f)+w]/k.T\}.k.T.g(E_a) \qquad (2.5.4)$$

The change in the activation energy of σ from E_0 to (E_a-E_f+w) was observed in the first glow discharge a-Si:H (Spear,Loveland and Al-Sharbaty, 1974) at $\simeq$ 250 K. In today's high quality a-Si:H, of low tail state and defect densities, there is evidence suggesting hopping transport at much lower temperatures ($\simeq$80 K) (Spear and Cloude, 1987).

2.5.3 Conduction by hopping at the Fermi level.

At low temperatures the major contribution to σ takes a path around E_f, and the electrons are most likely to hop to a distant state (not necessarily the nearest neighbour) at an energy equal to the energy $w \simeq k.T$ provided by the phonon (variable range hopping R).

$$\sigma_H(E_f) = (e.R^2/6).g(E_f).\nu_{ph}.\exp(-2.\alpha.R - w/k.T) \qquad (2.5.5)$$

According to Mott (Mott & Davis 1979, p32), the mechanism is due to a competition between the overlap factor and the energy factor, and R corresponds to maximum hopping probability, leading to Mott's $\sigma \approx T^{-(1/4)}$ law.

2.6 The dangling bond defect in a-Si

In addition to the band tail localised states arising from topological disorder, amorphous silicon (a-Si) also exhibits a significant density of gap states arising from dangling bond (DB) centres. This was first detected (Brodsky et al, 1969) in the ESR experiment as a singly occupied centre. Later ESR measurements (Thomas et al 1978) on very pure a-Si obtained in an ultrahigh vacuum evaporation system and on contaminated a-Si revealed that the center is a fairly localised structural defect which is very reactive and identifiable with a broken silicon bond, (Fig.2.6) which can be paired by an addition of impurities such as hydrogen. Indeed, hydrogenation of a-Si (eg preparation by glow discharge of silane) (Le Comber,Loveland and Spear, 1974) was found to decrease remarkably the spin density from $6.10^{19}cm^{-3}$ (in pure a-Si) to $6.10^{15}cm^{-3}$ (Knights et al, 1977). Further information on this centre was obtained from the temperature dependence of light induced ESR and photoluminescence in doped and undoped a-Si:H (Street and Biegelsen, 1980), and it is now known that the centre is neutral when unpaired (D^0) with a positive effective correlation energy U [the energy required for D^0 to capture an other electron and become doubly occupied (D^-)]; The D^0 centre can also lose its electron to give a third DB state D^+ (Fig.2.7). Electron transfer between D^0,D^+ and D^- states and the resulting equilibrium densities are controlled by the Fermi level position (cf sect.2.8).

2.7 Doping and the DB defect

Mott argued (Mott, 1969) that, according to the "8-N" rule, doping of a-Si by substitution with, for example, a pentavalent impurity such as P_3^0 is not possible since the accomodation of P_3^0 must satisfy the DB D^0. In other words, P_3^0 must be constrained to increase its coordination from 3 to 4. Moreover, in unhydrogenated a-Si of high mid-gap D^0 density, E_F is pinned (ie it can not be moved by doping). In hydrogenated glow discharge a-Si however, substitutional doping is possible (Spear and Le Comber, 1976) and has been shown to control the electronic properties of a-Si:H.

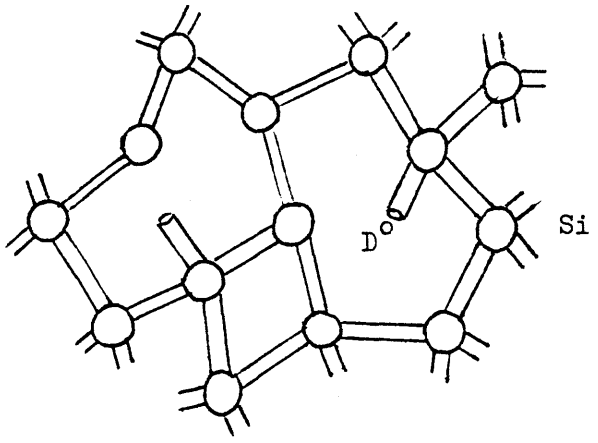

Figure.2.6. Identification of the dangling bond defect with a broken Si-Si bond singly occupied (D°).

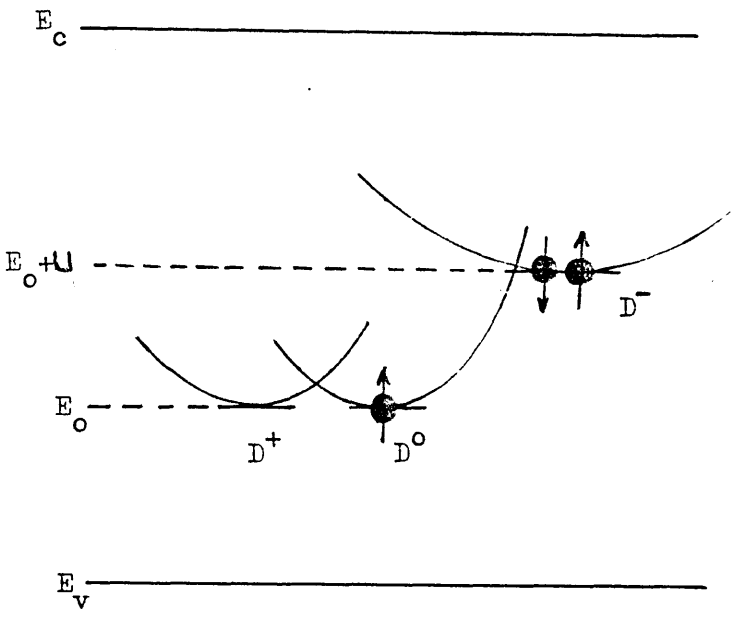

Figure.2.7. Illustration of the electron transfer between D°, D^{+}, and D^{-} states and the consequent configurational changes.

A solution for the doping mechanism was later given by the "Street model" (Street, 1982) suggesting that, during deposition, the P_3^0 atoms, after being ionised to P_4^+, satisfy the "8-N" rule leading to the reaction with the DB D^0, $P_3^0 + D^0 \longrightarrow P_4^+ + D^-$, in which the transfer $D^0 \longrightarrow D^-$ occurs. If E_0 is the D^0 energy level, the transfer to D^- occurs when E_F is shifted above the D^- level E_0+U. With the same mechanism, doping with a trivalent impurity such as B_3^0 is accompanied by the transfer to D^+ occurring when E_f is shifted below E_0 (Spear, Steemers and Le Comber, 1984). Typical values of E_0 and U are $\simeq$ 1.1-1.2 eV below E_c and 0.4 eV respectively (Le Comber and Spear, 1986).

2.8 Statistics of the dangling bonds at thermal equilibrium

Following the above discussion, the DB center is a two electron correlated state, and hence, it is a spin degenerate state. In the following, E_c will be taken as the energy reference, with negative energies below E_c.

The occupation functions F_0^0, F_0^- and F_0^+ of the three DB states are calculated from the electron (or hole) detailed balance at E_0 and at E_0+U, together with the DB conservation equation, $F_0^0 + F_0^- + F_0^+ = 1$, and are given by (Okamoto et al., 1984)

$$F_0^0 = \{ 1 + (1/2).\exp [(E_0-E_f)/k.T] + (1/2).\exp [(E_f-E_0-U)/k.T] \}^{-1}$$
$$F_0^- = F_0^0.(1/2).\exp [(E_f-E_0-U)/k.T]$$
$$F_0^+ = F_0^0.(1/2).\exp [(E_0-E_f)/k.T] \qquad (2.8.2)$$

2.9 Photoconductivity

The illumination of an amorphous semiconductor by uniformly absorbed light of an appropriate wavelength results in the photogenerated carriers being subjected to several processes:
(i) transport by diffusion in the extended states,
(ii) interaction with shallow and deep traps,
(iii) recombination into defect states (such as DB).

Under steady state illumination these processes occur simultaneously according to certain statistics. Whereas, in the transient regime, after light cut-off, carrier relaxation, by progressive thermalisation in the band tails, occurs prior to recombination. A review of recombination models in both regimes is presented in chapter.3. Herein, the basic concepts and elementary definitions that will be referred to in the next chapters are explained. The discussion will be in terms of electrons since the present study deals with n-type materials.

2.9.1 Lifetime and response time

The lifetime τ_n of free electrons is the average time spent in the extended states by the electrons, and is related to the excess free electron density by

$$n = G.\tau_n \qquad (2.9.1)$$

where G is the generation rate of electron-hole pairs (here $n \gg n_0$, the thermal equilibrium free electron density). τ_n is controlled by the recombination centers. If N_r is the density of these centres and σ_n their electron capture cross-section, τ_n is given by

$$\tau_n = 1/(N_r.v.\sigma_n) \qquad (2.9.2)$$

where v is the electron thermal velocity.

The response time τ_0 is the time required for the photocurrent to reach the steady state after photo-excitation (or, in practice, 50 % of the steady state value). Carrier traps are distinguished from the recombination centers by their thermal relation to the extended states, and therefore, they interact with them in determining the response time. For a single level of traps with n_t trapped electrons per cm^3,

$$n + n_t = G.\tau_0 \qquad (2.9.3)$$

and the response will be delayed by the traps to the time

$$\tau_0 = [1 + (n_t/n)].\tau_n \qquad (2.9.4)$$

2.9.2 Monomolecular and Bimolecular recombination

Consider the case of single levels of electron and hole traps (Fig.2.8). If the density of electron recombination centers N_r in the dark is high compared to the (free and trapped) electron density $n+n_t$, then τ_n remains unchanged as recombination proceeds, in accord with equation.2.9.2. The photoresponse as a function of G will be linear and the recombination is said to be *monomolecular*.

If, on the other hand, N_r is small compared to $n+n_t$, (which can occur at high excitations G), then τ_n may change as recombination proceeds. Since the electrons are the majority carriers, the excess charge neutrality condition is

$$n + n_t = N_r = (1 + k).n \qquad (2.9.5)$$

with $k = (N_t/N_c).\exp[(E_c-E_t)/k.T]$ the Boltzmann factor relating n_t to n. This Equation, with Eqns.2.9.1 and 2.9.2, yields a square root excitation dependence of n which is consequently observed in the photoresponse,

$$n \approx G^{(1/2)} \qquad (2.9.6)$$

Recombination processes occurring under these conditions are termed *bimolecular*.

2.9.3 Trap occupation function and trapped carrier Quasi-Fermi level

A trap state at an energy E in the gap is characterised by its electron and hole capture cross-sections σ_n and σ_p. Under steady state conditions, the four possible transitions, capture and release of electrons, and capture and release of holes, are in balance resulting in the trap occupation function (Simmons and Taylor, 1971)

$$f_t(E) = (v.\sigma_n.n + e_p)/(v.\sigma_n.n + e_n + v.\sigma_p.p + e_p) \qquad (2.9.6)$$

where

$$e_{n,p}(E) = v.\sigma_{n,p}.N_{c,v}.\exp\,[-|E_{c,v}-E|/k.T\,], \qquad (2.9.7)$$

is the electron (hole) release rate from the trap to the conduction (valence) band. For states located above E_f from which the emission of holes is unlikely to occur, equation.2.9.6 reduces to

$$f_t(E) = (v.\sigma_n.n)/(v.\sigma_n.n + e_n + v.\sigma_p.p)$$

$$= [1/(1 + r)].\{1 + \exp[(E-E^t_{fn})/k.T\ ]\} \qquad (2.9.8)$$

which has the form of a Fermi function modulated by the factor $(1+r)^{-1}$ (Fig.2.9) where the parameter r is given by

$$r = (\sigma_p.p)/(\sigma_n.n) \qquad (2.9.9)$$

and E^t_{fn} is the trapped electron quasi-Fermi level defined by

$$(1+r).n = N_c.\exp[(E^t_{fn}-E_c)/k.T] \qquad (2.9.10)$$

Replacing n by $N_c.\exp\ [(E_{fn}-E_c)/k.T\ ]$, one obtains for E^t_{fn}

$$E^t_{fn} = E_{fn} + k.T.\ln(1 + r) \geq E_{fn} \qquad (2.9.11)$$

E^t_{fn} represents a steady state demarcation energy between shallow traps and recombination centers.

2.9.4 The Rose model

In the case of a continuous distribution of trap states, such as the band tail in amorphous semiconductors, the photoresponse will be more complicated than simply linear or square root and will depend on the details of the distribution. The Rose model (Rose, 1963) which assumes an exponential band tail

$$g(E) = G_c.\exp[(E-E_c)/k.T_c], \qquad (2.9.12)$$

where $k.T_c$ is the tail width and G_c the extrapolation of g to E_c, accounts for power-law photoresponses with a power index $0.5<\gamma<1$. The lifetime τ_n decreases with increasing N_r as traps are converted into recombination centers with shifting QFL E_{fn} towards E_c. In calculating the converted trap density ΔN_r, one should use the modulated Fermi function (Eqn.2.9.8) and the QFL E^t_{fn}.

$$\Delta N_r = \int_{E_f}^{E^t_{fn}} g(E).f_t(E).dE$$

$$\simeq k.T_c.G_c.(1+r)^{(\alpha_c-1)}.(n/N_c)^{\alpha_c} \qquad (2.9.13)$$

This correction of the original Rose expression by the r factor is important, in that it includes the role of the minority carriers p, which may be particularly significant at high excitations G. In the

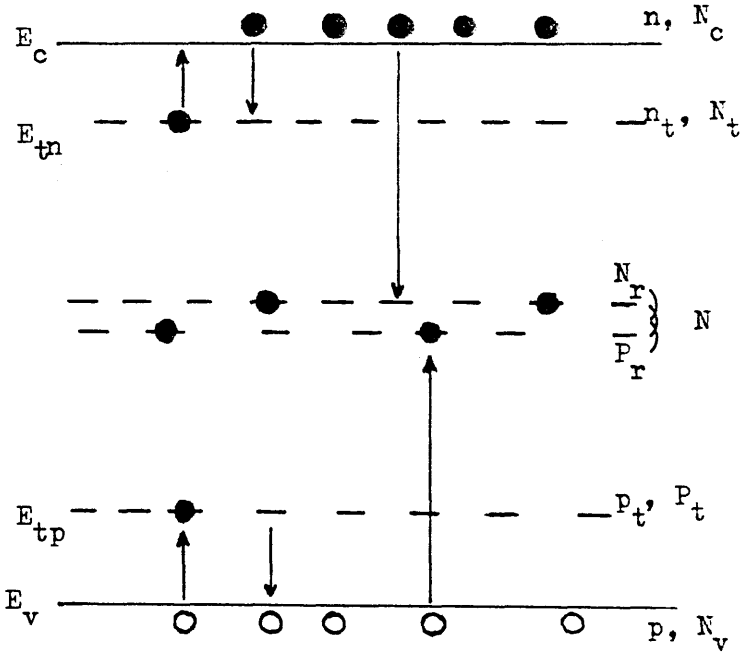

Figure.2.8. System of single levels of electron and hole traps and recombination centres.

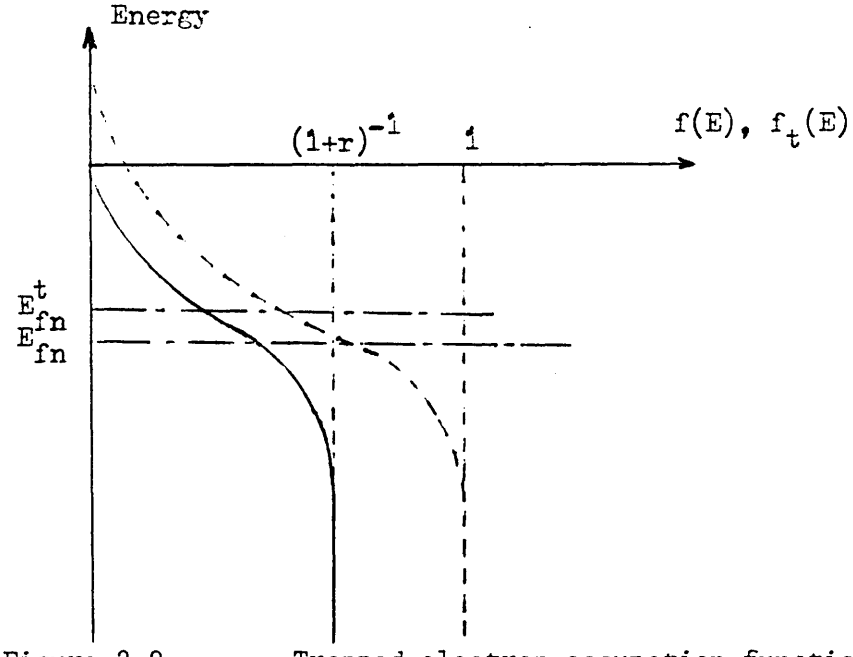

Figure.2.9. ——— Trapped electron occupation function.
----- Free electron occupation function (or Fermi distribution.

case where r is small (ie $\sigma_n.n >> \sigma_p.p$), the Rose model yields a photoresponse $n \approx G^{\gamma}$ with

$$0.5 < \gamma = 1/(\alpha_c+1) < 1 \ , \quad (\alpha_c = T/T_c < 1) \tag{2.9.14}$$

2.9.5 Dispersive transport

Again, consider the case of amorphous semiconductors where localised states form a band tail. The dispersive transport which arises from a spread in the release times as a result of the energy spread of the localised states follows the multiple trapping mechanism. A pulsed carrier density N_e will be rapidly trapped by localised states. While thermalising, the electrons fall into two groups of states:

(i) states in thermal equilibrium with the extended states and

(ii) states so deep that the probability of release within the measurement time t is negligible.

The demarcation level E_d separating these two state groups is defined by the relation

$$e_n(E_d).t = 1, \tag{2.9.15}$$

since the electrons are released only once from E_d in the time t. The release rate $e_n(E)$ is given by Eqn.2.9.7 with $\sigma_n.v.N_c = \nu$, an "attempt to escape" frequency of the order of $10^{12}sec^{-1}$. Hence, the electrons thermalise in the form of a packet with the peak at E_d (Fig.2.10) such that

$$E_c - E_d = k.T.\ln(\nu.t) \tag{2.9.16}$$

A treatment of the time evolution of the photoresponse (Orenstein et al, 1982), for low N_e based on dispersive transport with free electron recombination via trapped holes has led to a two region decay of the transient photocurrent I_{TPC} (Fig.2.11),

$$I_{TPC} \approx t^{(\alpha_c-1)} \ , \text{ for } t < t_r$$

$$I_{TPC} \approx t^{(\alpha_c+1)} \ , \text{ for } t > t_r \tag{2.9.17}$$

where t_r is the effective recombination time.

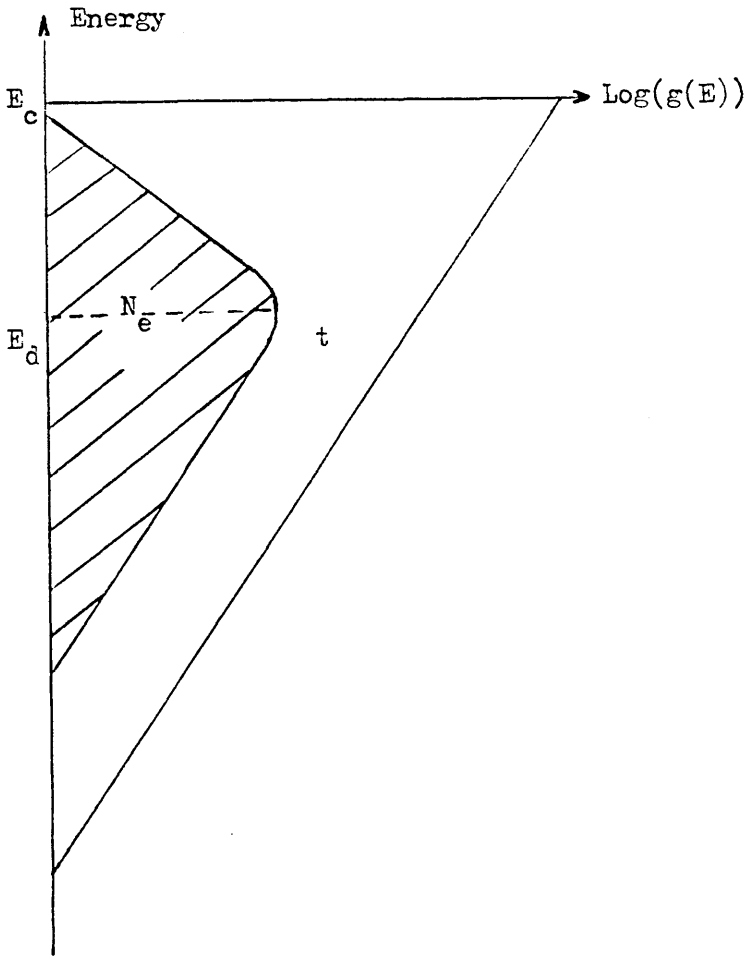

Figure.2.10. Electron thermalisation into an exponential CBT (see details in the text).

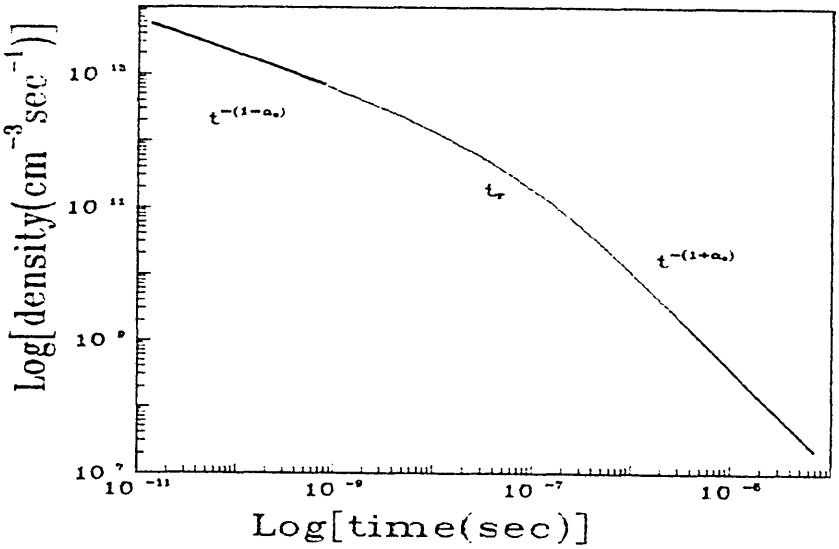

Figure.2.11. TPC decay, showing the two regions expressed by Eqn.2.9.17.

CHAPTER.3

REVIEW OF RECOMBINATION MODELS IN STEADY STATE AND TRANSIENT PHOTOCONDUCTIVITY

3.A. Transient photoconductivity.

The basic 'TROK' approach dealing with multi-trapping electron thermalisation in band-tails (Tiedje and Rose, 1982, and Orenstein and Kastner, 1982) (cf sect.2.9.5) has been confirmed by observations from time-of flight (TOF) measurements in undoped a-Si:H (Tiedje, 1984) and from the coplanar transient photoconductivity (TPC) method (Hvam and Brodsky, 1981). The inclusion of *recombination* in the multi-trapping models has been more recent development, to account for features observed in the TPC decay which are not in agreement with the simple 'electron multi-trapping thermalisation ' picture. In particular, attempts have been made to explain the effects of optical bias and the very long dispersive decays in n-type a-Si:H.

Pandya and Schiff (1984) observed, in undoped a-Si:H, TPC responses with a steep decay at short times (10^{-7}-10^{-6}sec). This was interpreted as a changeover from band-tail trapping at very short times ($t < 10^{-7}$s) to trapping in dangling bonds. On applying optical bias, the photocurrent in the time region 10^{-6}- 10^{-4}s was observed to *increase*. Pandya and Schiff interpreted this in terms of a change in the occupation of D^0 centres with constant illumination, leading to a reduced trapping rate by dangling bonds.

In contrast with the above, at times *longer* than 10^{-4}sec, the effect of optical bias is to *hasten* the decay of the TPC. In an attempt to explain this observation, Zeldov and Weiser (1984) proposed that the steady illumination would lead to saturation of the conduction band tail states - i.e. filling of states up to a quasi-Fermi level. Then when electron thermalisation is complete down to this level, recombination can proceed. As the optical bias increases, raising the electron quasi-Fermi level, then the time at which recombination commences shortens. A bimolecular recombination process was assumed.

Compared to the undoped case, the TPC in n-type a-Si:H is characterised by a much longer decay time (10^{-5}-10^{-4}sec) separating a nearly flat region with a small dispersive parameter (power law index < 0.25) from a long slow decay, observed with some structure (Oheda, 1987) or as a power-law decay (Main, 1987). The initial region was assigned (Oheda, 1985), according to its temperature dependence, to trapping in states located 0.2 eV below E_c, while Main et al. identified this non-dispersive region with trapping in shallow states distributed down to 0.17 eV below E_c.

The difficulty of attributing the long-time dispersive decay to *electron* thermalisation has been pointed out by Street et al. (Street, Beigelson and Weisfield, 1984), who argued that electron thermalisation to the Fermi level in n-type material should be completed within 100ns, after which there can be no further dispersion in the electron mobility. (It should be noted here that the model of Zeldov and Weiser for the effects of optical bias, originally applied to the *undoped* case would also break down in the case of n-type a-Si:H, for the same reason)

Both Oheda (1987) and Main et al.(1987) resolved the above difficulty by proposing that the long time recombination decay was controlled by the *minority* carriers (holes), but different interpretations were given for the cause of the slow dispersive decay. While Oheda adopted electron bimolecular recombination and attributed the dispersion in the decay to a very wide distribution of the hole recombination coefficients, Main adopted hole monomolecular recombination via D^- states and attributed the long power-law decay to the distribution of trapped hole release times which would occur during hole thermalisation in the VBT (Valence band tail). This last argument implies that there is no recombination between free electrons and trapped holes (in VBT states). McMahon (1990) has more recently proposed the existence of 'safe hole traps' in a-Si:H, which have this property.

3.B. Steady state photoconductivity.

Steady state photoconductivity (SSPC), although experimentally straightforward, has been a most efficient method in revealing

information on the gap defect states involved in the recombination process. The excitation and temperature dependences are very sensitive to changes in these defects, and therefore, they are readily affected by the preparation conditions of the material. Hence, the technique has been regularly applied to monitor material quality. In this chapter, the general features of steady state photoconductivity in amorphous semiconductors are reviewed, with particular emphasis on amorphous silicon.

The general and common characteristic features in the temperature dependence (Fig.3.1.a) and excitation dependence (Fig. 3.1.b) of the SSPC for a-Si:H and also many chalcogenides are,

i)- A maximum region (I) near the intercept with the dark current. At temperatures around and above this maximum, the excitation dependence is linear ($\gamma = 1$).

ii)- An activated region (II) over a wide range below room temperature, for which the excitation dependence is *sublinear* ($\gamma < 1$).

iii)- A low temperature flat region (III) for which the excitation dependence *returns* to linearity.

The excitation dependence should thus be characterised at a *given temperature* by a change from being linear ($\gamma = 1$) at low excitation to sublinear ($\gamma < 1$) at moderate excitation, followed by a further transition to linearity at very high excitation and/or low temperatures.

The first measurements on chalcogenide glasses were interpreted in terms of various models regarding the energy distribution of the gap states, and the transitions involved in the recombination process: While Main and Owen (1973) proposed a simple model in which the localised states (LS) are represented by two discrete levels near the band edges acting as recombination centers for the free carriers, neglecting transitions between localised states (LS-LS), Arnoldussen et al (1972) had to postulate a sharp decrease of the effective density of recombination centers near the band edges, in a model which assumed a continuous energy distribution of the localised states, in order to obtain reasonable agreement with the experimental data for the activated region (II). LS-LS recombination was also necessary in this model.

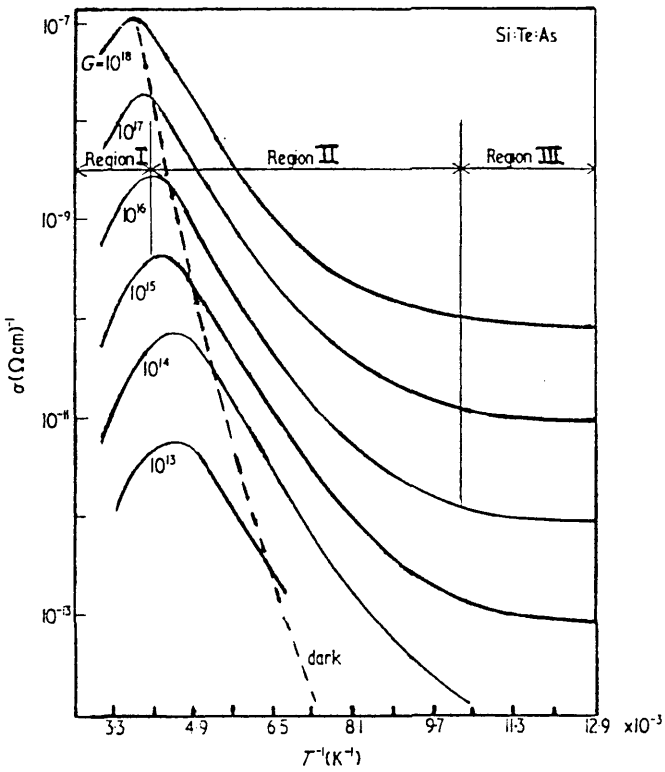

Figure.3.1. (a). Temperature dependence of the photoconductivity with excitation as parameter in Si:Te:As (Simmons and Taylor, 1974)

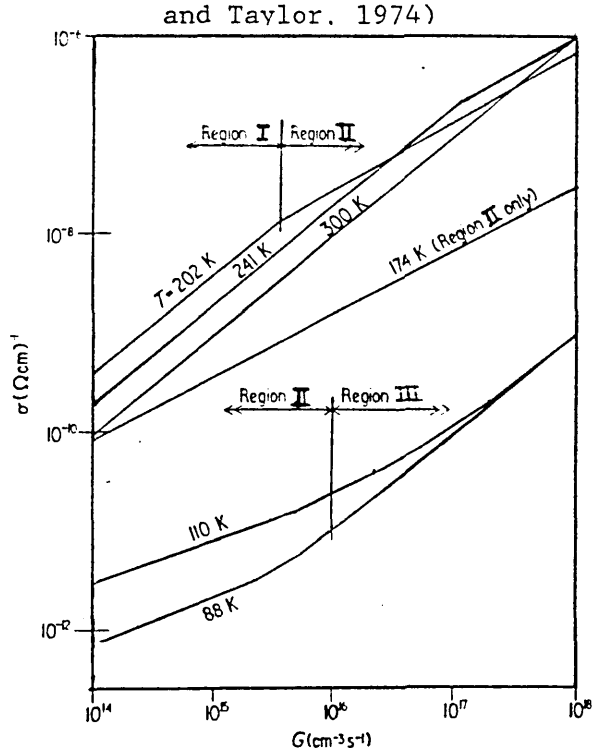

Figure.3.1. (b). Excitation dependence of the photoconductivity with temperature as parameter (Complement of (a))

In an earlier model suggested by Weiser et al (1970), the carriers recombine from LS at specific levels ($\simeq$ 0.18eV from the mobility edges) called "recombination edges" reached when further migration towards midgap is opposed by large spatial extentions of the states wavefunctions. Adopting the Mott-Cohen, Fritzsche, Ovshinsky (M-CFO) model of exponential trap tails (see Cohen et al 1969), Simmons and Taylor (1973) were able to obtain an exellent correlation with some observed data using extended Shockley-Read statistics (Shockley and Read 1952, and Simmons and Taylor, 1970) which involve both carrier types. The same authors reported later (Taylor and Simmons, 1974) that the M-CFO model predicts a substantially weaker temperature dependence of characteristics than is observed (eg, it does not predict the low temperature flat region), and that the discrete-level model is more appropriate, and they concluded that such levels might have the origin of an excess or a deficit of a specific atom required for the theoretically complete bonding structure in the material. The low excitation linear region is followed by a sublinear region in the excitation dependence which in chalcogenides, is exclusively a square root-law, and was interpreted as a transition from monomolecular to bimolecular recombination (see Main and Owen, 1973).

In the early samples of undoped a-Si:H produced by the glow discharge decomposition of silane (cf sect.4.1), two levels were identified by the field effect technique (Spear, Loveland and Al-Sharbaty, 1974) as peaks in the density of states located round 0.4 eV and 1.1-1.2 eV below the conduction mobility edge, and suggested to be associated with dangling bond defects (Madan and Spear, 1973) using evidence from ESR measurements (Brodsky et al, 1970). Again, this material shows more or less the same temperature and excitation dependences as those obtained with the chalcogenides. This behaviour was explained (Spear, Loveland and Al-Sharbaty) in a model assuming electron recombination from LS in a sharply decreasing tail at an energy 0.18 eV below the conduction mobility edge, via trapped holes around the 1.2 eV peak, and trap-controlled charge neutrality. The low temperature second transition to region (III) taking place at 250K (independently of the excitation) was interpreted in terms of phonon-assisted hopping, occurring at the same level from which recombination occurs at higher temperatures, with hopping activation energy of $\simeq$ 0.09 eV.

In contrast, Wronski and Daniel (1981) measured in their intrinsic material an increase in the activation energy for region II, E_{pc} at $T \simeq 200K$, from 0.1 to 0.2 eV, and concluded that the SSPC is controlled by free electrons over the whole temperature range above and below 200 K. This second transition in the activation energy was accompanied by a transition in the power index γ of the excitation dependence from 0.5 to values as low as 0.4. Their model of recombination based on the concept of the Rose model (see sect.2.9.4) included mainly hole occupied centers located below midgap, having small capture cross-section ($\simeq 10^{-19}cm^2$), and acting as recombination centers, with the presence of other types of centers above midgap and an important high density of shallow electron traps ($10^{19}cm^{-3}$) which act as desensitisers when approached by the electron QFL. They attributed the first transition of E_{pc} from 0 to 0.1 eV and γ from 0.83 to 0.5 to the shift of the QFL up to the trap level, and explained the second transition, where γ falls below the Rose limits (0.5-0.4), by the saturation of the deep-lying recombination centers, due to the high density of electron traps, and the involvement of other types of centers, thus decreasing the electron life time. The basic Rose model (sect.2.9.4) appears to be too limited to explain the widely varying temperature dependence of the index γ from one sample to an other, even though γ falls mostly within its limits (0.5-1) as reviewed by Crandall (1984).

More recently, after it was shown possible to dope the intrinsic a-Si (Spear and Le Comber, 1975, 1976) steady state photoconductivity measurements were carried out on doped a-Si:H by Anderson and Spear (1977) on a series of boron and phosphorus-doped a-Si:H. Adopting the field effect measured density of states they associated the change from the maximum region (I) to the activated region (II) with a transition from monomolecular to bimolecular recombination occurring at a critical energy above the 0.4 eV localised state peak (i.e. at $\simeq 0.33$ eV below E_c) which was reached by E_{fn} at the appropriate temperature and excitation. This interpretation was a consequence of the observed saturation of the SSPC having its onset when the QFL is at $\simeq 0.33$ eV below E_c, and the correlation of this with the abrupt fall of γ from about 0.9 to 0.55 at the same time.

The specific effect of doping on the SSPC in terms of the dark Fermi level E_{F0} was studied by many reseachers (Anderson and Spear, 1977, Rehm et al, 1977, and Vanier et al, 1981). The SSPC was found to rise rapidly with increasing P-doping, attain a saturation level, and start decreasing when E_{F0} is at $\simeq$ 0.4 eV below E_c. According to Anderson and Spear, the introduced low concentrations of P-dopant neutralise part of the hole occupied recombination centres above E_{F0}, thus increasing the electron life time; At high doping levels, the electron occupied states below the QFL become effective electron recombination centers after capture of holes under illumination, which results in the saturation and subsequent decrease of the SSPC, with onset at $E_{F0} \simeq$ 0.4 eV below E_c being assigned to the peak in the density of states. However, later combined studies based on ESR and DLTS measurments (Cohen et al, 1982) have shown a minimum in the density of states at 0.4 eV below E_c rather than a peak.

Kagawa et al (1983) used intrinsic a-Si:H in a MOSFET structure to investigate the effect of shifting E_{F0}, by charge injection, on the SSPC. They observed a monotonic increase of the SSPC and a gradual decrease in γ over the range 0.85-0.35 with shifting of E_{F0} up to 0.25 eV below E_c, and concluded that the saturation and decrease in the SSPC and the abrupt fall of γ observed when E_{F0} is moved by doping is due to defects introduced in the gap by the dopant, mainly changes in the tail state profile. Their model assumed free carrier recombination via centers near midgap limited by the capture of holes. With the same aim of study, Hack et al (1984) proposed a model in which the free carriers recombine to a continuous distribution of donor and acceptor-like states in the form of exponential tails with dopant-created defects and shallow steeper tail traps. The increase of the SSPC with doping was assigned to change in the recombination path from donor to acceptor-like states as E_{f0} moves towards E_c. A reasonable fit to the Anderson data on the doping dependence of SSPC required a high ratio (10^3) of charged to neutral state capture cross-section.

There is evidence, from ESR studies in particular, that the dangling bond defects are the predominant recombination centers in a-Si:H (Street 1982 and Dersch et al 1983). It was found that these defects are correlated with a positive correlation energy U (Street

and Biegelsen, 1980). Their relative occupation depends on the doping level (ie the position of the dark Fermi level) (Spear, Steemers, Le Comber, 1984).

Okamoto et al (1984) developed statistics for the SSPC based on recombination via correlated defects, in which the tail states were assumed as "trap reservoirs" for the free carriers and included only in the charge neutrality. More recently, Vaillant et al (1988) adopted the same statistics for the dangling bonds, but allowed recombination to tail states according to Simmons and Taylor statistics, in this way they obtained an exellent fit for data on undoped a-Si:H above 150 K, including thermal quenching, however they had to assume a rapid increase of the tail states' electron capture cross-section with increasing energy towards E_c to account for the temperature dependence below 150 K.

Very recently, Bube and Redfield (1989) developed a simple numerical model by generalising the single recombination centre Rose model, with exponential trap tail states, for the dangling bond centre in the case of a-Si:H. These authors used a numerical solution based on the particle conservation relation, and assumed recombination of free carriers via dangling bonds only. Since the occupation of the divalent dangling bond center depends on the dark Fermi level location, this relation changes with shifting the Fermi level by means of doping or optical degradation. Reasonable agreement was obtained with previous results on the effect of doping and light soaking on the excitation dependence of the SSPC. However, the questions of whether the model also predicts the observed features of the temperature dependence of SSPC were not addressed by Bube and Redfield. These questions will be answered while dealing with the model proposed in the present work (Chap.5, sect.5.B).

The above review illustrates that there are many different and sometimes conflicting interpretations for steady state photoconductivity in a-Si:H, in which new states appear to be invoked when necessary to explain new results. This makes a coherent assessment of models as was done in (3.A) above for the transient case, very difficult. Nevertheless, there are some common features emerging particularly from the more recent work. These are-

i) the dominance of correlated dangling bonds as recombination centres

ii) the role of distributed tail states mainly as charge reservoirs

These ideas form the basis of the model developed and described in chapter 6. Additionally, the possibility of recombination mediated by transitions between shallow band-tail states and dangling bonds will be studied, and the importance of *minority* carrier distributions, often ignored in the literature, will be demonstrated.

CHAPTER.4

EXPERIMENTAL METHODS

In this chapter the fabrication and the pre-experimental treatment of the samples is described. A description then follows, of the experimental techniques employed in the work. The different parts of the experimental arrangement are subsequently detailed. Finally the experimental variables and the difficulties encountered in the measurements are discussed.

4.1. Experimental Samples

4.1.1. Glow discharge technique (G-D)

The method used to prepare the a-Si:H samples studied in this work was glow discharge plasma deposition. This is a radio frequency (r.f.) deposition technique where the basic gas component, silane (SiH_4) is subjected to decomposition into radicals (species such as Si, Si-H, etc) which, in turn, deposit onto a substrate held in contact with the plasma, thus forming a thin layer of a-Si:H. Additional components may include a diluent inert gas (usually Ar or H) used as a carrier gas and PH_3 or B_2H_4 as apropriate dopant gases. These are usually premixed with the gas matrix SiH_4. Other dopant gases such as AsH_3 can also be used. The silane decomposition results from the plasma electrons which, despite their low concentration in the plasma ($\leq 10^{11} cm^{-3}$ at a pressure of 0.1 torr), are at high temperature and energy ($T \simeq 10^4$ K, E$\simeq$ 2-7 eV). However, this energy is below the dissociative ionisation energy (11eV), and the dominant reaction is neutral radical formation (Hirose, 1984). Built in spectroscopic techniques may be used to study the plasma reactions, and hence to optimise the deposition conditions which the physical properties of the growing material depend on. A typical range of discharge parameters is presented in Table.4.1.

Depending on the method of coupling the r.f. excitation into the plasma, G-D deposition systems fall into two types, namely, inductively coupled systems and capacitatively coupled systems such as the system used in the Dundee University laboratories (Spear. W. E and Le Comber. P. G, 1984).

Parameter	Range
SiH_4 concentration	10-100% in H_2
Total gas flow rate	20-200 sccm
Total pressure	.05-2 torr
rf power	1-100 W
rf frequency	13.56 MHz
Substrate temperature	200-300°C
Substrate bias	mostly zero

Table 4.1. Typical range of deposition conditions

The samples studied in this work originate from two sources; Arsenic doped samples prepared at I.B.M. laboratories, and Phosphorous doped samples deposited in the Dundee system. For the Dundee samples, Aluminium electrodes were vacuum deposited on top of the a-Si:H layer by evaporation from a tungsten filament. The coplanar structure was obtained using a copper mask with two adjacent windows separated by a 0.5mm diameter wire defining the gap. For the I.B.M samples, the electrodes were in the form of Cr stripes 2mm apart underneath the silicon film. A silver "dag" conductive paint and a fine Al wire served to connect the sample to the external circuit. The contact thus formed was checked to be ohmic, and the current/voltage characteristics are shown in figure.4.1 (b). The two sample structures are shown in Fig.4.1 (a), and the details of the samples are summarised in Table.4.2.

Sample origin	I.B.M		DUNDEE	
Sample	Arsenic doped		P - 619	P - 272
Doping level	.05 As %	.01 As %	2 Vppm	3 Vppm
Deposition temperature	300 °C	300 °C	320 °C	295 °C
Growth rate	not avble	not avble	1.85 A°/s	1.85 A°/s
Plasma pressure	0.1 Torr	0.1 Torr	0.1 Torr	0.1 Torr
rf power	1.2 W	1.2 W	8 W	8 W (40 MHz)
Film thickness	1.2 μm	1.0 μm	0.7 μm	1 μm

Table 4.2. Details of the samples

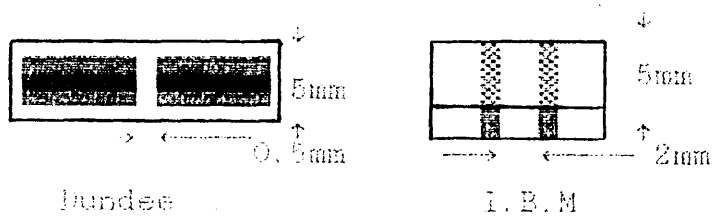

Figure.4.1 (a). Configuration of the samples

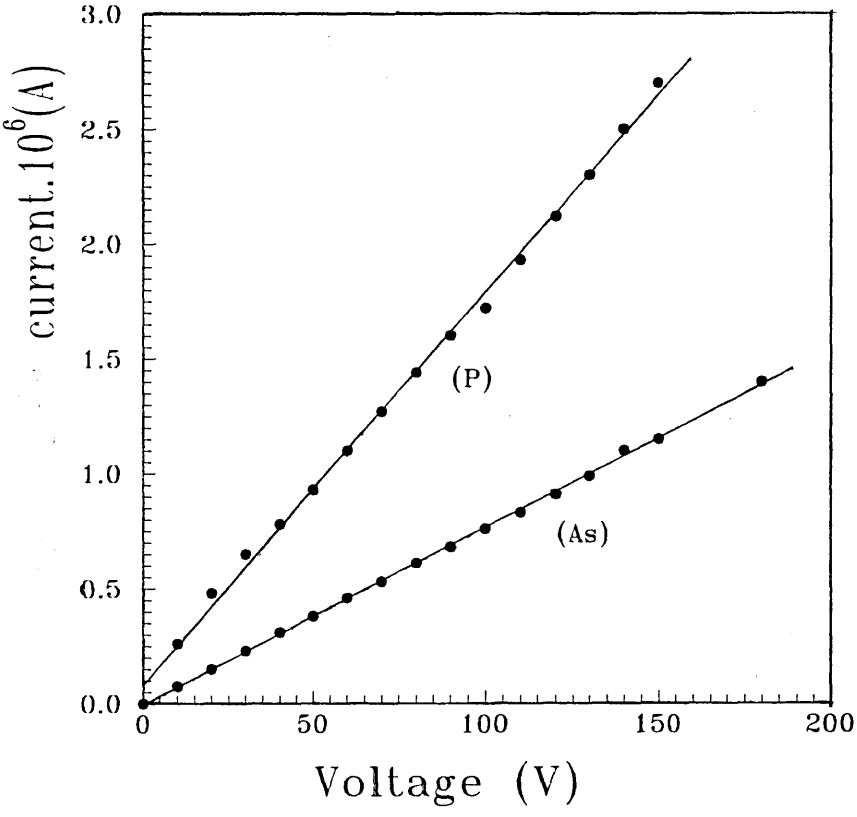

Figure.4.1 (b). Current/voltage characteristic of the samples

4.1.2. Dundee deposition system

As an example of a typical G-D capacitatively coupled preparation system, the Dundee deposition system is presented in Figure.4.2. The notation for the parts composing the apparatus is given below the figure.

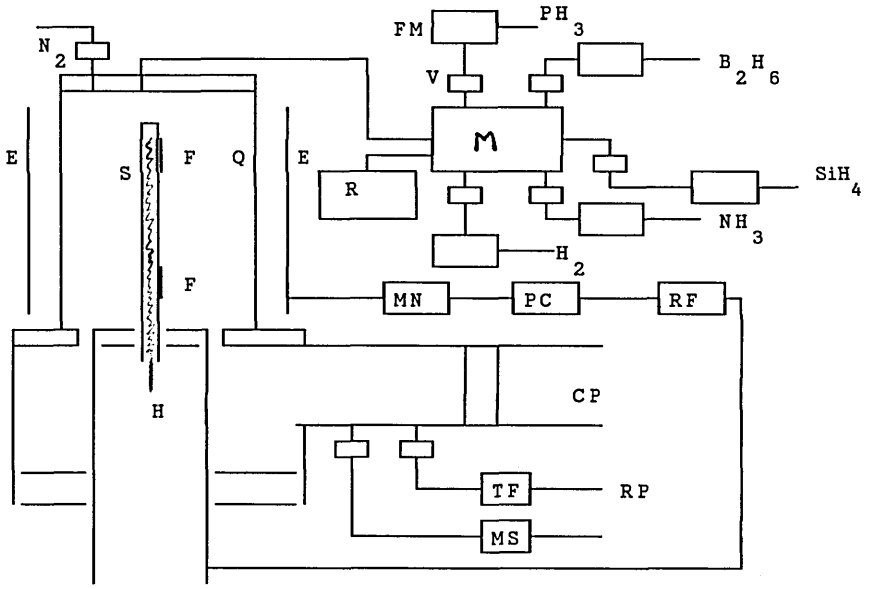

Figure.4.2. Dundee deposition system

Notation for Fig.4.2

S,H,F: Specimen holder mounted vertically with its heater, and rotatable Flaps for substrate shading.

Q: Demountable quartz enclosure.

E: Electrodes (capacity plates) adjusted parallel to S.

RF,PC,MN: Radio-frequency generators connected, through a power controller and a matching network, between E and S.

FM,V: Flow meters, and piezoelectric Valves for five gas channels

M,R: A chamber for mixing the five gases, and reservoirs for premixed gases.

N_2: Nitrogen flushing lines for operation safety.

CP,RP,TF: 3000 1/s cryopump producing high vacuum, and operating after a deposition run to reduce the previous run gas contamination, a rotary pump operating during deposition to maintain the gas flow, and a tubular furnace in front of RP to decompose the hydrides, preventing contamination of the pump oil.

MS: The mass spectrometer for examining the gas sample.

4.2. Characterisation techniques

The technique employed to characterise the different samples studied in this project was photoconductivity applied in three different regimes :

i).Steady state photocurrent (SSPC)

A constant photon-flux was directed on to the sample gap surface, and the generated photocurrent was directly read (see section 4.4) at a time much longer than the response time τ_r. The dark current was measured in the same way, and subtracted from the total current to obtain the net photocurrent.

ii).Transient photocurrent (TPC)

A light pulse of fixed magnitude and duration was directed on to the sample gap surface, and the generated photocurrent decay was detected and displayed (see section 4.4).

iii).Transient photocurrent with Optical Bias (OB)

Steady excitation was first applied, then the transient excitation was superimposed on the steady illumination. Figure.4.3 shows a schematic illustration of the three regimes.

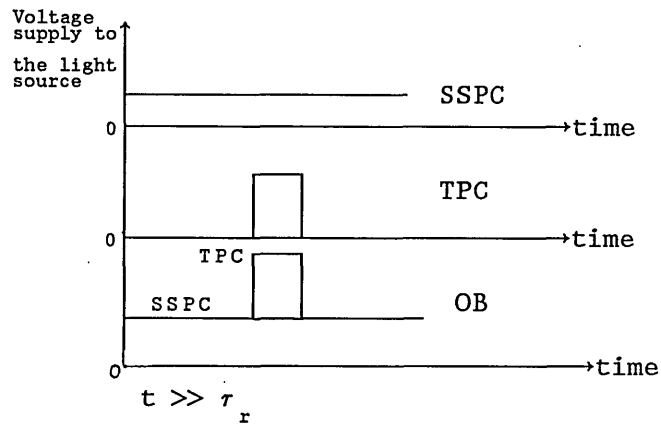

Figure.4.3. Schematic illustration of the photocurrent techniques employed in this work

4.3 Experimental Arrangement

An outline of the experiment set-up is presented in Figure.4.4. In the following, the main parts of the experimental arrangement are described.

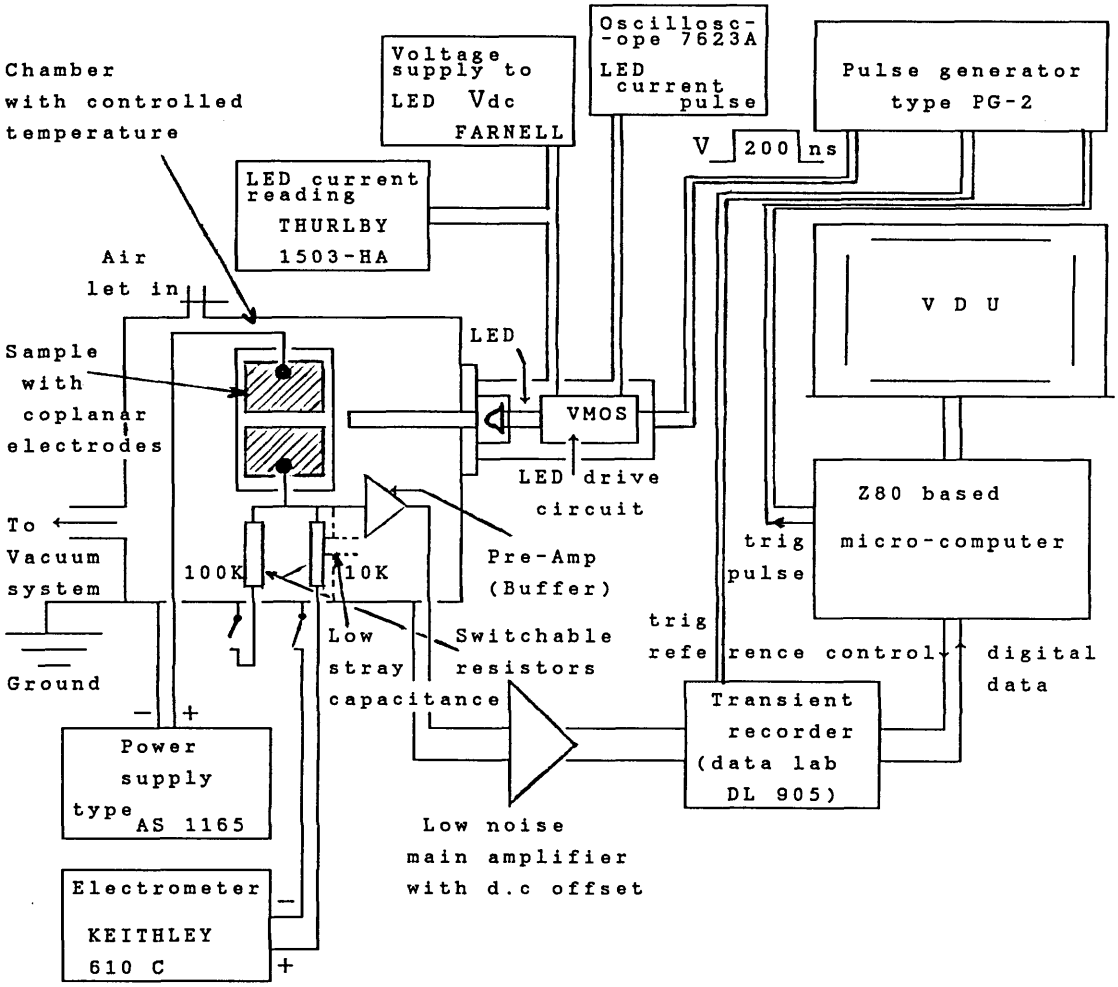

Figure 4.4. Experimental arrangement (LED as optical source).

4.3.1. Sample chamber and sample holder

Figure.4.5. shows the sample holder mounted in the vacuum chamber (system used in Dundee Institute of Technology): The sample was placed onto a brass block with electrical insulation by an interposed alumina plate. The brass block was vertically screwed onto a brass bobbin which holds a heater coil. This was also screwed onto a long copper bar "cold finger" through tubular washers of selectable size to control the cooling rate. Cooling down to 150K was obtained by

immersing the "cold finger" into liquid nitrogen. The temperature was monitored with a flat Thin film Pt-resistance sensor placed onto the alumina plate next to the sample, and controlled to ± 0.2 K by an Oxford instrument temperature controller (model 3120). The holder was vertically mounted in the chamber ,and a vacuum of 10^{-4}torr was established by diffusion and rotary pumps. Electrical connections to the external circuit were made by BNC vacuum lead-throughs.

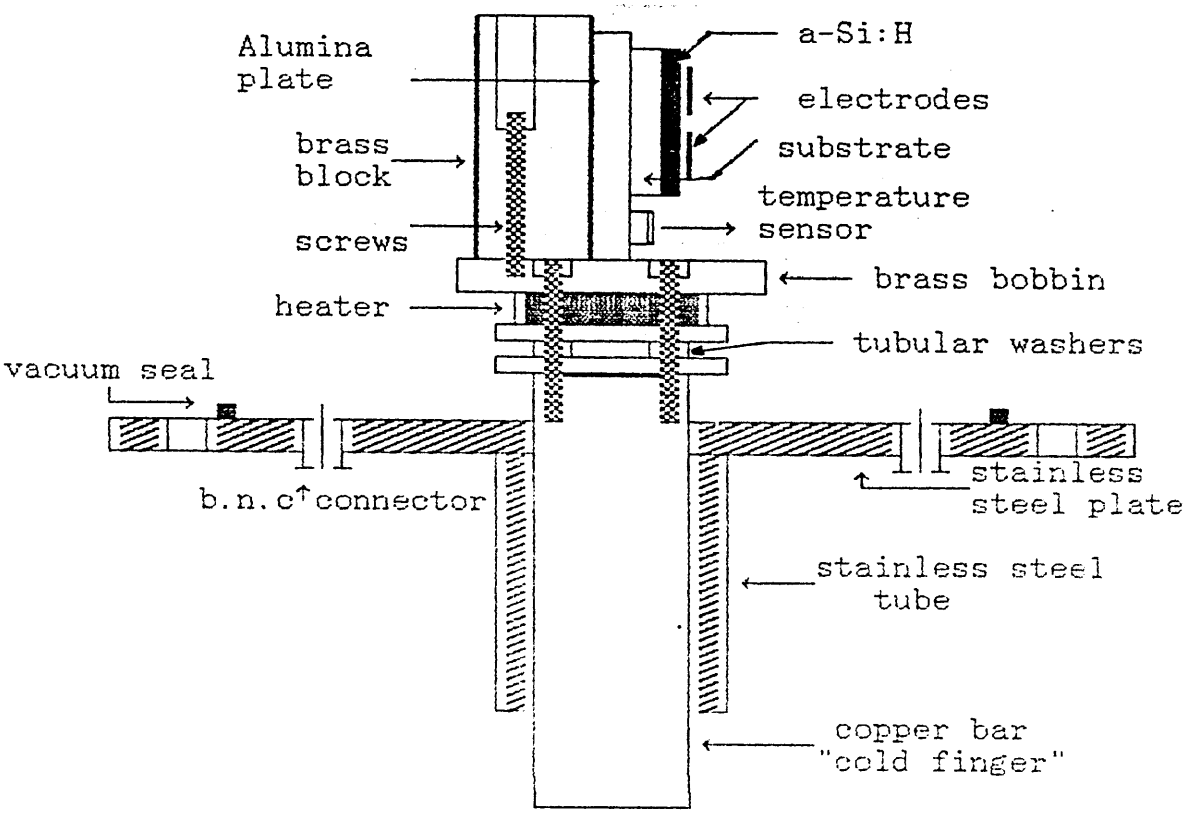

Figure.4.5. The sample holder

4.3.2 Optical sources

Depending on the experimental requirements, two different optical excitation sources were used.

4.3.2.1. Light emitting diode (LED).

A LED (Stanley type H 3000) which emits at a mean wavelength around 655nm (ie a photon energy of 1.89eV), giving reasonably uniform

absorption in a-Si:H, was used in most of the work for the three regimes of photoconductivity.

LED drive circuit.

The LED drive circuit is laid out in figure 4.6 . As can be seen, the LED is driven by a two stage VMOS switch to produce a current pulse of up to 8 Amps at a pulse width of 200 ns depending upon the input voltage pulse V, and the dc supply voltage V_{dc}. The LED d.c current, in the case of 'SSPC' or 'OB' measurements is varied by adjusting V_{dc} and/or the potentiometer P (with d.c switch on), and read on a digital multimeter (Thurlby) placed in series with the d.c voltage supply (Fig.4.4).

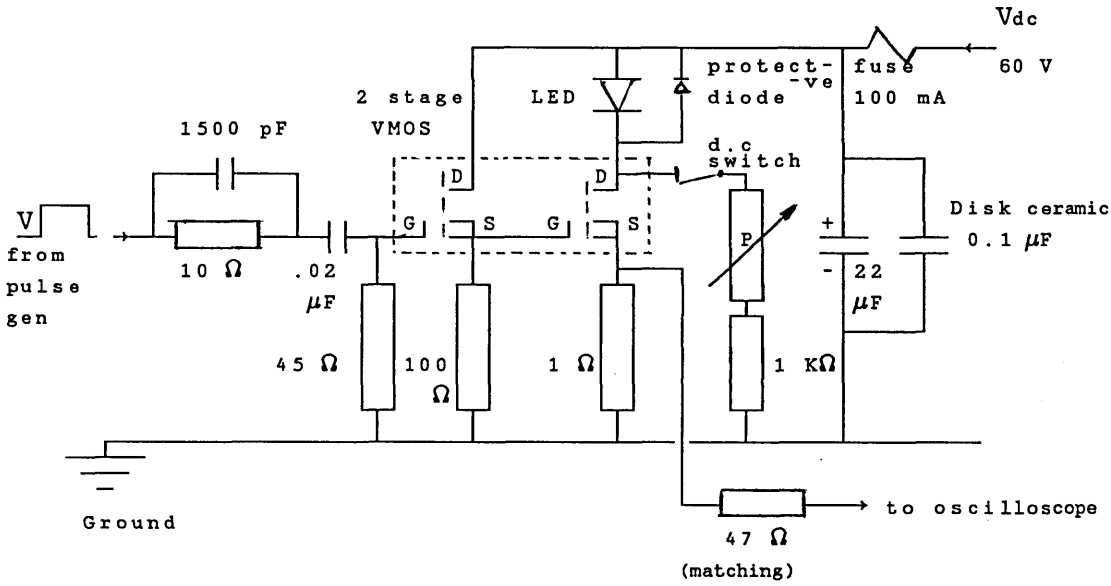

Figure.4.6. The dual-purpose (d.c and transient) LED drive circuit

It is worth noting that this circuit design produces a time response (rise and fall times) for the LED of $\simeq$40 ns, short enough to fit the experimental range of time.

LED calibration

A 0.2 mm^2 area fast pin photodiode (Hewlett-Packard, type 5082-4200 series, rise time 1ns) was used as a detector to calibrate the LED. Calibration of the photodiode sensitivity in terms of photodiode current to photon-flux (I_Φ/F) was necessary, and for this a

thermopile (Oriel type 7103) was used, of a known V/F calibration *viz* 1Volt≡9.3 W/cm^2 ≡3.07×10^{19} photons/s.cm^2 (λ=655nm), itself previously calibrated against a standard radiometer (Scientech model 362). The photodiode current to flux relation was found to be

$$F = (8.27).10^{20}\ I_{\Phi}\ (s^{-1}cm^{-2}) \qquad (4.1)$$

For c.w. calibration, the dc side of the LED supply circuit was used. The current output from the photodiode I_{Φ} was simply read on a Keithley 610C electrometer, whereas the LED current I_{LED} was monitored by a Thurlby digital multimeter 1503-HA inserted in series with the dc voltage supply. The position of the LED with respect to the photodiode was arranged in such a way as to give a maximum I_{Φ}. In the case of pulses, the pulse section of the VMOS circuit was used (with d.c switch 'off'), and I_{LED} was measured on an oscilloscope (Tektronix type 7623A) in storage mode.

Spatial distribution of the LED light beam

The light was guided to the sample through a quartz pipe with polished flat ends, of diameter 7 mm, ending about 1 mm above the sample gap. Although the whole gap was illuminated, the beam intensity was not distributed uniformly. An overestimate of the LED calibration had thus been made by measuring the maximum I_{Φ} rather than an average photodiode current $I_{\Phi av}$. Figure.4.7 (a) illustrates the procedure for the correction of this error; assuming axial symmetry, half of the distribution was measured by scanning the photodiode across the radius of the pipe section starting from the central position of the maximum I_{Φ}. Assuming also that the beam was uniformly normal to the gap surface, $I_{\Phi av}$ was determined by equating the distribution area to a rectangular area as wide as the gap length and centered at I_{Φ}. $I_{\Phi av}$ had then to be equal to the height of the averaging area. The correction factor was consequently defined as, $c = I_{\Phi av}/I_{\Phi}$ (Table.4.3) and the calibration relation was corrected to

$$F_c = (8.27).10^{20}.I_{\Phi}.c\ (s^{-1}cm^{-2}) \qquad (4.2)$$

LED calibration result

The LED calibration (I_{LED}/F) is shown in figure.4.7 (b). As can be seen, below 20 mA the plot in the logarithmic scale shows some curvature towards lower photon fluxes, (i.e. superlinear) whereas above 20 mA dc and up to current *pulses* of the order of 4 Amps the photon flux increases linearly with the LED current.

In the transient case, the light output or the number of emitted photons N_ϕ in one pulse per cm^2 was also measured.

$$N_\Phi = (8.27).10^{20}.c.I_m.t \ (cm^{-2}) \qquad (4.3)$$

t is the pulse width ($\simeq$ 200ns) and I_m=6 mA the photodiode signal current measured on the oscilloscope as a result of I_{LED}=4A.

Taking account of a reflection coefficient R≈0.3, and assuming a quantum efficiency η=1, The pulsed electron density was determined as,

$$N_e = N_\Phi.(1-R).\eta.\alpha \ (cm^{-3}) \qquad (4.4)$$

The absorption coefficient α was calculated after measuring the transmission T (the ratio of the I_{LED} through the substrate,glass and film, to I_{LED} through the glass) at the particular wavelength (655nm) of the LED.

$$\alpha = (1/d).\log(\frac{1-R}{T}) \ \ (cm^{-1}) \qquad (4.5)$$

4.3.2.2. Dye Laser

The response to high excitation in the transient regime was examined by the use of high intensity short duration pulses from a nitrogen pumped dye laser (Laser Science type 337 with sealed nitrogen pump and dye type Rhodamine 101) emitting coherent light in the red region at a photon energy of 1.91 eV .

Figure.4.7. (a)
Spatial distribution of the LED beam intensity across diameter of the light guide.

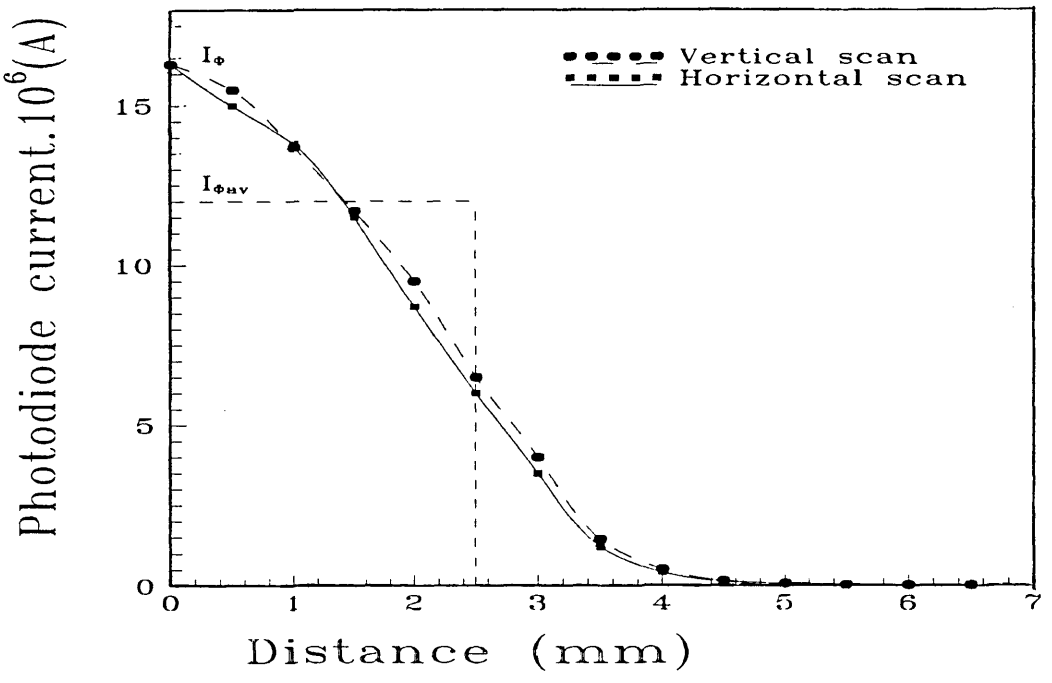

Figure.4.7. (b)
Calibration of the LED (I_{LED}/F)

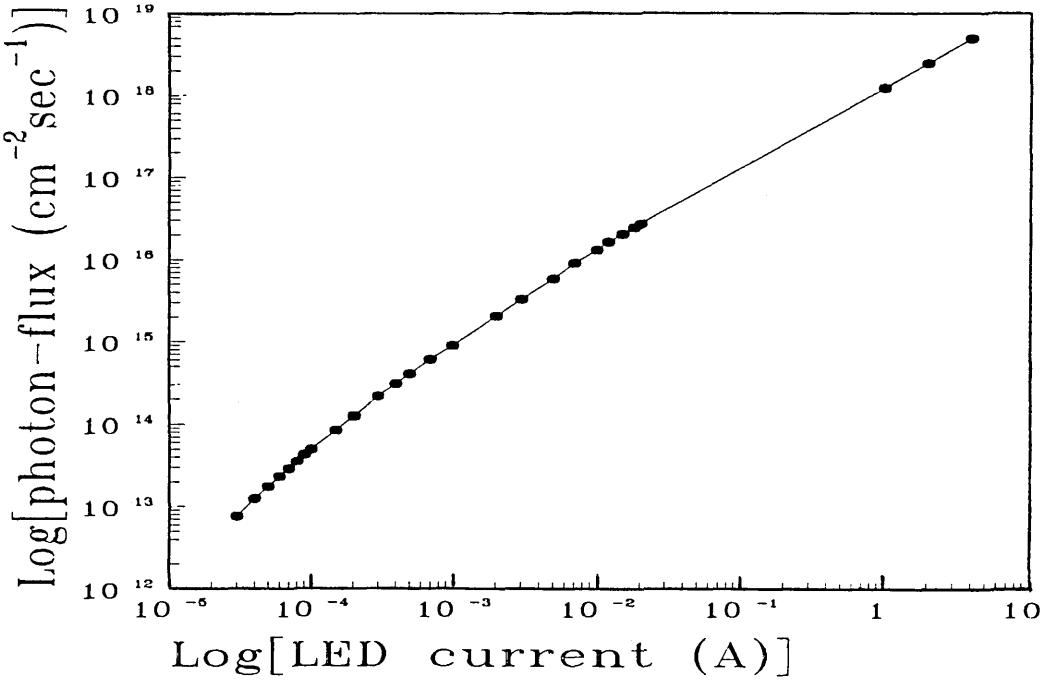

Measurement of the light output

The laser source was kept outside the chamber at a distance of 40 cm from the specimen gap which was oriented horizontally and perpendicular to the beam. The beam reached the specimen through a quartz window on the chamber side facing the source, and was seen as a rectangular bar across the gap (Figure.4.8 (a)). The same distance (40cm) was fixed, for calibration, between the laser aperture and the pin photodiode detector while measuring the spatial distribution of the laser beam intensity (Figure.4.8 (b)). An attenuation by means of neutral density filters by a factor $A_t=10^{-4}$ was necessary to avoid saturation of the photodiode. The current pulse displayed on the oscilloscope showed a time distribution of the beam intensity which was Gaussian in shape. The pulse duration corresponding to the width at half height of the pulse was $t \simeq 5ns$.

In contrast to the case of the LED, the spatial distribution of the laser source (Fig.4.8. (b)) was so sharp that only part of the gap length (l_{eff}) was effectively illuminated. This effective length was approximated by the width of the distribution at the point where it starts to rise sharply ($l_{eff} \simeq 2$ mm). The photodiode current was then spatially averaged over l_{eff} in the same way that was applied to the LED; the average current I_{mav} was taken to be the height of a rectangle centered at the distribution peak I_m, and having width l_{eff}. The whole distribution was scanned and shows an axial symmetry of the beam. The laser output, ie the number of emitted photons in one pulse per cm^2 is then given by

$$N_\Phi = A_t^{-1}.(8.27).10^{20}.t.c.I_m \quad (cm^{-2}) \tag{4.6}$$

where c is the averaging factor given by $c = I_{mav}/I_m$ (Table.4.3). The electron density generated by one pulse is .

$$N_e = N_\Phi.(1-R).\eta.\alpha \quad (cm^{-3}) \tag{4.7}$$

The results of the procedure above described for both sample types and both light sources are summarised in table.4.3 below,

			Dundee	I.B.M
			$\alpha = (1.8).10^{4} cm^{-1}$	$\alpha = (1.2).10^{4} cm^{-1}$
	c	N_Φ (cm^{-2})	N_e (cm^{-3})	N_e (cm^{-3})
LED	0.74	$(6.07).10^{11}$	$(9.2).10^{15}$	6.10^{15}
Laser	0.62	$(1.82).10^{14}$	$(2.5).10^{18}$	$(1.67).10^{18}$

Table.4.3. Estimated photon-flux N_Φ in the light pulse and electron density N_e generated by this pulse.

4.3.2.3. Combination of two sources in the OB regime

The OB regime of the photocurrent was measured by two complementary methods:

i).Using the LED with a fixed pulse defined by N_Φ in table.4.3, and applying a range of steady state dc bias (I_{LED}= 100 μA to 20 mA, giving F = $5x10^{13}$- $2.73x10^{16} cm^{-2}s^{-1}$).

ii).Using two laser sources; A source for the transient pulse, which was a N_2-pumped dye laser (Rh6G), similar to that used in the non biased transient regime, producing pulses of photon energy 1.88 eV and duration 10 ns, resulting in an estimated maximum electron density, $N_e \simeq (4.2).10^{17} cm^{-3}$, varied by attenuation from neutral density filters down to 32 % N_e, and a cw biasing source which was a He-Ne laser of a fixed photon-flux F = 25 mW/cm^2.

The first method was carried out in the D.I.T. laboratory on both types of sample using the single source (LED) dual purpose (dc and pulse) circuit detailed above. The second method was achieved at Odense University by I.K.Kristensen in collaborative work (Main et al, 1990) on the 0.01 % Arsenic-doped sample.

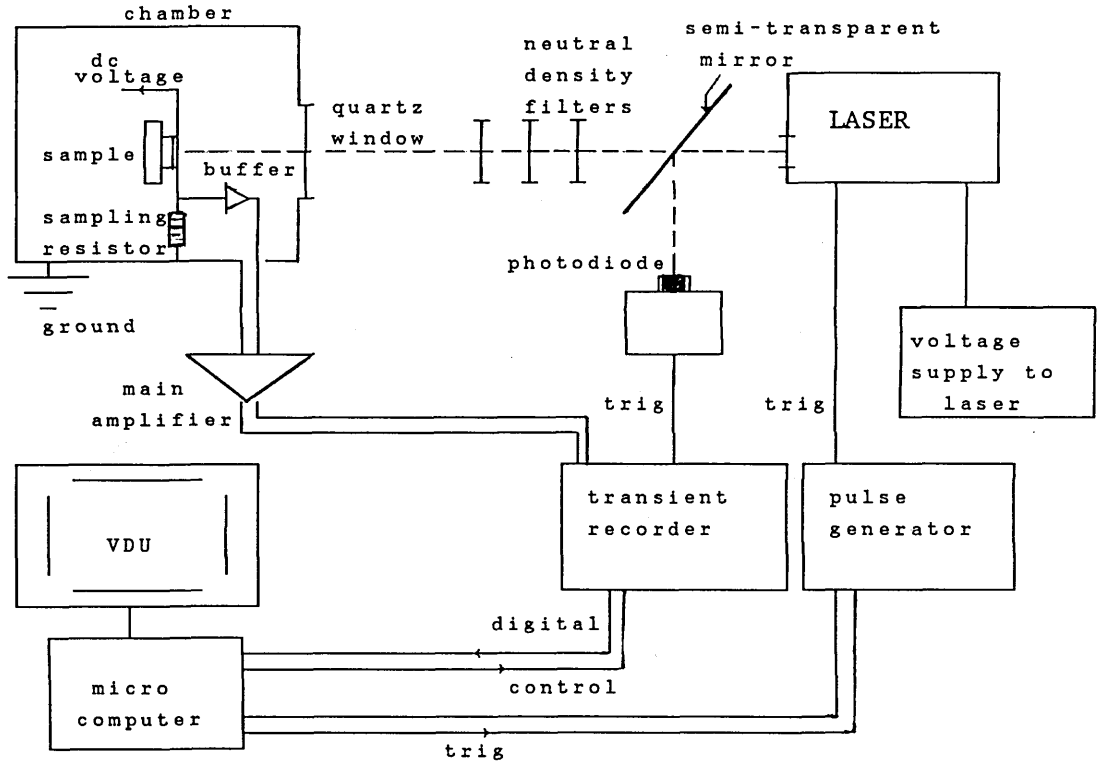

Figure.4.8 (a). Laser characterisation method

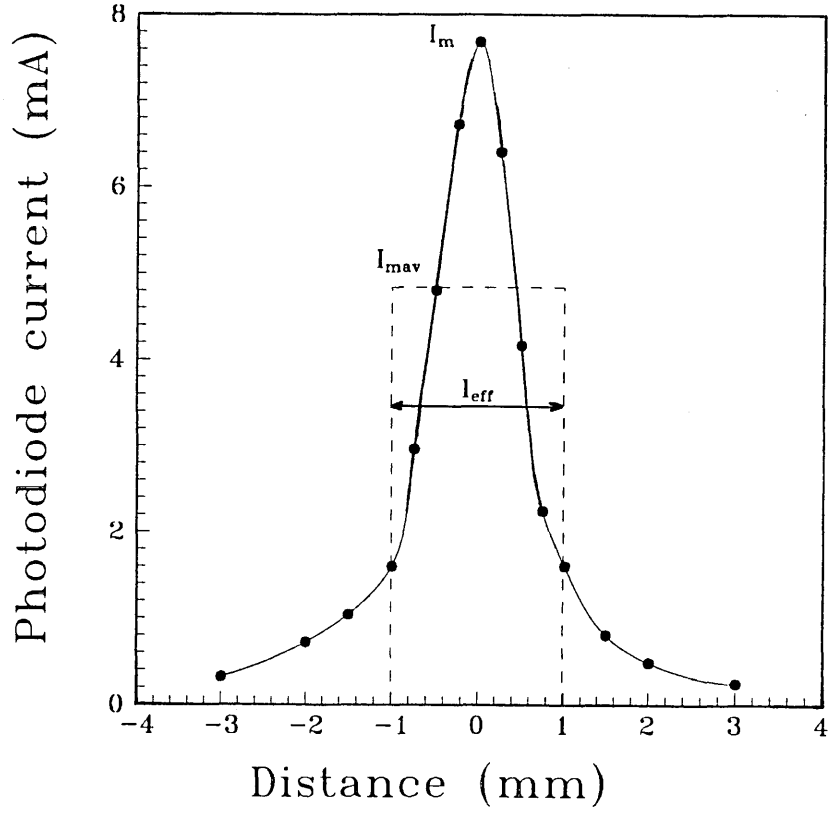

Figure.4.8 (b). Spatial distribution of the laser beam intensity

4.3.3. Current detection and sensitivity

4.3.3.1. Dark current and Steady state photocurrent

The Keithley model 610C electrometer was used in the 'fast' mode to measure the dark current and SSPC via the 10 KΩ resistor, bypassing the FET buffer amplifier (see fig.4.4). Voltages in the range 100 to 150 Volts were applied across the sample gap from a power supply (Solartron type AS 1165) . In the SSPC case, the calibrated LED was used in the dc mode with the light intensity being varied by adjustment of the potentiometer and/or the dc voltage as stated above in the 'OB regime' case.

4.3.3.2.Transient photocurrent (TPC regime)

In standard systems, a sampling resistor r_s of a chosen value placed in series with the sample is used for transient photocurrent detection (see Figure.4.9): The light pulse induced photocurrent decay is monitored by measuring the resulting voltage across the sample resistor by direct connection to an oscilloscope of high input impedance.

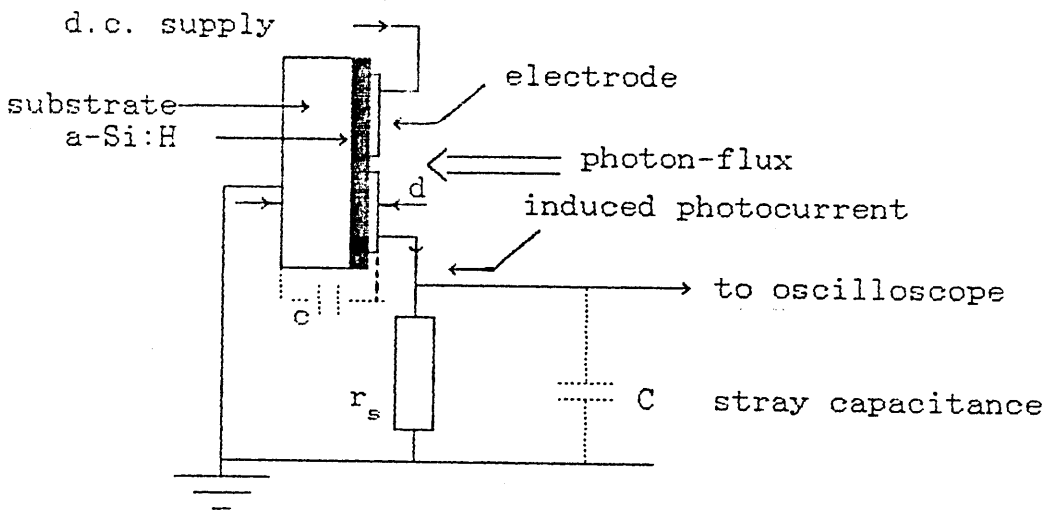

Figure.4.9. Standard transient photocurrent detection system planar structure.

To observe the transient response at short times, r_s must be low to reduce the time constant (the response time) of the system,

$$\tau = r_s.(c + C) \qquad (4.8)$$

where c is the capacitance due to the sample geometry. In the present work, c represents the capacitance between the Al electrode and the grounded brass block, and it can be calculated by considering the Alumina plate and the glass substrate as two adjacent dielectrics (see Fig.4.5).

$$c = \epsilon_o.S.\ [(d_1/\epsilon_{r1}) + (d_2/\epsilon_{r2})\ ]^{-1} \qquad (4.9)$$

where $\epsilon_o \simeq 9.10^{-12}$ F/m is the free space permittivity, $\epsilon_{r1} \simeq 5$ and $\epsilon_{r2} = 8$ are the relative permittivities of the glass and the alumina respectively, $d_1 = 0.82$mm and $d_2 = 0.98$mm are the thicknesses of the substrate and the plate respectively, and $S \simeq (8x5)mm^2$ is the typical electrode area. With these parameter values c is only 1.3pF. C is a stray capacitance mainly due to the coaxial cable which transfers the signal to the oscilloscope (a typical figure for this is 100 pF per meter cable).

In these conditions, to observe the signal at times longer than 100 ns, r_s must have an upper limit of 1 KΩ. Reducing r_s solves the response time problem, but at the expense of the response sensitivity. This is a problem, particularly at low temperatures, low pulse excitation and/or long decay times where the signal is overcome by background noise. The method used in this work (described below) has the advantage over such systems by reducing τ through reduction of C itself rather than r, thus keeping r high enough to produce a high signal to noise ratio (ie sensitivity). The new modification consists of (see Figure.4.10).

i).interposing a low input capacitance pre-amplifier of a unity gain within the vacuum chamber as a buffer.

ii).neutralising the stray capacitance of the signal lead between the sample and the buffer by using a screening lead driven by the output of the unity gain buffer, which equates its ac potential to that of the signal lead. The remaining stray capacitance between the screening lead and the ground has a very small effect on the time

constant of the circuit. The coaxial cable and signal lead to the oscilloscope were connected to the buffer output, which has a small output resistance of 10 Ω, giving a fairly short time constant (1ns for 1m cable).

iii).using two switchable sampling resistors: A resistor of 10 KΩ for short times ($t \leq 10\mu s$) in order to exploit the reduction of τ, and a higher resistor (100 KΩ) for longer times to increase the sensitivity. Even at short times the 10 KΩ resistor was high enough to allow currents as low as 10^{-10} A to be detected (see chapter 6, section.6.A).

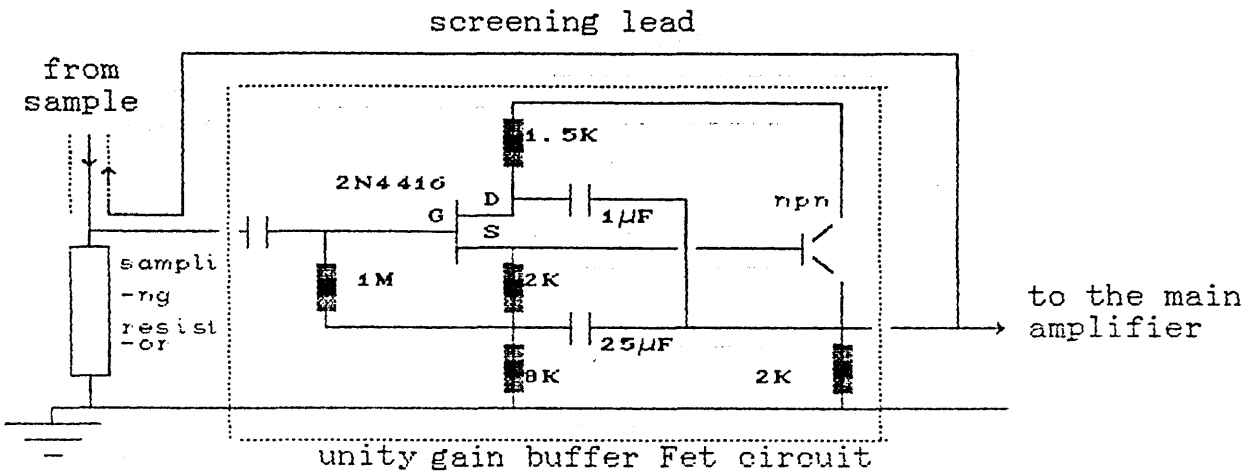

Figure.4.10. "Buffer and bootstrapped lead" method to reduce the stray capacitance

Hence the buffer amplifier provides a combination of short response time and high sensitivity for transient photocurrent measurements. However, it introduces a dc off-set to the monitoring circuit. Therefore, the main signal amplifier following the buffer was equipped with a dc off-set adjustment to compensate the introduced off-set. The main amplifier was a low noise two stage amplifier with voltage gains 10 and 100, employing two low noise operational amplifiers (Burr-Brown type OPA37) . The response time of the system (corresponding to 63 % rise time) and the gains without the main amplifier, with the times 10 stage, and with the times 100 stage were measured for both sampling resistors using a small voltage pulse from a resistor source of 50Ω in series with the sampling resistor (figure.4.11). Results are shown in table.4.4.

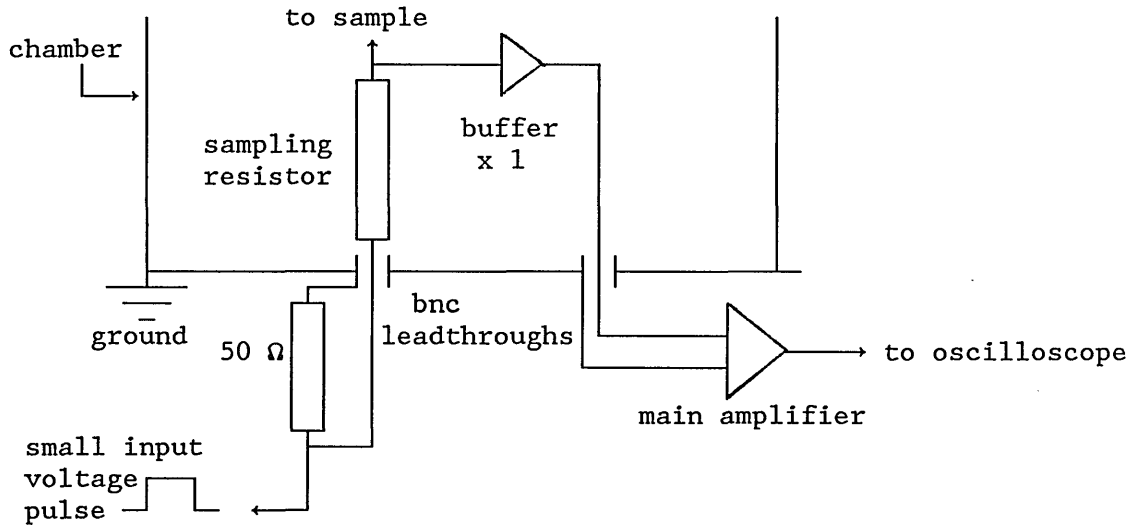

Figure.4.11 .Time response measurement method

Samp Resistor	Main Amplifier	Gain	Resp time
10 KΩ	without main Ampl (buffer only)	0.92	30 nsec
100 K			700 nsec
10 KΩ	with the times 10 stage	9.5	60 nsec
100 K			700 nsec
10 KΩ	with the times 100 stage	95	100 nsec
100 K			700 nsec

Table 4.4. Measured gain and response time of the detection system

As can be seen from the table, the buffer gain was less than unity, leading to a slight reduction (5 %) of the total gain at the output of the main amplifier; also, introduction of the main amplifier led to an increase of τ from 30ns to 60ns and 100ns when the 10 KΩ resistor was used in short time measurements. However, the time resolution of the transient recorder employed (see below) was 200ns, well above the response time and equal to the pulse width to allow detection of the photocurrent due to the whole pulse. The total stray capacitance with the 10 KΩ resistor in place is only $\simeq$ 3 pF, i.e. typically $\simeq$ 33 times smaller than in the standard unbuffered systems.

4.3.3.3. Transient signal digitising and processing

Having been amplified, the signal was fed into an 8 bit transient recorder (Datalab model DL905) whose sweep time could be altered between 0.2ms and 10s. The number of samples taken per sweep was 1024, and therefore the minimum time resolution was 200ns. The TPC decay was normally measured from 200ns to 5s after the light pulse. This time range could be covered by three sweeps (mostly 0.2ms ,50ms and 5s) resulting in three overlapping portions of the decay.

The transient measurement was controlled by a Z80 based micro-computer. The control program allowed control of the number of pulses used and the inter-pulse pause time, and performed digital filtering. In addition, a multichannal averaging function was performed. In a transient run the signal was aquired and processed as follows (see fig.4.4).

i)-The micro-computer triggers the pulse generator, and the latter pulses the LED and the transient recorder simultaniously.

ii)-The transient recorder takes 824 voltage measurements over the sweep time and places 200 pretrig measurements in front of the 824. It averages these 200 points to give the background dc level which forms the baseline of the TPC decay .

iii)-The digitised data are fed to the micro-computer, where they are smoothed using the technique of variable band-width digital filtering. This technique is favoured since it smooths the data more as the sweep time increases and the signal gets smaller and noisier .

vi)-After a pre-set time, the process is repeated until the required number of sweeps has been taken. The sweeps are then averaged on a multichannel basis and the voltages converted into currents.

v)-The TPC data are then displayed graphically on the VDU. These could be stored on floppy disks.

Two checks were necessary, to avoid spurious effects:

i)-The TPC decay should be independent of the voltage polarity applied to the sample.

ii)-The inter-sweep pause should exceed a critical value comparable to the overall relaxation time of the carriers after the pulse, particularly at long sweep times and/or low temperatures. In either case, sufficient time between sweeps is required for the sample to relax sufficiently closely to thermal equilibrium.

4.4. Measurement summary

4.4.1. Measured quantities

The main measured parameter throughout the work was the photocurrent (I_{pc}), but other parameters were varied in the measurements depending on the technique in use.

In the basic SSPC method, the variables were the temperature (T) and the generation rate (G). Therefore, the dependences of I_{SSPC} on T and G were measured. Additionally, the temperature dependence of the dark current (I_d) had to be measured since it represents the thermal equilibrium "reference" for the SSPC I_{pc}.

In the TPC regime, the time (t) was introduced as another variable, thus leading to the necessity of measuring the dependence on t of the transient photocurrent (I_{TPC}). For example, if it was possible to identify, at a particular time, the occurrence of an important feature in the decay, then the temperature and excitation (N_e) dependences of the feature were measured. In the OB regime, the steady state optical bias photocurrent I_{SSPC} (ie the OB level) was used as a varible depending on which I_{TPC} was measured. Temperature and excitation dependences were also measured at a fixed OB level.

Control of the quasi-Fermi level (QFL) E_{Fn} was possible by adjustment of the OB level and the temperature. Thus the effect of E_{Fn} position on the temperature dependence of I_{TPC} was measured.

4.4.2. Experimental problems

The major unavoidable experimental difficulty was the effect of light exposure during the measurement (Staebler-Wronski effect) (Steabler and Wronski, 1977). This could only be minimised by careful measurements :

i).reducing as much as possible the time of exposure while reading the SSPC current, and the time between two consecutive readings.

ii).reannealing The sample (420 K for 1hr) after a complete set of measurements at various temperatures. It was assumed that light exposure had a small effect as long as the dark current I_d (checked at different temperatures while measuring the I_{SSPC}) lay on a previously measured I_d versus 1/T curve.

CHAPTER.5

THEORY AND MODELS

As an extension to the models and theories developed in previous studies related to this work, some analysis and models developed in this project will be presented in this chapter to underpin the observed results that will be presented in chapter.6. The chapter is divided into two sections: A -the transient regime and B -the steady state regime. The optically biased transient case will be treated in the transient regime section A as a transient modulated by the steady state, in a linear superposition approach, rather than a transient perturbation introduced to the steady state regime (Schiff, 1985).

5.A. The Transient Regime

5.A.1 Recombination free transport

The early treatment of the TPC decay after pulse generation of the carriers in amorphous semiconductors by Tiedje and Rose (1980) , and Orenstein and Kastner (1981) , known as the TROK model, considered essentially within a linear approach, the "small signal" case in which a small excess packet of charge thermalises in an exponential tail of "empty" states. This approach ignores the possibility of the tail states' prior thermal equilibrium (or steady state) occupancy, and it avoids also the possibility of the excess packet saturating the tail states on top of the steady state distribution.

Saturation of the tail states was first approached by Schiff (1981) who postulated a time dependent occupation function to describe the thermalising carrier packet,

$$f_d(E,t) = F(t).\ \frac{1}{1 + \exp\left(\frac{E - E_d}{k.T}\right)} \qquad (5.A.1)$$

with $E_d(t)$, a time dependent quasi-Fermi level which represents the demarcation level of the packet given by equation.2.9.16 and F(t), an occupancy function (independent of energy) whose significance is the occupation below E_d ($E >> E_d$). This approach also ignored the pre-existing thermal equilibrium (or steady state) distribution.

The "large signal" case taking account of both the steady state occupation and the possibility of tail states' saturation was first treated by Kristensen and Hvan (1984) and further developed, in collaboration with Kristensen, in this project (Main et al, 1990). Here the effects of equilibrium or steady state occupation on the availability of tail states for thermalisation are included. Hence the problem becomes that of a pulsed excess electron density thermalising in an "effective" distribution of tail states g'(E,T) which represents the available empty states after the steady occupation has been subtracted. For this, a major assumption was made, that the thermal equilibrium (or steady state in the case of the optical bias regime) occupancy is considered to be "frozen" over the time scale of the thermalisation.

$$g'(E,T) = g(E)\ [1 - f_t(E,T)\ ] \quad (cm^{-3}eV^{-1}) \qquad (5.A.2)$$

where g(E) is the total density of states (DOS) assumed to be exponentially distributed in the first instance (Eqn.2.9.12) and $f_t(E,T)$ is the trapped electron occupation function (Eqn.2.9.8). In the following, the mobility edge E_c will be taken as an energy reference and energies below E_c are negative.

5.A.1.a. Distribution of the thermalising excess electron packet

The thermalising excess electron density $\delta n(E,T,t)$ can be determined by attributing to the transient regime a Fermi distribution f_d similar to that given by Eqn.5.A.1. δn will then be given by,

$$\delta n(E,T,t) = g'(E,T)\ .\ f_d(E,T,t) \quad (cm^{-3}eV^{-1}) \qquad (5.A.3)$$

and the integrated volume density N_e is

$$N_e = \int_{-\infty}^{+\infty} \delta n(E,T,t)\ dE \quad (cm^{-3}) \qquad (5.A.4)$$

N_e is, in practice, the pulsed excess electron density given by equation 4.7, and should be constant in the absence of recombination. After substitution from Eqns 5.A.1, 2 and 3 and calculation (see Appendix), the following expression is obtained for N_e,

$$N_e = \frac{F(t).N_{fnt}}{1- \exp \frac{E_{fnt}-E_d}{k.T}} .\{ (1+r).[\exp \frac{E_d-E_{fnt}}{K .T_c} - 1]$$

$$+ r.[\exp \frac{E_d-E_{fnt}}{k.T_c} .\exp \frac{E_{fnt}-E_d}{k.T} - 1] \} \qquad (5.A.6)$$

where $\alpha_c = (T/T_c) < 1$ is the dispersion coefficient of the conduction band tail (CBT), and N_{fnt}, the SSPC trapped density below the trapped electron quasi-Fermi level E_{fnt}, is given by

$$N_{fnt} = \int_{-\infty}^{+\infty} g(E) \; . \; f_t(E,T) \; dE$$

$$= \frac{1}{1+r} .k.T_c.G_c .\frac{\pi.\alpha_c}{\sin(\pi.\alpha_c)} .\exp(\frac{E_{fnt}}{k.T_c}) \qquad (5.A.8)$$

The parameter r (see Eqn.2.9.9) is related to the steady state occupancy of deep states below E_{fnt} as described by Simmons and Taylor (1971).

For group V impurity-doped samples, n is much higher than p, and therefore the parameter r will tend to zero (particularly in the dark or low biased transient regime). In such a case, E_{fnt} coincides with the free electron QFL, E_{fn} (or the dark Fermi level in the non biased transient regime) (see Eqn.2.9.11), and f_t coincides with the free electron Fermi occupation function f_n. N_{fnt} will be written now as N_{fn} and the expression of N_e (excess electron packet density) given by Eqn.5.A.6 will reduce to

$$N_e = F(t).N_{fn}.\frac{1 -\exp [(E_d - E_{fn})/k.T_c]}{\exp [(E_{fn} - E_d)/k.T] - 1} \qquad (5.A.9)$$

The effective density of states has the following energy and temperature dependence (see Fig. 5.A.1),

$$g'(E,T) = G_c.\exp(E/k.T_c) \; .\frac{1}{1 + \exp(\frac{E_{fn}-E}{k.T})} \qquad (5.A.10a)$$

This gives,

$$g'(E) = g(E), \qquad \text{for } E >> E_{Fn} \qquad (5.A.10b)$$

$$g'(E_{fn}) = 1/2.g(E_{fn}) \qquad (5.A.10c)$$

$$g'(E,T) = G_c.\exp(-E_{fn}/k.T).\exp(E/k.T'_c), \quad \text{for } E<<E_{fn} \qquad (5.A.10d)$$

Figure.5.A.1
The available density of states for electron thermalisation in the CBT for two positions of the QFL E_{fn}.
The total CBT DOS is also shown for T_c=470 K.

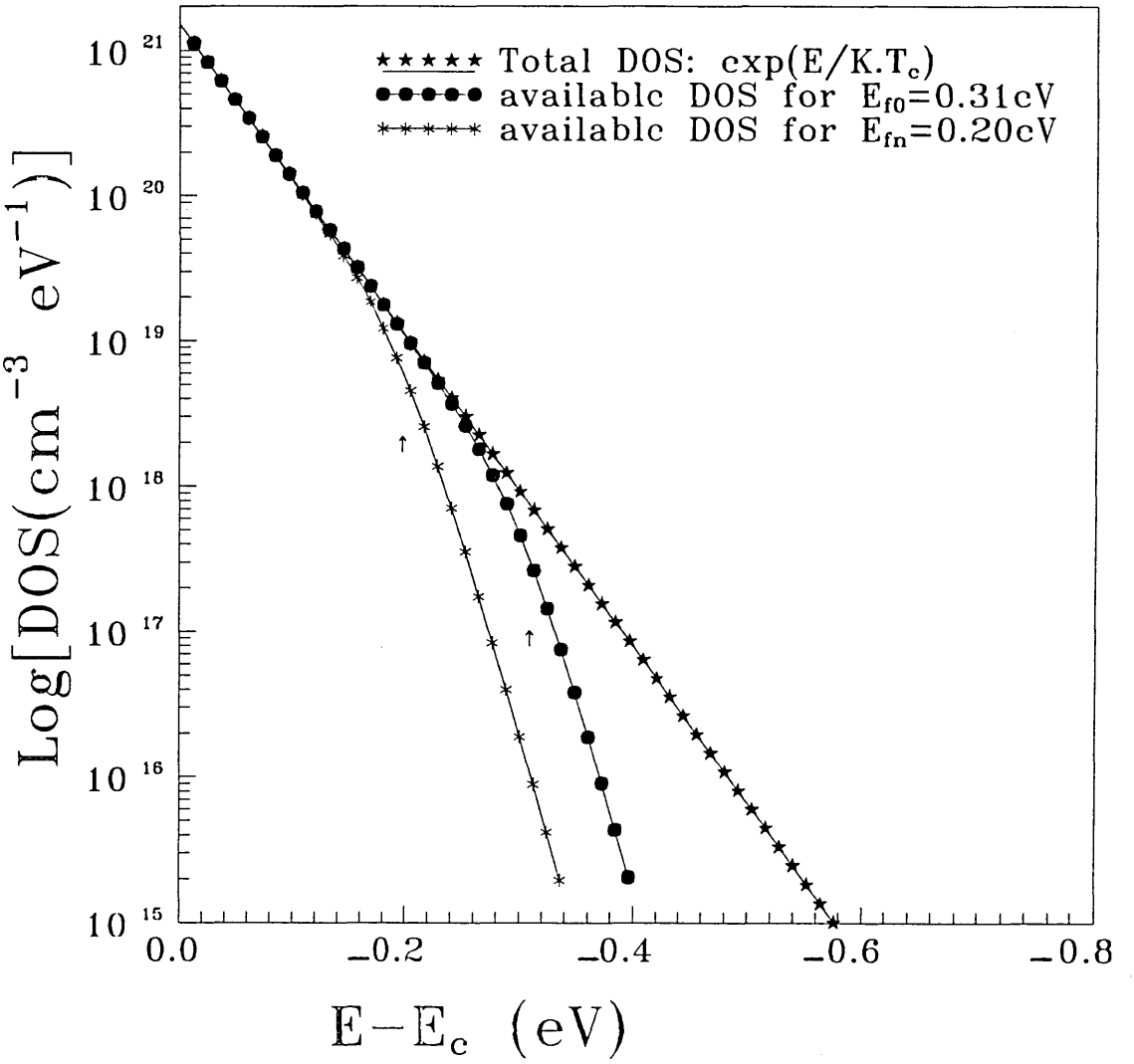

The last of these equations shows that below E_{fn}, g'(E,T) falls exponentially more sharply than above E_{fn} with a characteristic temperature $T'_c = T.T_c/(T+T_c)$ which is always less than the measurement temperature T. This fact implies that in the case of low pulse excitations the excess electron packet resides mainly around E_{fn} at complete thermalisation (Fig.5.A.2.b) although, as will be seen later, E_d can still "sink" below E_{fn} (Kristensen and Hvan, 1988).

In the thermalisation process, the time t (before any recombination to deep states) can be associated with the electron release from the tail traps at E_d as this advances towards deep states. If t_0 is the time by which E_d reaches E_{fn} then,

$$E_{fn} = E_d(t_o) = - k.T.\log(\nu.t_0) \qquad (5.A.11)$$

Replacing E_d and E_{fn} by their time values (Eqn.5.A.11) into equation.5.A.9, one obtains the following time expression for the occupation below E_d,

$$F(t)=(N_e/N_{fn}).\frac{(t/t_0) - 1}{1 - (t_0/t)^{\alpha_c}} \qquad (5.A.12)$$

with the asymptotic values,

$F(t) \simeq (N_e/N_{fn}).(t/t_0)^{\alpha_c}$ for $t \ll t_0$ i.e. $(E_d \gg E_{fn})$

$F(t_0) = (N_e/N_{fn}).\alpha_c^{-1}$ $(E_d = E_{fn})$, and

$F(t) \simeq (N_e/N_{fn}).(t/t_0)$ for $t \gg t_0$ i.e. $(E_d \ll E_{fn})$

(The value of F at t_0 i.e. $F(t_0)$ needs L'Hopital's rule).

Returning to the energy distribution f_d of the thermalising excess electron packet (Eqn.5.A.1), the effect of the steady state occupation (ie the change in the sharpness of the available density of states) on the evolution of the packet during the course of thermalisation can be understood in terms of time and energy (fig.5.A.2a) as follows:

Before E_d reaches E_{fn}, the packet density δn is such that, above E_d $(E \gg E_d)$, the occupation follows Boltzmann statistics and decreases with time as $t^{\alpha_c - 1}$,

$$f_d \simeq (N_e/N_l).(\nu.t)^{\alpha_c - 1}.\exp(-E/k.T), \qquad (E \gg E_d) \qquad (5.A.13)$$

Figure.5.A.2
Calculated $f_d(E)$ at three different times for the pulsed electron density $N_e=10^{12}/cm^3$, $T_c=470$ K and $E_{f0}=-0.31$ eV.

(a)

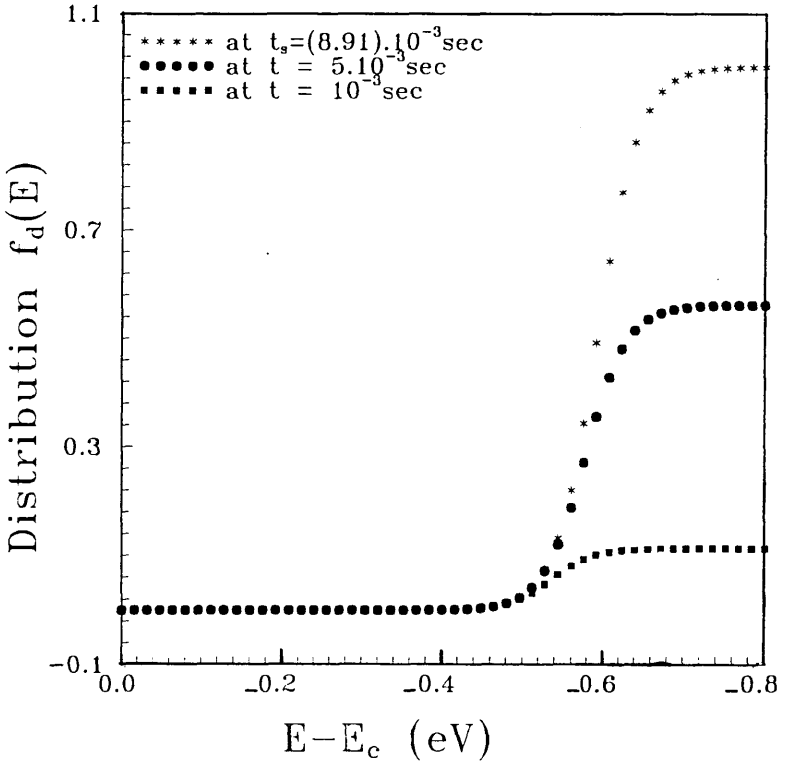

Calculated $\delta n(E)$ at the indicated times for the pulsed electron density $N_e=10^{12}$ cm^{-3}, $T_c=470$ K and $E_{f0}=-0.31$ eV.

(b)

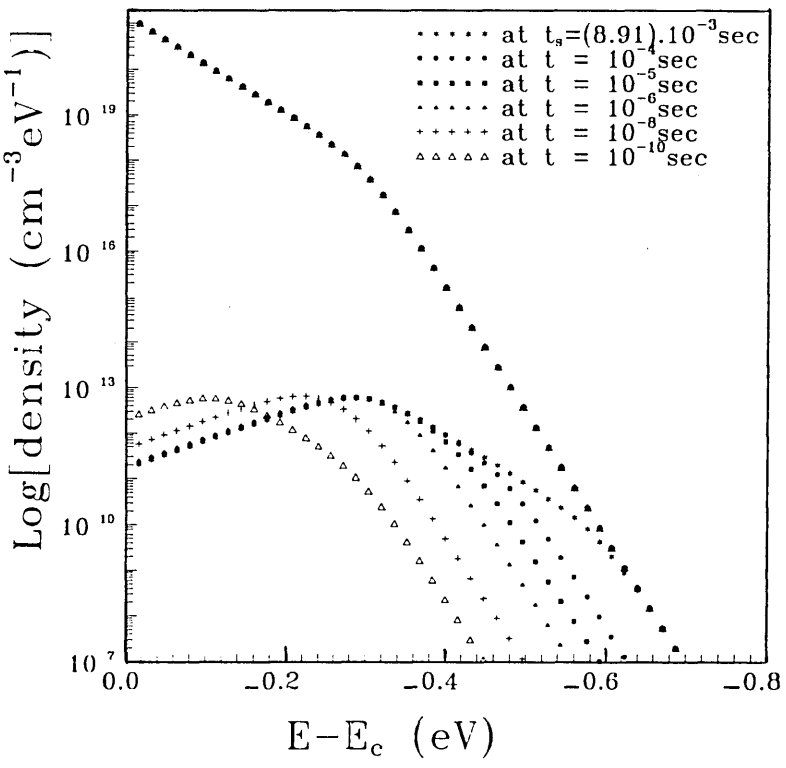

and below E_d, the occupation is independent of energy and increases with time as t^{α_c} resulting in the packet density $\delta n = f_d.g'$ being parallel to the density of states g', with

$$f_d \ (N_e/N_l).(\nu.t)^{\alpha_c} (E << E_d) \qquad (5.A.14)$$

N_l here denotes the total integrated tail state trap concentration

$$N_l = k.T_c.G_c.\pi.\alpha_c/\sin(\pi.\alpha_c) \qquad (5.A.15)$$

It should be noted that the same distribution of the packet density was calculated by Orenstein et al (1981) using the capture and release rate equations and Laplace transforms.

Additionally, the present theory predicts a distribution of the packet in the case of low excitation densities ($N_e << N_{fn}$) where E_d crosses E_{fn} and advances further below it ($t >> t_0$): In this time range the packet density δn is such that, above E_d the occupation follows Boltzmann statistics independently of time,

$$f_d \simeq (N_e/N_{fn}) \ . \ \exp\ [(E_{fn}-E) \ / \ k.T], \qquad (5.A.16)$$

and below E_d, the occupation increases proportionally with time as E_d advances until the latter stops at complete thermalisation (or saturation) (see section.5.A.1d below)

$$f_d \simeq (N_e/N_{fn}).(t/t_0). \qquad (5.A.17)$$

The packet density $\delta n = f.g'$ calculated at different times to illustrate the thermalisation process is shown in figure.5.A.2b as a complement to figure.5.A.2a. As can be seen, the packet has its maximum centered at E_{fn} at any time longer than t_0 (ie $E_d < E_{fn}$).

5.A.1.b The dispersive transport

The time dependent excess free electron density which determines the photocurrent is given by

$$n(t) = \int_0^\infty g''(E). \ f_d(E,t) \ dE \qquad (5.A.18)$$

where g"(E) is the density of states above the mobility edge (E >0). If N_c is the effective density of states at the mobility edge

expressed as,

$$N_c = \int_0^{\infty} g''(E).\exp(-E/k.T)\ dE \qquad (5.A.19)$$

then n(t) will have the value,

$$n(t) = F(t).N_c.\exp(E_d/k.T) = F(t).N_c.(\nu.t)^{-1} \qquad (5.A.20)$$

Consequently, the dispersive transport occurring at short times ($t \ll t_0$) before E_d reaches E_{fn} is depicted by the power-law photocurrent decay,

$$I_{TPC}(t) = \mu_0.\epsilon.A.(N_e/N_1).N_c.(\nu.t)^{(\alpha_c - 1)} \qquad (5.A.21)$$

where μ_0 is the free electron mobility, ϵ is the electric field across the gap and A is the conducting cross-section (the gap length times the absorption depth). This last expression is, formally, the same as that found by Orenstein et al (1982), but derived here with more rigour.

5.A.1.c. Complete thermalisation and saturation.

The condition for complete thermalisation (or saturation) is that the states below the demarcation level E_d are all occupied, i.e. $F(t_s)=1$, t_s being the complete thermalisation (or saturation) time. Inserting this condition into equation.5.12 leads to a very important relation for calculating t_s,

$$\frac{1 - (t_0/t_s)^{\alpha_c}}{(t_s/t_0) - 1} = \frac{N_e}{N_{fn}} \qquad (5.A.22)$$

This equation together with equation.5.A.11 gives, after being numerically solved, t_s as well as the position of the corresponding energy level E_{ds} for complete thermalisation (or saturation), given the Fermi level position E_{fn}.

Saturation of the states in the portion of the tail located below E_d can occur for low excitation densities ($N_e \ll N_{fn}$) as well as for

high excitation densities ($N_e >> N_{fn}$). In the former case, the saturation occurs below the QFL E_{fn} at $t_s > t_0$, whereas in the second case, it occurs above E_{fn} at $t_s < t_0$. The "transition" case should therefore be a saturation occurring at t_0 when $E_{ds}=E_{fn}$. Refering to Eqn.5.A.12 and the saturation condition for t_0 $F(t_0)=1$, the excitation density N_{e0} required for this "transition" saturation to occur is

$$N_{e0} = \alpha_c . N_{fn} \qquad (5.A.23)$$

5.A.1.d. Low excitation ($Ne << N_{eo}$) and linear response

The TPC response, in the short time ($t << t_0$) dispersive transport discussed above, decays as a power law of index $\alpha_c - 1$ (Eqn.5.A.21). At t_0, the "upper part" of the electron packet stops thermalising (Fig.5.A.2b) and E_d "leads" the "lower part" further below E_{fn}. At long times ($t >> t_0$) (without recombination effects) the TPC levels out and a non dispersive "plateau" response follows, its time independent value being readilly obtained from Eqns.5.A.12 and 5.A.20,

$$I_{TPC} = \mu_0 . \epsilon . A \; . \; N_c . (N_e/N_{fn}) \; . (\nu . t_0)^{-1}$$
$$= I_{SSPC} . N_e/N_{fn} \qquad (5.A.24)$$

where $I_{SSPC} = \mu_0 \; . \epsilon . A . N_c . (\nu . t_0)^{-1}$ is the dark current (or the SSPC in the case of OB regime). The TPC starts to level out at t_0, but the saturation time t_s depends on the pulse excitation density N_e. Eqn.5.A.22 gives

$$t_s \simeq t_0 . N_{fn}/N_e \qquad (5.A.25)$$

The TPC, in this time range, should be experimentally observed in a logarithmic plot as a flat response which depends linearly on the pulse excitation density N_e. Figure.5.A.3 (a) shows calculated TPC decays n(t) at different N_e values over the time range including both the power-law and the "plateau" regions of the recombination free regime and Figure.5.A.3 (b) shows the corresponding $\delta n(E)$ at the saturation times t_s.

Figure.5.A.3. (a)
Calculated pre-recombination n(t)(decay) for different pulsed electron densities lower and higher than N_{e0}, $E_{f0}=-0.3$ eV $T_c=470$ K, $T=300$ K, t_0 and t_s are indicated on the curves.

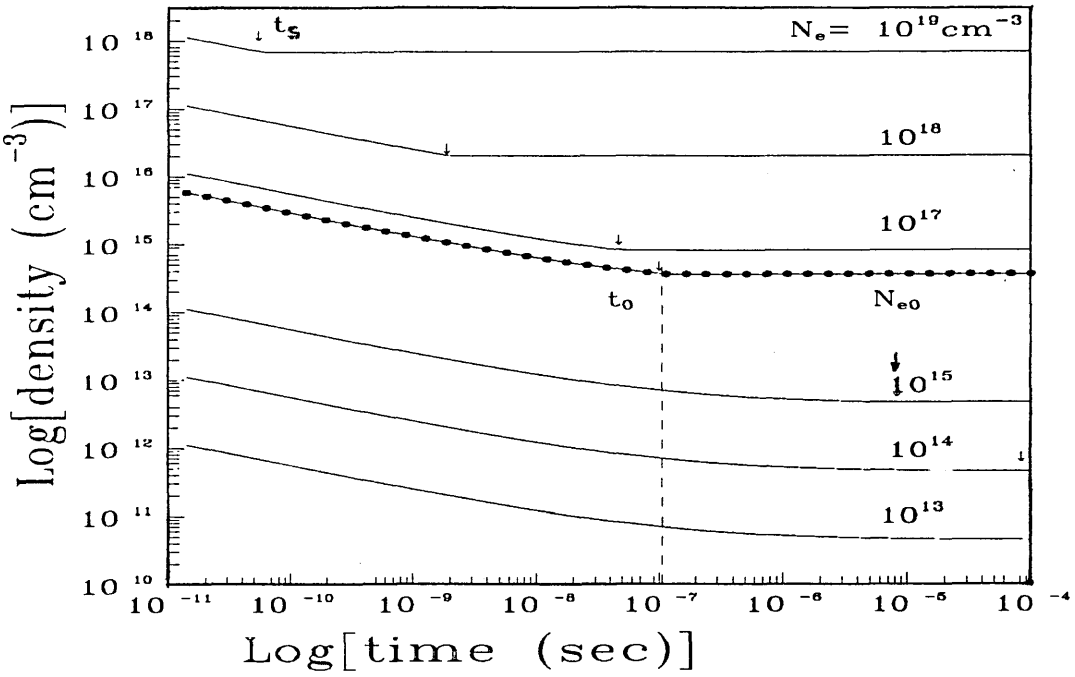

Figure.5.A.3. (b)
Calculated $\delta n(E)$ associated with n(t) in fig.5.A.3.(a) at the saturation time t_s for the same pulsed electron densities N_e. The saturation levels E_{ds} are indicated for each N_e value.

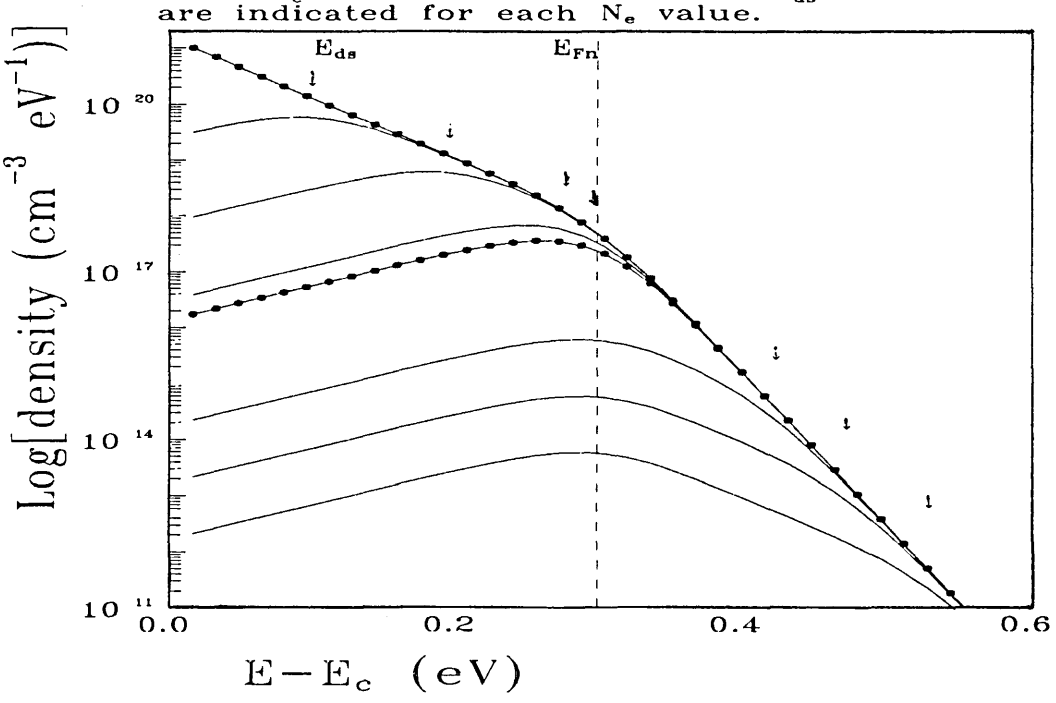

5.A.1.e High excitation ($Ne \gg N_{eo}$) and superlinear response

In the case of high excitation densities $N_e \gg N_{e0}$ the saturation of states above E_{fn} by the injected N_e is attained. In this situation, the saturation time t_s is less than t_0 ($t_s \ll t_0$), and the free excess electron density at saturation ,$F(t_s)=1$, is given by (Eqn.5.A.20),

$$n_s = N_c.(\nu.t_s)^{-1} \tag{5.A.26}$$

Equation 5.A.22 gives for t_s the value

$$t_s \simeq t_0.(N_{fn}/N_e)^{(1/\alpha_c)} \tag{5.A.27}$$

The TPC response at saturation is then

$$I^s_{TPC} = \mu_0.\epsilon.A.n_s = \mu_0.\epsilon.A.N_c.(\nu.t_0)^{-1}.(N_e/N_{fn})^{(1/\alpha_c)}$$

$$= I_{SSPC} \cdot (N_e/N_{fn})^{(1/\alpha_c)} \tag{5.A.28}$$

As long as recombination is not effective, E_d will not go below its saturation value E_{ds}, and the TPC response in the time range $t \geq t_s$ is constant and equal to I^s_{TPC} indicating a non dispersive transport region. Calculated TPC decays for high Ne in the time range $t<t_s$ and $t \geq t_s$ are also included in figure.5.A.3a.

Since α_c^{-1} is greater than 1 at all the measurement temperatures, the TPC response after saturation is superlinear with increasing superlinearity as the temperature decreases.

Figure.6.A.6 (in chapter.6, section.6.A.1) shows calculated "I_{TPC} versus N_e" curves at three different temperatures (to fit the experimental data) indicating the linear and superlinear responses, and the changing point at N_{e0}.

5.A.1.f. The tail state characteristic temperature T_c

It should be remarked that the characteristic temperature of the exponential tail (T_c) can be experimentally determined in three

different ways:

i) From the time dependence of the TPC in the short time dispersive region with the help of Eqn.5.A.21. The power-law index (α_c-1) is represented by the slope in a logarithmic plot.

ii) From the transition from low excitation linear response to high excitation superlinear response via equation.5.A.23.

iii) From the excitation dependence of the TPC in the non dispersive plateau region of the decay using Eqn.5.A.28. The power-law index ($1/\alpha_c$) is represented by the slope of the superlinear region in a logarithmic plot.

5.A.1.g. Non exponential density of tail states (DOS)

The assumption of an exponential energy dependence of the conduction band tail was the starting point for the derivation of the TPC expressions in the preceeding sections. Thus, an experimental confirmation of this theory, ie an ideal fit of the response observation to the theoretical prediction, is at the same time a confirmation of an exponential tail, and a deviation of the experimental data response from the theory reflects a deviation of the band tail from being an exponential; The closer the theory-data fit, the closer the DOS is to an exponential tail.

A most useful relation was noted in the course of this work that the ratio R of t_s to t_0 is equivalent to the ratio of the SSPC to the TPC at complete thermalisation, which is experimentally measurable,

$$R = I_{SSPC} / I^{s}_{TPC} = \exp\,[(E_{fn} - E_{dS})/k.T\,] = t_s/t_0 \qquad (5.A.29)$$

Having defined an effective density (cm^{-3}) of tail states by

$$g_{eff}(E) = k.T_c.[\pi.\alpha_c/\sin(\pi.\alpha_c)].g(E) \qquad (5.A.30)$$

and taking account of Eqns.5.A.9 and 2.9.12, one obtains for g_{eff} at E_{fn} and E_{ds} respectively,

$$g_{eff}(E_{fn}) = N_e.\frac{R - 1}{1 - R^{-\alpha_c}} \qquad (5.A.31a)$$

$$g_{eff}(E_{ds}) = N_e.\frac{R - 1}{R^{\alpha_c} - 1} \qquad (5.A.31b)$$

Two methods can be defined to probe $g_{eff}(E)$, each in accordance

with one of these two Equations:
i)-Using Eqn.5.A.31a, R and N_e are experimentally measured. The position of E_{fn} is determined from the dark current and the SSPC.
ii)-Using Eqn.5.A.31b, E_{fn} is kept constant and E_{ds} is determined by use of Eqn.5.A.29.

In the first method E_{fn} is shifted by varying the SSPC in the OB regime, and in the second method E_{ds} is shifted by the saturation effect through variation of N_e. Despite the pre-assumption of an exponential CBT, these methods are also applicable to a non exponential tail if a "local" T_c is used to describe a variable slope DOS. However a DOS varying too rapidly with energy, where the Fermi level lies below the sharp fall off, does not allow the methods to be applied (sect.5.A.1h below).

5.A.1.h. Sharply varying band tails

High quality a-Si:H samples show a tail density of states with a shoulder at a shallow level ($E_t \simeq$ 0.13-0.17eV), and a sharp fall off below this level (Spear, 1988, and Marshall et al, 1985).

In lightly phosphorous-doped samples of such a quality the dark Fermi level E_{f0} is located 0.5 to 0.4eV below the conduction mobility edge (Spear et al, 1984). In this case, the electron density N_e (injected charge) is trapped within a short time, $t = \nu^{-1}.\exp(E_t/k.T)$, and found peaking close to E_t, in quasi-thermal equilibrium with the extended states.

The drift mobility μ_d is related to the extended state mobility μ_0 (see Mott and Davis, 1979, p.248) in the equation

$$\mu_d = \mu_0.(N_c/N_t).\exp(E_t/k.T) \qquad (5.A.32)$$

with N_t the effective density of states at E_t. The TPC is then,

$$I_{TPC} \simeq \mu_d.\epsilon.A.N_e = \mu_0.\epsilon.A.(N_c/N_t).\exp(E_t/k.T).N_e \qquad (5.A.33)$$

This equation indicates that such material is characterised by a linear excitation response. In terms of free electron density equation 5.A.33 can be written,

$$n = N_e.(N_c/N_t).\exp(E_t/k.T) \qquad (5.A.34)$$

Increasing the pulsed electron density N_e to high levels does not affect the position of the dominant trap level E_t but adds proportionally to the free electron density n. Eqn.5.A.34 also predicts no effect of steady state biasing on the TPC in the recombination free region since E_{f0} is located deeper in the tail compared to the dominant trap level E_t. In other words, E_{f0} has to be shifted upwards by $E_t - E_{f0} \simeq 0.25$ eV in order to observe such an effect. This may occur only at high OB levels and/or low temperatures.

An estimation of the effective density of states at E_t can be obtained from Eqn.5.A.33,

$$N_t = (\mu_0.\epsilon.A.N_c/I_{TPC}).[\exp\ (E_t/k.T)].N_e$$

$$= R\ .\exp\ [(E_t - E_{fn})/k.T\ ].\ N_e \qquad (5.A.35)$$

R is again the ratio of the SSPC (in the optically biased transient case) or the dark current to the TPC in the non dispersive "plateau" (recombination free) region, $R = I_{SSPC}/\ I_{TPC}$, and E_{fn} is the QFL (in the optically biased transient case) or the dark Fermi level E_{f0} as before.

5.A.2. Transport in the presence of recombination

In the preceeding section, the electron thermalisation in the CBT was treated with no regard to the behaviour of the (minority carriers) holes in the valence band tail (VBT). This has always been the case for undoped or n-type material in the absence of recombination when there is no dynamic relation between the two carrier types. In fact even in the presence of recombination, the early transient studies (Tiedje and Rose, 1980, Orenstein et al, 1982, Hvam and Brodsky, 1980, Oheda, 1985 and 1987) were concentrated on the electron behaviour, and just extended the thermalisation process to include recombination of the electrons via trapped holes with the appropriate analysis involving only the CBT parameters and avoiding the description of the hole dynamics (sect.3.A).

In contrast to the above, a number of recent studies (Main, 1987, Oheda, 1987, Werner, 1988 and McMahon 1988 and 1989), particularly that published by Main et al, of which part of the present work is an extention, considered the hole thermalisation in the VBT as being the controlling process to account for the long time TPC decays in n-type a-Si:H.

In the model proposed by Main the TPC decay presents four distinctive stages (fig.5.A.4 illustrates the correlation between the hole thermalisation (a) and the TPC decay during these stages):
stage(i): Initial trapping of holes and electrons occurring at the start of the decay, just after the excitation cut-off.
stage(ii): Electron (and hole) thermalisation in the CBT (and the VBT) without recombination.
stage(iii): Complete thermalisation of the electrons at the Fermi level or a shallower level while the holes are still thermalising without recombination.
stage(iv): The holes reach a stage where the probability of further hole capture is balanced by the probability of hole recombination via deep states (for example, doubly occupied dangling bonds (DB)) where they are subsequently annihilated by electron capture.

In the following, the recombination process in stage (iv) will be treated, together with the hole behaviour in stage (iii) as this serves as the initial conditions for stage (iv).

5.A.2.a. Recombination in the absence of optical bias

The case which will be focussed on is the case of low pulse excitation which gives a linear response in the recombination free regime (sect.5.A.1d, and stage(iii) in figure.5.A.4).

Without optical bias, the Fermi level E_{f0} in n-type material is well above mid-gap and, in contrast to the case considered above for CBT states, all the states in the VBT are available for trapping and thermalisation of excess holes.

The electron transport in stage(iii) of the TPC decay is characterised by a constant electron photocurrent with free and

Figure 5.A.4. Illustration of the decay of excess electrons and holes following pulsed excitation, with no optical bias. Parameters: T_C=470K T_V=600K (computer-simulation data)

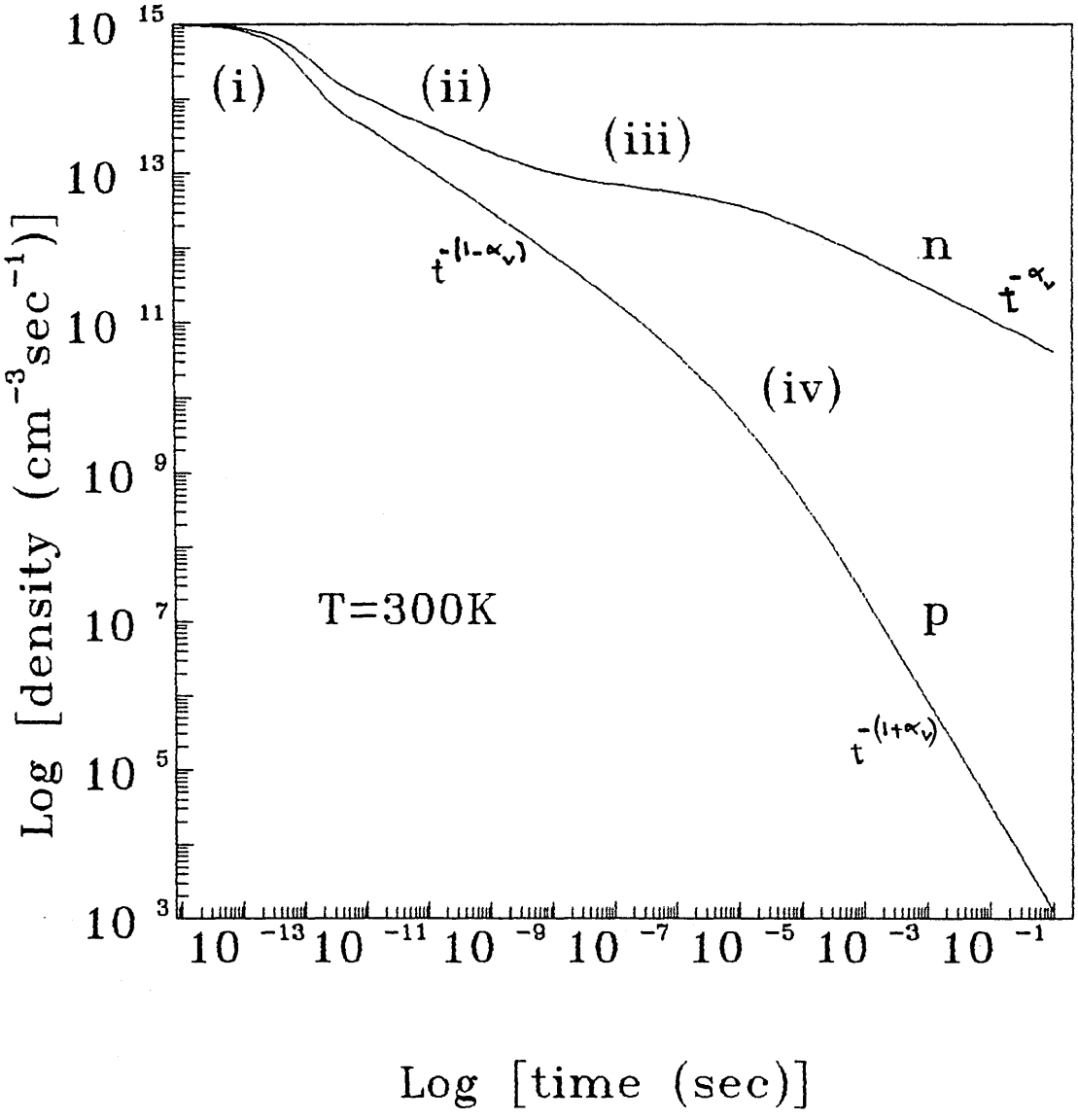

trapped electrons in quasi-equilibrium after complete thermalisation. Simultaneousely in the same stage, the hole thermalisation proceeds in the VBT without recombination.

Assuming an exponential VBT,

$$g_v(E) = G_v \,.\exp\,[(E_v-E)/(k.T_v)\,] \qquad (5.A.36)$$

(G_v is the extrapolation of g_v to the valence mobility edge E_v and $k.T_v$ is the energy characteristic of the VBT), the thermalising hole packet can be described, in the same way as for the electrons, by the transient occupation function (Eqn.5.A.1),

$$f_{dp}(E,t) = F_p(t).\frac{1}{1+\exp(\frac{E_{dp}-E}{k.T})} \qquad (5.A.37)$$

E_{dp} is the trapped hole demarcation energy related to the time t by

$$E_{dp}-E_v = k.T.\log(\nu.t) \qquad (5.A.38)$$

and $F_p(t)$ is the energy independent occupation function (occupation above E_{dp}).

The integrated trapped hole density in the packet is

$$P_t(t) = \int_{-\infty}^{+\infty} g_v(E).f_{dp}(E,t)\,dE$$

$$= F_p(t).N_{lv}.(\nu.t)^{-\alpha_v} \qquad (5.A.39)$$

where $N_{lv}=k.T_v.G_v.[\alpha_v.\pi\ /\sin(\alpha_v.\pi)]$ is the VBT trap cocentration and $\alpha_v=T/T_v$ is the hole dispersion coeficient.

In this stage there is no loss of carriers by recombination, and most of the generated holes (like the electrons) are trapped. P_t is then practically equal to the excitation density N_e. Therefore, the occupancy above E_{dp}, in this stage, increases as t^{α_v} as E_{dp} advances upwards,

$$F_p(t) = (N_e/N_{lv}).(\nu.t)^{\alpha_v} \qquad (5.A.40)$$

The recombination stage(iv) of the TPC decay starts at a time

associated with the effective hole recombination life time t_r when E_{dp} reaches a critical level E_r in the VBT above which the hole trapping probability is equal to the probability of hole recombination via defect states. This criterion can be expressed as follows,

$$\int_{E_c \neq 0}^{E_r} \beta_p(E).g\,(E)\,dE = C_p.N_r \qquad (5.A.41)$$

The right hand side of this equation represents the probability of monomolecular recombination to centers of a concentration N_r assumed constant (see below) and a hole recombination coefficient C_p (product of the recombination cross-section σ_p of the defect and the thermal velocity v_p of the free holes). The left hand side of the equation represents the probability of hole trapping by a time decreasing density of "hole-empty" VBT states (of capture coefficient β_p) represented by the integral. The minimum value of this integral (or the critical value) below which the criterion.5.A.41 is in favour of recombination is attained at t_r when E_{dp} reaches E_r,

$$E_r - E_v = k.T.\log(\nu.t_r) \qquad (5.A.42)$$

Once the recombination starts at t_r, P_t is no longer constant; The hole packet "stops" at E_r and starts losing holes by emission from below E_{dp} to the valence band and subsequent recombination as E_{dp} continues advancing. In this situation the occupancy F_p above E_{dp} will remain constant during the recomination stage(iv),

$$F_p = F_p(t_r) = (N_e/N_{lv}).(\nu.t_r)^{-\alpha_v} \qquad (5.A.43)$$

Replacing F_p into Eqn.5.A.39, one obtains the time dependence of the trapped hole density during stage(iv) of the decay,

$$P_t(t) = N_e.(t_r/t)^{\alpha_v} \qquad (5.A.44)$$

The assumptions made here are:

i)- The probability of the electrons recombining via capture by trapped holes in the VBT states is negligible (Cleve and Thomas, 1990, and Main et al, 1990) due to the small probability of the necessary multi-phonon emission processes (Okushi et al, 1982).

ii)- The recombination of excess free holes is monomolecular, in a

process in which the rate limiting step is the emission of trapped holes to the valence band. The recombination centers in n-type material are supposed here to be, mainly doubly electron occupied dangling bonds (DB) (D^-) (Spear, Steemers and Le Comber, 1984 and Bube and Redfield, 1989). The reaction involved in such a mechanism is simply a reversible transfer between doubly and singly electron occupied DB,

$$D^- \underset{+\ e}{\overset{+\ h}{\rightleftharpoons}} D^0$$

iii)- One more simplifying assumption is included in the mechanism, that the occupation at the D^- states does not change significantly, and therefore the charge neutrality is controlled by the excess free and trapped charges (in the band tails). Moreover, at long times of the stage(iv) range, most of the carriers are trapped. In such a condition, the charge neutrality is given by,

$$n_t = P_t \qquad (5.A.45)$$

On the other hand, the trapped electron density n_t in the CBT, during this stage, must decay from its initial value N_e (sect.5.A.2) as the recombination proceeds. However, it is still in thermal equilibrium with the free electron density n(t). For sharply varying CBT, Eqn.5.A.34 is rewritten in this stage as follows

$$n(t) = (N_c/N_t).\exp(E_t/k.T).n_t(t) \qquad (5.A.46)$$

As a result, the free electron density and consequently the TPC response, combining Eqns.5.A.44, 45 and 46, decays as $t^{-\alpha_v}$,

$$I_{TPC}(t) = I_{SSPC}.(N_e/N_t).\exp\left[(E_t-E_{fn})/k.T\right].(t_r/t)^{\alpha_v} \qquad (5.A.47)$$

I_{SSPC} is the dark current (or the SSPC in the case of very low OB) and E_{fn} is the dark Fermi level E_{f0} (or the QFL).

Experimentally, the TPC response presents a power-law decay of index α_v identified by the slope, in a logarithmic plot, which increases linearly with the temperature. It can then be concluded that the present approach is an alternative physical view for the TROK analysis to account for the observed long time TPC decay in n-type

a-Si:H (see results in chap.6, sect.6.A.2).

5.A.2.b. Recombination in the presence of OB

The steady state OB splits the dark Fermi level E_{f0} into electron and hole QFLs E_{fn} and E_{fp} which shift towards the conduction and valence bands respectively; considerable shifts can be obtained using high OB levels. The effect of OB will then result from the introduction of a steady state trapped hole distribution in the VBT above E_{fp}. Therefore, the approach should be modified to involve the effect of this distribution in a similar way to the electron case (sect.5.A.1).

The density of available states for hole thermalisation in the VBT will be

$$g'_v(E) = g_v(E).[\ 1 - f_p(E)\ ] \qquad (5.A.48)$$

where f_p is the hole Fermi occupation function . In this case, the integrated hole density in the thermalising hole packet has a similar expression to that given for the electron case in Eqn.5.A.9,

$$P_t = \int_{-\infty}^{+\infty} g'_v\ .f_{dp}\ dE$$

$$= F_p(t)\ .N_{fp}.\frac{1 - (t_p/t)^{\alpha_v}}{(t/t_p) - 1} \qquad (5.A.49)$$

where $t_p = \nu^{-1}.\exp\ [(E_{fp} - E_v)/k.T\ ]$ is defined (similarly to t_0 for the electron thermalisation) as the time by which E_{dp} reaches E_{fp}, and N_{fp} is the trapped hole density above E_{fp},

$$N_{fp} = \int_{-\infty}^{+\infty} g_v\ .f_p\ dE\ = N_{1v}.(\nu.t_p)^{-\alpha_v} \qquad (5.A.50)$$

In the following, it will be admitted that the same assumptions made above for the non optically biased case are also applicable for the OB case.

As mentioned above, very low OB levels have no effect on the TPC (stage(iv)) compared to the non OB case, since E_{fp} is still at the top of the VBT well above E_v; In terms of time, t_p is much longer

than t_r, and lies beyond the experimental time range. For significant OB levels, the recombination criterion (Eqn.5.A.41) is rewritten, with consideration of the steady state distribution introduced by the OB as follows

$$\int_{E_c=0}^{E'_r} \beta_p(E).g_v(E).[(1-f_p(E)]\ dE = C_p.N_r \qquad (5.A.51)$$

The OB becomes more and more significant as E_{fp} gets closer to E'_r. A new critical energy E'_r for hole recombination must now be defined which moves with E_{fp} as required by equation.5.A.51. Hence, one of the OB effects is to shorten the effective hole recombination time t_r (or the "turnover" time of the TPC decay).

Since $g_v(E)$ increases with decreasing energy in the VBT, E_{fp} shifts by larger amounts than the shift of E'_r. In other words, the energy difference $E_{fp}-E'_r$ decreases with increasing OB level and E_{fp} tends to "catch" E'_r. Figure.5.A.5 shows <u>calculated</u> $g'_v(E)$ and $\delta p(E)=g'_v(E).f_{dp}$ for different OB levels and the relevant positions of E'_r. As can be seen, at high OB levels E'_r can be located in the rapidly varying region of $g'_v(E)$ <u>above</u> E_{fp}. In this case, E_{dp} will reach E_{fp} before E'_r during thermalisation (in stage(iii)).

Consider this last case of high OB level: At short times ($t \ll t_p$) before E_{dp} reaches E_{fp}, the occupation F_p above E_{dp} is found (Eqn.5.A.49) to increase as t^{α_v}, and the free hole density p (analogously to n) decays as $t^{(\alpha_v-1)}$. By the time E_{dp} passes E_{fp}, most of the hole density peaks at E_{fp} (Fig.5.A.5). Thus within the small time range $t_r > t > t_p$ the free hole density p will *level out*, as a result of multiple trapping near E_{fp}, which can be expressed by an equation similar to Eqn.5.A.24. When E_{dp} reaches E'_r at time t_r, the recombination criterion will then be satisfied, and for the remaining time range $t \geq t_r$, the hole recombination will proceed by hole emission from around E'_r and subsequent recombination to D^- DB's follows according to the hole rate equations

$$dP_t/dt = - e_r.P_t \qquad (5.A.52a)$$

$$dp/dt = e_r.P_t - C_p.N_r.p \qquad (5.A.52b)$$

Figure.5.A.5.
Calculated $\delta p(E)=g'_v(E).f_{dp}(E)$ at t_r
for different positions of the hole QFL E_{Fp}
(ie different OB). The parameters used are:
T=300K, T_c=600K, $G_v=4.10^{21}eV^{-1}cm^{-3}$,
$N_v=k.T.G_v$, $N_e=10^{14}cm^{-3}$, $\nu=10^{12}$/sec,
$C_p=10^{-8}cm^3sec^{-1}$, $N_r=10^{16}cm^{-3}$, $E_v=-1.8eV$.

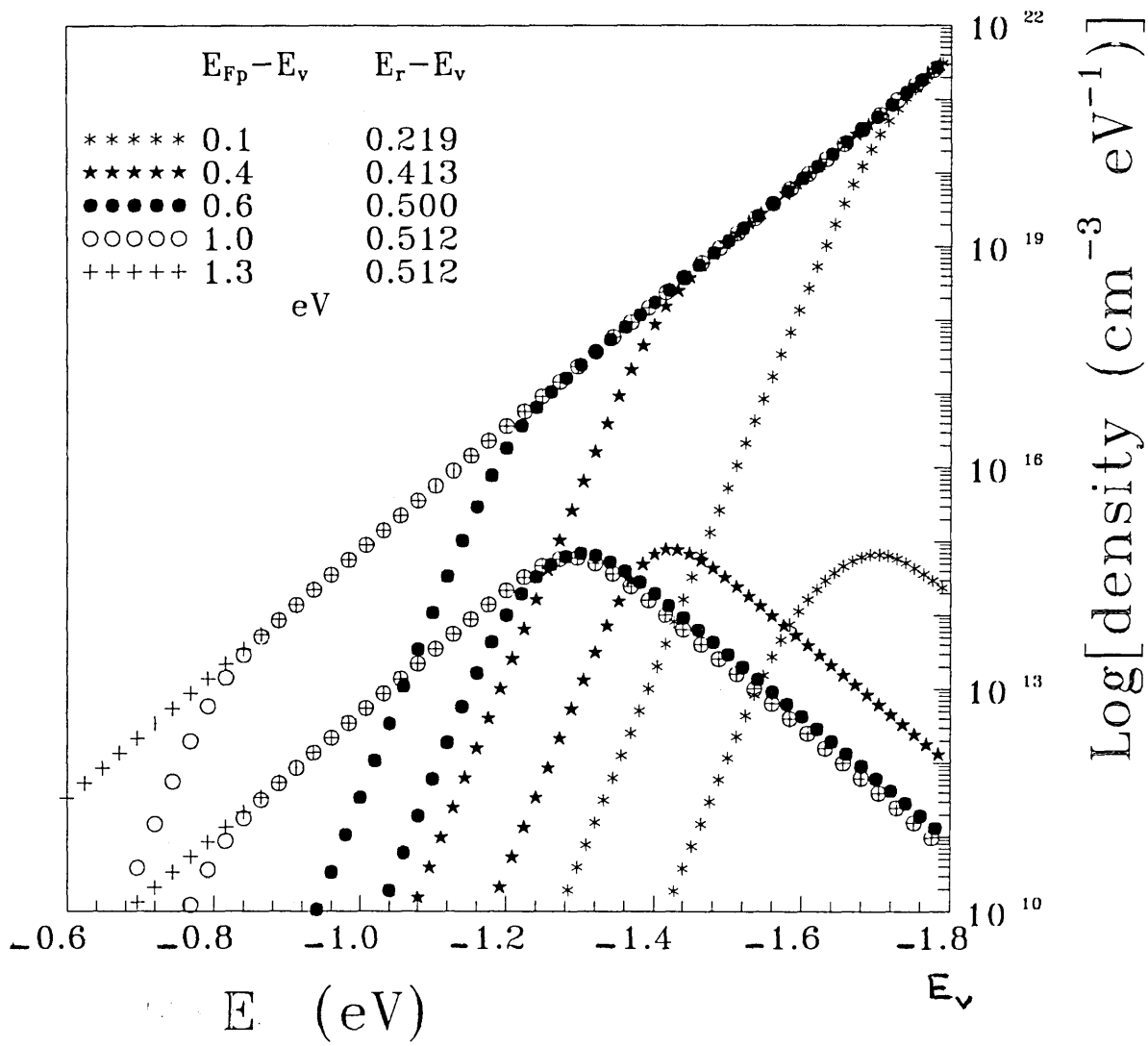

e_r being the hole emission coefficient from E'_r to the valence band, $e_r = 1/t_r$. The decay law of P_t is exponential,

$$P_t = N_e.\exp(-\ t/t_r) \qquad (5.A.53)$$

Recalling the long time charge neutrality assumption (Eqn.5.A.45) and Eqn.5.A.46, one thus obtains for a sharply varying CBT an exponential time dependence of the TPC response,

$$I_{TPC}(t) = I_{SSPC}.(N_e/N_t).\exp\ [(E_t-E_{fn})/k.T\ ].\exp\ (-t/t_r) \qquad (5.A.54)$$

As for intermediate OB levels which locate E_{fp} above E'_r (ie $t_p > t_r$) and for which t_p lies in the observed experimental time range, the TPC in the recombination stage (iv) should decay first as $t^{-\alpha_v}$ for $t_r < t < t_p$, and then an exponential response follows for $t > t_p$.

A sketch of the decays p(t) and n(t) is given in figure.5.A.6 to illustrate the effect of the OB level on the TPC decay. This should be compared with Fig.5.A.4.

5.B. The steady state regime

The "sub-square-root" excitation dependence for the steady state photocurrent (SSPC) observed experimentally in the P-doped material in this study cannot be explained by the standard model of Rose described in chapter.2. To recap, Rose's analysis predicts an excitation index, γ, in the range $0.5 < \gamma < 1.0$, (Eqn.2.9.14), the magnitude *increasing* steadily to 1.0 as temperature is reduced toward absolute zero. In the present work, not only were γ values of less than 0.5 observed, but over a wide range of temperature (region II of fig.3.1), γ was observed to be *independent* of temperature.

Sub-square root response in the SSPC excitation dependence has been observed in previous work in a-Si:H and given different interpretations (see chap.3): Kagawa et al (1983) found $0.4 < \gamma < 0.5$ for large shifts of E_{f0} (0.4 -0.25 eV below E_c) in thin film transistor structures with positive gate bias. In Kagawa's model, a fixed density of recombination centers near mid-gap was assumed, with free

Figure 5.A.6. Illustration of the decay of excess electrons and holes following pulsed excitation, with high optical bias. Parameters: T_c=470K T_v=600K (computer-simulation data)

(a)

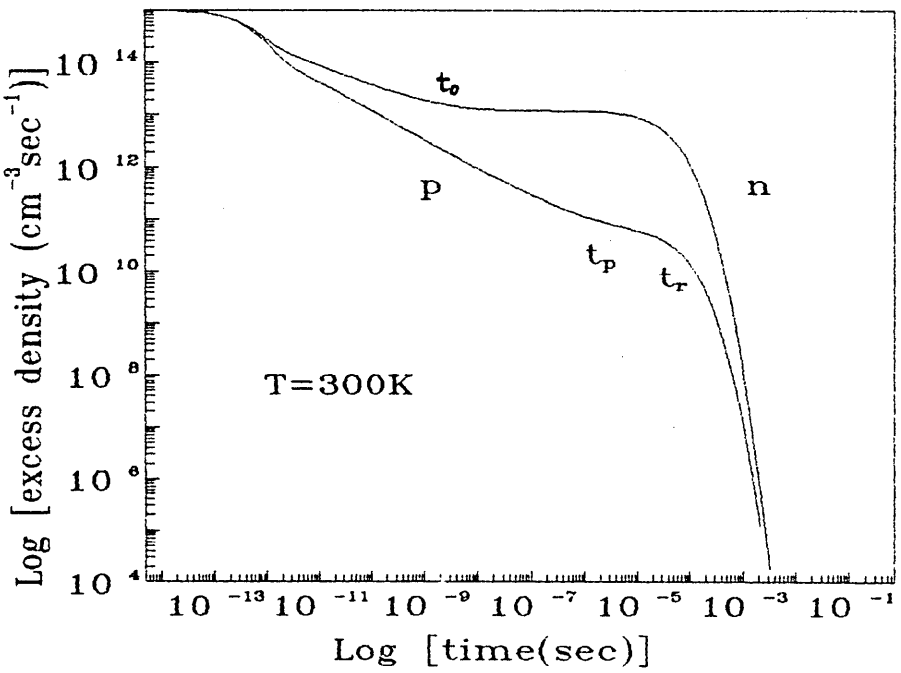

Illustration of the decay of excess electrons and holes following pulsed excitation, with intermediate optical bias. T_c=470K T_v=600K (computer-simulation data)

(b)

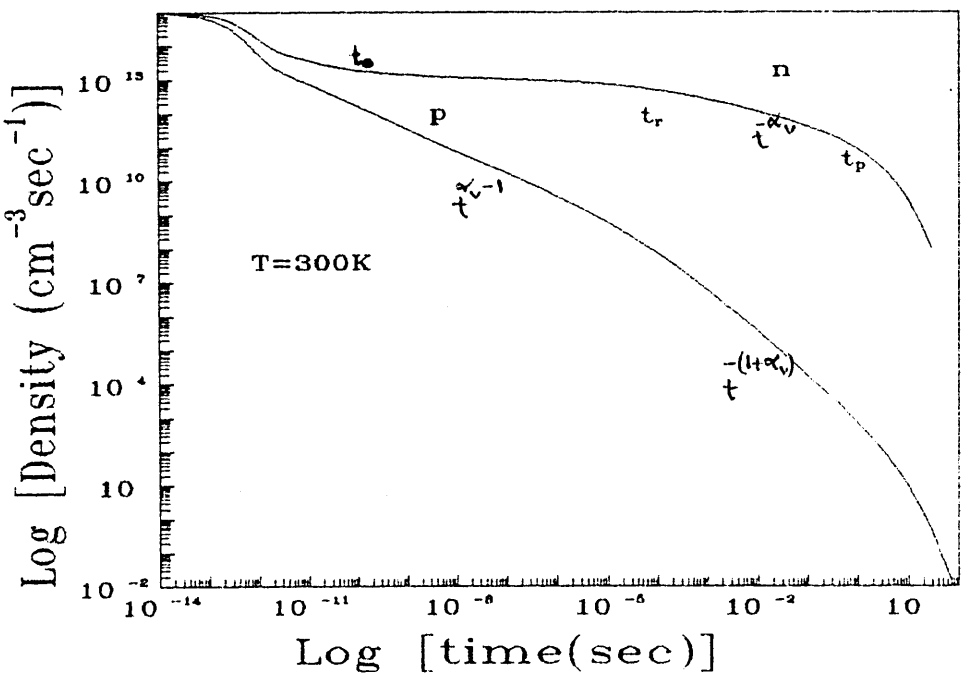

carrier recombination. A density of exponential tail states was proposed, which become steeper as toward the mobility edges, in disagreement with the measured density of CBT states by the "time of flight" technique (Marshall et al, 1986) which shows a sharp decrease below a shoulder at a shallow level. With this gap state distribution, the recombination centers had to be donor-like states and the recombination limited by free hole capture to explain γ values less than 0.5.

In the model proposed by Hack et al (1984) γ values less than 0.5 observed with light P-doping needed very high excitation intensities ($\simeq 10^{22} cm^{-3} s^{-1}$). The interpretation given for the special case of high illumination and heavy P-doping corresponds to the change in the space charge neutrality condition due to the introduced dopant concentration. It should be noted that the range of excitation required by this model to give such low γ values was very limited compared to the *actual* range observed to do so in the present work. The proposed density of gap states was similar to that proposed by Kagawa et al.

5.B.1. The proposed model.

The model proposed in the present work represents an improvement on the model already proposed by the research group at Dundee Institute of Technology (Main et al, 1987). Before describing the details, some general points can be made:

(i) The proposed model predicts extreme sublinearity ($\gamma < 0.5$) over a wider range of excitation than Hack's model, and is in agreement in this respect with experiment.

(ii) The model predicts an activated temperature dependence of photocurrent in the very sub-linear regime in good agreement with experiment, while other models (e.g. that of Vaillant et al, 1988) do not.

(iii) The proposed model also predicts other effects - such as thermal quenching at high temperatures, and low temperature behaviour in qualitative accord with experiment.

(iv) The model parameters are consistent also with the *transient* photoconductivity. This is probably not true for any of the other SSPC models proposed for a-Si:H.

(v) Non-participation of tail-states in recombination (by Shockley-Read mechanism) is an essential feature of the proposed model and distinguishes it from other models (Hack, Vaillant, ..). This is entirely consistent with the *transient* model and all of the observed photoconductive behaviour in the present study.

5.B.1.a. Model assumptions.

In the present model, it is assumed that the electrons recombine by tunneling from shallow localised tail states located mainly at the shoulder of the sharply varying CBT, to dangling bonds. This assumption may be partly justified by the fact that the shallow level is highly populated under steady state conditions (particularly at high temperatures) due to the sharp shoulder in the density of states profile at E_t. While this condition may not apply at *low* temperatures it is assumed in the model that recombination still proceeds via tunneling from states near E_t to dangling bonds. It can only be speculated that this may be due to a combination of the high density of states at E_t and the greater spatial extent of the electron wavefunctions of such shallow states which allows electron tunneling to the recombination centers (Dersch et al, 1983) in preference to free electron capture or transitions from tail states near the expected occupation peak at E_{Fn}.

The recombination centers are predominantly DB defects (Street and Biegelsen, 1980), and other gap states intervene only in the charge neutrality condition. The correlation effects among the DB defects and related statistics are taken into account (Okomoto et al, 1986). The holes are assumed to recombine from extended states, although this is not an essential feature .

Figure.5.B.1 shows the transitions involved in the model and the sharply varying CBT.

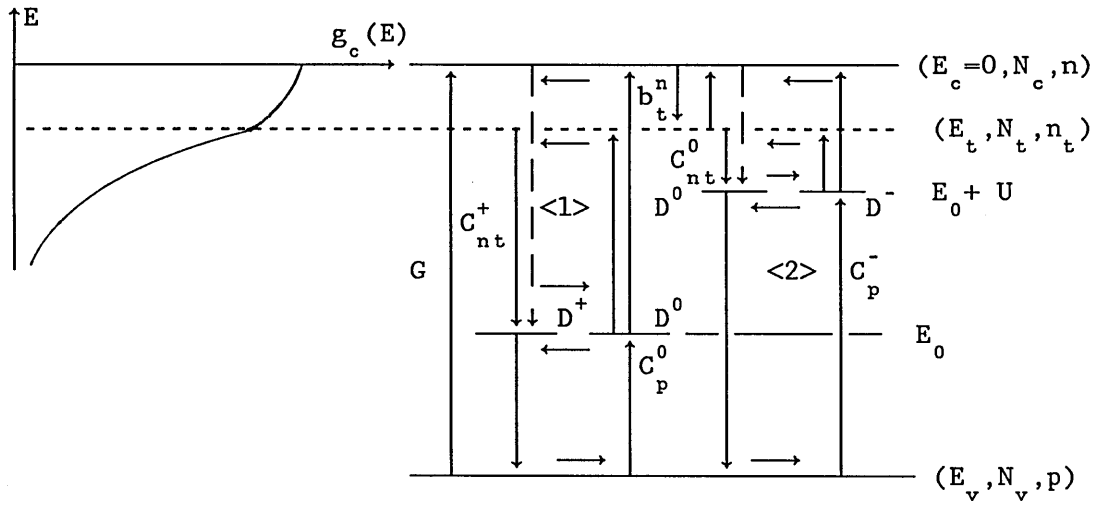

Figure.5.B.1. The model for the SSPC, (the CBT shown on the left)

On figure 5.B.1, the transfers between DB states are indicated by the horizontal arrows (eg, the hole capture transition by the D^- state leads to the transfer $D^- \longrightarrow D^0$).

5.B.1.b. Model parameters.

The conduction band-tail states involved in recombination are represented by a discrete level at E_t with an effective density of states N_t (cm^{-3}) related to the effective density of states in the conduction band, N_c by $N_t = N_c.g(E_t)/g(E_c)$, with N_c approximated to $k.T.g(E_c)$ in the analysis. The density of states *below* E_t is assumed to fall as a steep exponential distribution with density

$$g(E) = g(E_t).\exp\,[(E-E_t)/k.T_c]$$

where the characteristic temperature T_c is less than 300K. Other parameters used in the analysis are listed below.

n_t — the trapped electron density in tail-states at E_t

n, p — free electron and hole densities.

b_t — electron trapping coefficient in tail states

C_n^0, C_n^+, C_p^0, C_p^- — capture coefficients of, respectively, a free electron by D^0 state, a free electron by D^+ state, a free hole by D^0 state, and a free hole by D^- state

C_{nt}^0, C_{nt}^+ — capture coefficients of trapped electrons by D^0 and D^+ states respectively.

E_0 energy (assumed discrete) of D^+/D^0 level.

U correlation energy.

$E_0 + U$ energy of D^0/D^- level.

G electron/hole pair generation rate.

E_c is taken as the energy reference, and energies below E_c are negative

5.B.2. The model calculations.

5.B.2.a. Rate equations.

The rate equations for the steady state in terms of the excess charges at different transition levels are,

$$\text{at } E_c: \quad dn/dt = 0 = G - b_t.(N_t - n_t).n + b_t.N_c.\exp(E_t/k.T).n_t + n_1^0.C_n^0.N.F^- + n_1^+.C_n^+.N.F^0 \qquad (5.B.1)$$

$$\text{at } E_t: \quad dn_t/dt = 0 = b_t.(N_t - n_t).n - b_t.N_c.\exp(E_t/k.T).n_t - n_t.N.(C_{nt}^0.F^0 + C_{nt}^+.F^+) + n_{t1}^0.C_{nt}^0.N.F^- + n_{t1}^+.C_{nt}^+.N.F^0 \qquad (5.B.2)$$

$$\text{at } E_0+U: \quad dF^-/dt = 0 = n_t.C_{nt}^0.F^0 - (C_{nt}^0.n_{t1}^0 + C_n^0.n_1^0).F^- - p.C_p^-.F^- + p_1^-.C_p^-.F^0 \qquad (5.B.3)$$

$$\text{at } E_0: \quad dF^+/dt = 0 = (C_{nt}^+.n_{t1}^+ + C_n^+.n_1^+).F^0 - n_t.C_{nt}^+.F^+ + p.C_p^0.F^0 - p_1^0.C_p^0.F^+ \qquad (5.B.4)$$

F^0, F^-, F^+ are the occupation fractions of the D^0, D^-, D^+ DB states respectively and N the total density of DB's,

$$F^0 + F^- + F^+ = 1 \qquad (5.B.5)$$

Although the free electron recombination represented by the dashed line transition in figure.5.B.1 is required by the detailed balance in the equilibrium condition, this is slow compared to the electron tunneling process from localised states at E_t because of the high density of trapped electrons n_t ($C_{nt}^{+/0}.n_t >> C_n^{+/0}.n$). The terms n_1^0 and n_1^+ are 'electron emission densities' from D^- and D^0 to the extended states, obtained by detailed balance considerations of the release and capture rates, and defined along with respective hole emission terms as-.

$$n_1^+ = (0.5).N_c \exp(E_0/kT) \qquad n_1^0 = 2.N_c \exp[(E_0+U)/kT]$$

$$p_1^0 = 2.N_v \exp[(E_v-E_0)/kT] \qquad p_1^- = (0.5).N_v \exp[(E_v-E_0-U)/kT] \qquad (5.B.6)$$

The other terms n_{t1}^0 and n_{t1}^+ are the electron 'emission densities' from D^- and D^0 to the localised states at E_t given by similar equations to the n_1 terms ,

$$n_{t1}^0 = 2.N_t.\exp\,[(E_0+U-E_t)/k.T\,] \qquad (5.B.7a)$$

and

$$n_{t1}^+ = (0.5).N_t.\exp\,[(E_0-E_t)/k.T\,] \qquad (5.B.7.b)$$

Simplifications can be introduced before solving, as follows-

First, define

$N_1^0 = C_n^0.n_1^0 + C_{nt}^0.n_{t1}^0$, and $N_1^+ = C_n^+.n_1^+ + C_{nt}^+.n_{t1}^+$ the total probability of electron emission from D^- and D^0 to the extended and localised states.

Similarly-

$N^+ = n_t.C_n^+ + p_1^0.C_p^0$ the probability of the transfer $D^+ \longrightarrow D^0$,

$N^0 = n_t.C_n^0 + p_1^-.C_p^-$ the probability of the transfer $D^0 \longrightarrow D^-$,

$P^- = p.C_p^- + N_1^0$ the probability of the transfer $D^- \longrightarrow D^0$,

$P^0 = p.C_p^0 + N_1^+$ the probability of the transfer $D^0 \longrightarrow D^+$.

(5.B.8)

5.B.2.b. Net electron recombination rate.

The generation rate G which should be equal to the net electron recombination rate R_n is obtained by the combination of rates for paths <1> and <2>,

$$G = R_n = [n_t.C_{nt}^+.N.F^+ - N_1^+.N.F^0\,] + [n_t.C_{nt}^0.N.F^0 - N_1^0.N.F^-\,]$$

$$= \qquad R_n^1 \qquad + \qquad R_n^2 \qquad (5.B.9)$$

Hence two independent recombination paths are identified: the path noted by <1> involving the reversible transfer $D^+ \rightleftarrows D^0$, with the net recombination rate R_n^1, and the path noted by <2> involving the reversible transfer $D^0 \rightleftarrows D^-$, with the net recombination rate R_n^2.

The occupation fraction of the D^0 state is obtained by combination of 5.B.1-8.

$$F^0 = (N^+.P^-) \;/\; [N^+.P^- + P^0.P^- + N^0.N^+] \qquad (5.B.10)$$

5.B.2.c. Charge neutrality.

No explicit assumptions are made about the charge neutrality control as this may be temperature dependent (ref Vaillant). Expressed in terms of excess charge in all the states, the charge neutrality condition is,

$$(n - n_0) + n_t + \Delta n_t + N.(F^- - F_0^-) - (p - p_0) - \Delta p_t - N.(F^+ - F_0^+) = f(n, n_t, p) = 0 \qquad (5.B.11)$$

where n_0 and p_0 are the dark thermal equilibrium densities of free electrons and holes defined by the dark Fermi-level E_{F0}. The thermal equilibrium DB occupation fractions F_0 (Eqn.2.8.2) are subtracted. Δn_t and Δp_t are the trapped charges below and above the electron and hole QFLs respectively,

$$\Delta n_t \simeq k.T_c.g(E_t).\exp\,[(E_{F0} - E_t)/k.T_c].[\,(n/n_0)^{\alpha_c} - 1\,] \qquad (5.B.13a)$$

$$\Delta p_t \simeq k.T_v.G_v.(p/N_v)^{\alpha_v} \qquad \alpha_{c,v} = T/T_{c,v} \qquad (5.B.13b)$$

For consistency with the TPC model (cf sect.5.A) which is based on the assumption that, in n-type a-Si:H the recombination rate limiting step is the capture of a hole by the D^- state, path <2> will dominate in the SSPC.

5.B.2.d. Solution.

Given these simplifications, D^+ states can be neglected and one can proceed towards solving the problem by reducing the charge neutrality condition (eq. 5.B.11) to a function of only two variables n and n_t as follows,

G and F^0: $G = R_n^2$, can be expressed as a function of F^0 and n_t , and $F^0 = P^-/(P^- + N^0)$ as a function of p and n_t

p : p can be deduced as a function of n_t, $p(n_t)$

F^- : replaced by $1-F^0$, it can be expressed as a function of n_t and p.

Taking account of p (n_t) above, Eqn.5.B.1. leads finally to a *quadratic* equation in n_t with coefficients depending on n, i.e.

$$A(n).n_t^2 + B(n).n_t + C(n) = 0 \qquad (5.B.14)$$

Hence the charge neutrality equation 5.B.11. can be solved numerically for n by a simple bisection method. The SSPC is then given by,

$$I_{SSPC} = e.\epsilon.A. \left[\mu_0.(n - n_0) + \mu_{0h}.(p - p_0) \right] \qquad (5.B.15)$$

where μ_{0h} is the free hole mobility.

The physics and the parameters of the model will be discussed in chapter.6 in the light of the observed SSPC results.

CHAPTER.6

RESULTS
INTERPRETATION and DISCUSSION

In this chapter, the experimental results will be presented in the same sequence followed in chapter.5, so as to interpret them according to the models developed in the work, and to show at the same time the deficiencies of these models. The discussion will also involve comparison with other related works.

The samples are characterised by measured activation energies, -0.5 eV for the P-doped sample and -0.31 to -0.36 eV for the As-doped sample, which give the dark Fermi-level position (assumed fixed with varying temperature).

6.A.Transient Photoconductivity results

First, an overall description of the TPC decay features will be given. The results corresponding to the two regions of the TPC, the short time (or pre-recombination) region and the long time (or recombination) region (including the effects of optical bias and high excitation band tail saturation) will then be discussed separately since they reflect different carrier processes. Presented in this way, it is more convenient for the sake of comparison, to show the results from the P-doped and As-doped samples side by side, and interpret and discuss them on the basis of the theory in chapter.5.

6.A.1.Overall description

Figure.6.A.1 shows TPC decays at three temperatures, for the P-doped sample (a) and the As-doped sample (b), obtained at a LED pulsed electron density $N_e \simeq 6.10^{15} cm^{-3}$ (Table.4.3), plotted in log-log scale. The TPC presents two distinctive regions: a very slow decay region showing small slopes (almost flat) at short times, and a long power-law decay region at long times after a gradual turnover. As the temperature decreases, the turnover time increases in both doping cases. The slope of the long time region decreases considerably with decreasing temperature in the P-doped case, but shows only a slight

Figure.6.A.1.
TPC decays at 3 different temperatures
for the P-doped sample

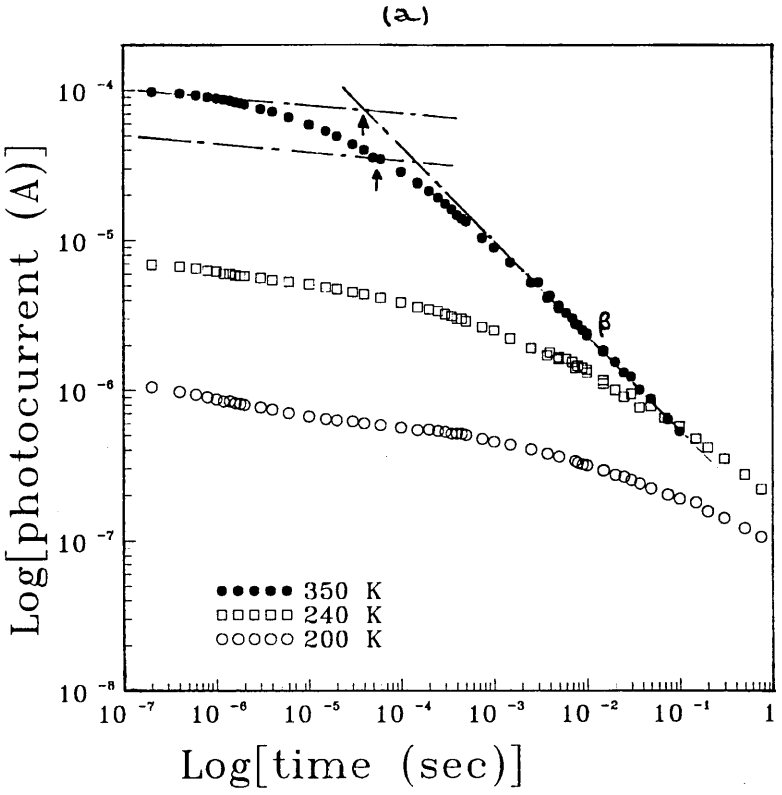

Fig.6.A.1
TPC decays at 3 different temperatures
for the As-doped sample

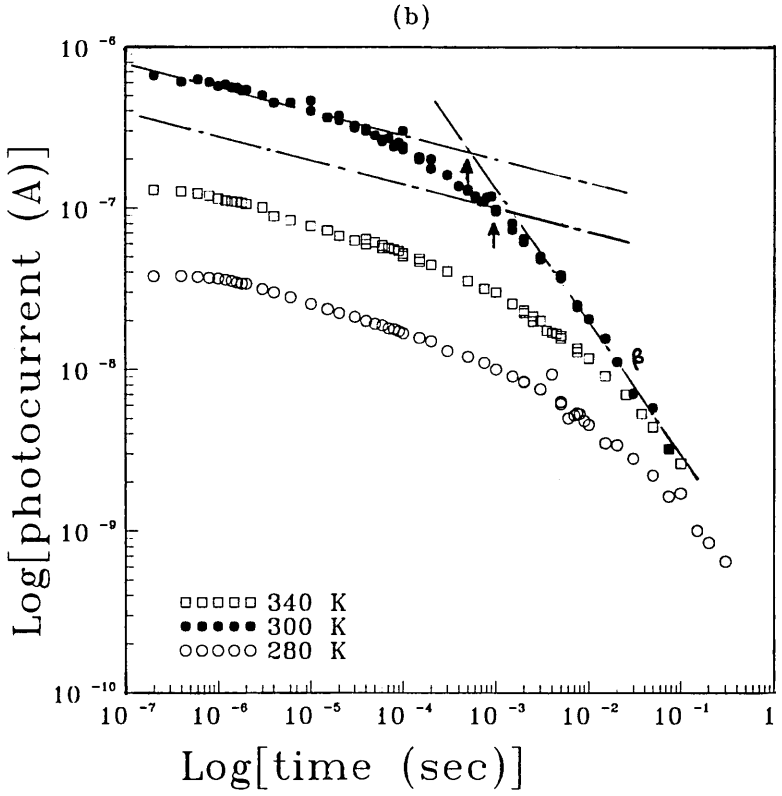

decrease in the case of As-doping. The small slope region at short times depends weakly on temperature.

6.A.2.The short time region of the TPC decay

This region covers the time range up to the turnover time. (For example at 300 K, $t \leq 10^{-4}$sec for the P-doped sample and $t \leq 10^{-3}$sec for the As-doped sample). This region can be identified with recombination free transport described in sect.5.A.1, and the turnover time identified with the recombination time t_r (sect.5.A.2). The time t_r is supposed to correspond to the point when the TPC falls 50 % below the extrapolated pre-turnover line (Seynhaeve, PhD thesis, 1989) (see arrow indications).

Because of the experimental time limitation ($t > 0.2$ μsec), the electron dispersive regime of the recombination-free transport can only be observed at low temperatures. Figure.6.A.2 shows low temperature TPC decays for (a) the P-doped and (b) the As-doped samples. The two sets of data present the same features: A well defined transition from dispersive transport at short times, characterized by a temperature dependent slope, to a smaller slope region which characterises the non dispersive transport. The dashed line on the figure separates the two regions and the indicated intercepts represent the observed "complete thermalisation times".

Figure.6.A.2.
The short time region of the TPC decay at low temperatures showing thermalisation in the CBT states and complete thermalisation at the indicated times t_t for the P-doped sample.

(a)

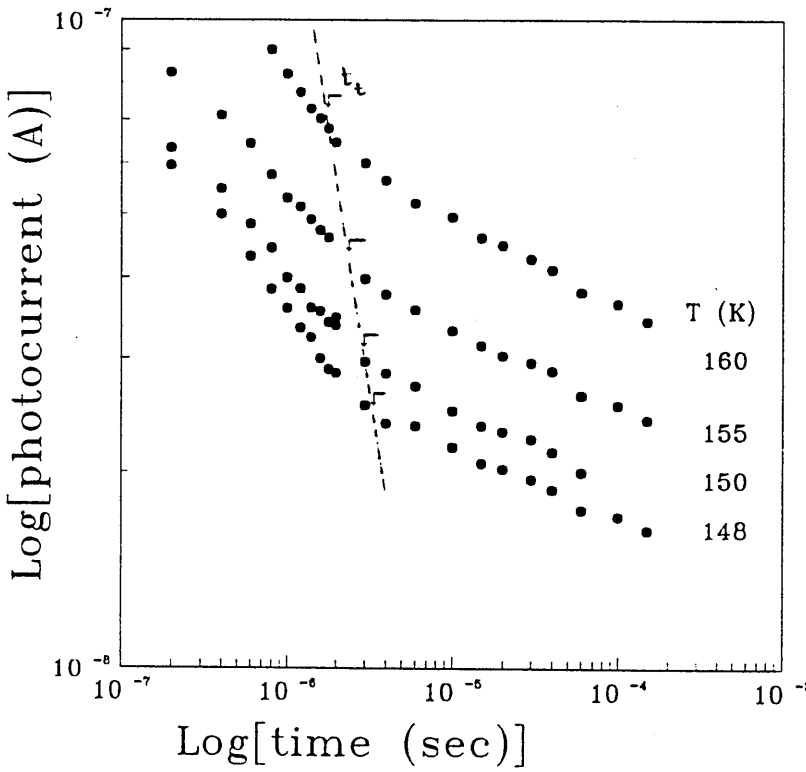

The short time region of the TPC decays at low temperatures showing thermalisation in the CBT states. The observed and actual complete thermalisation times t_0 and t_s are indicated by the arrows, for the As-doped sample.

(b)

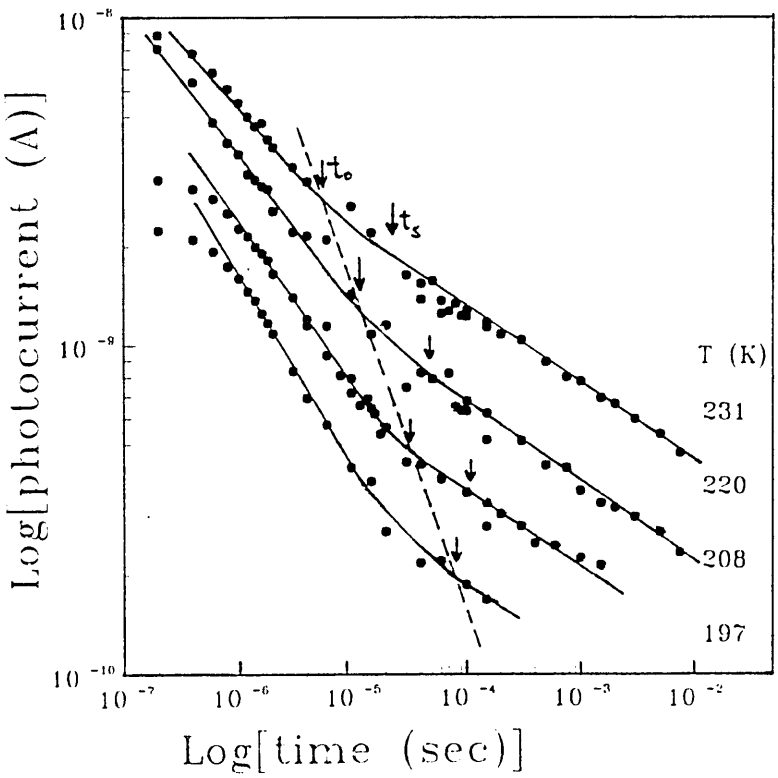

6.A.2.a.In the absence of optical bias

For the As-doped sample, the slopes of the dispersive region allow the determination of an average CBT characteristic temperature $T_c \simeq 470$ K (Eqn.5.A.21). As the temperature increases above $\simeq$ 250 K, this slope becomes comparable to the small slope in the non dispersive region and the transition can no longer be distinguished. Figure.6.A.3 (curve (As)) shows the Arrhenius plot of the electron drift mobility μ_d (Eqn.5.A.24) obtained from the non dispersive TPC taken at t = 200 nsec for T > 250K, and at the observed time of complete thermalisation t_0 (at the intercept points) for the temperatures of figure.6.A.2 (curves (b)). It turns out that the activation energy coincides with the dark Fermi-level position $E_{f0} \simeq$ -0.31eV indicating that the observed complete electron thermalisation occurs when the excess electron packet reaches E_{f0}. The choice of a delay time 200 nsec to replace t_0 above 250 K gives no significant error since the non dispersive TPC decays very slowly. In fact, the actual complete thermalisation (or saturation) occurs at $t = t_s$ calculated, for the present case of a moderate $N_e \simeq \alpha_c . N_{fn}$, by solving numerically Eqn.5.A.22 and indicated in figure.6.A.2 (b) by the arrows.

As for the P-doped sample, the transitions from dispersive to non dispersive transport are observed at shorter times and lower temperatures than for the As-doped sample. This indicates that the apparent complete thermalisation level is shallower than in the As-doped sample (Eqn.2.9.16). The Arrhenius plot in figure.6.A.3, curve (P), of the non dispersive μ_d (Eqn.5.A.32) measured at 200 nsec for T > 170 K, which includes also the low temperature values obtained from the TPC's of figure.6.A.2, curves (P), taken at the transition times t_t, yields an activation energy $E_t \simeq$ -0.17 eV which is much shallower than the E_{f0} position.

Since the TPC starts to level out at t_t, one immediately concludes that, in contrast to the As-doped case, the CBT in the P-doped case must present a sharp energy variation below E_t (Spear, 1988). The difference between the two cases is that, in the former case the increase in the steepness of the available or <u>effective</u> CBT DOS at E_{f0} (fig.5.A.1) arises from the existing thermal equilibrium or steady

Figure.6.A.3.
The Arrhenius plots of the electron drift mobility μ_d, As: As-doped sample, P: P-doped sample. The activation energies are indicated.

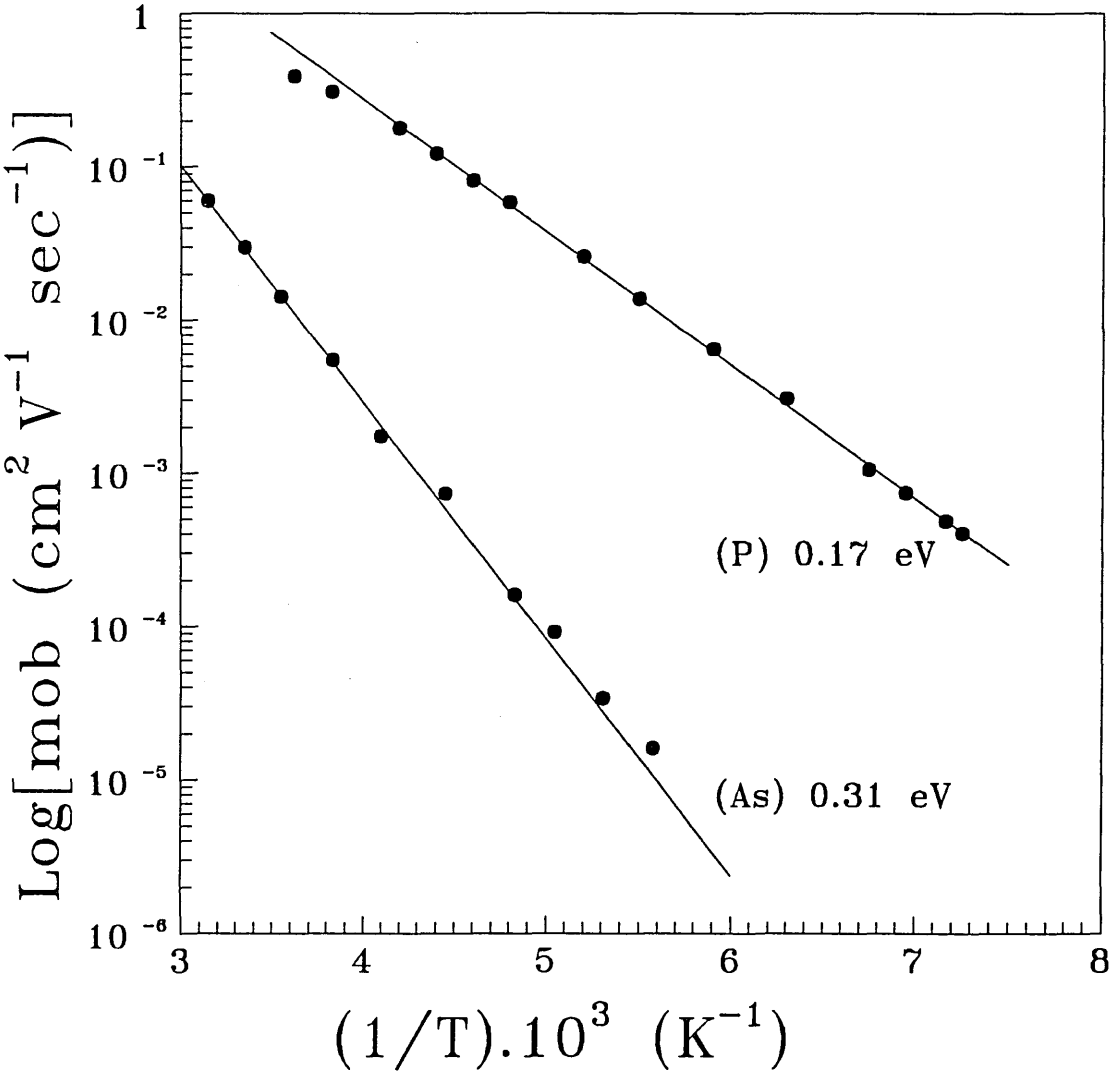

state occupation (the actual CBT is exponential above and below E_{f0}), whereas in the latter, the steepness in the actual CBT below E_t is structural and related to the sample quality. The pre-transition dispersive region in fig.6.A.2. shows slopes which yield, if an exponential g(E) is assumed above E_t, T_c values of $\simeq$ 218 K. If this is true, T_c will fall below 218 K for $E < E_t$, in disagreement with frequently reported T_c values ($\simeq$ 300 K) in the literature (for exemple, Furukawa and Matsumoto, 1983). It is concluded that the TPC over the time range below t_t does not reflect an exponential g(E) (Bhattacharya and Narasimhan, 1983). The location of the CBT "shoulder" at 0.17 eV agrees with the upper limit of the "time of flight" drift mobility result (0.14 -0.17 eV) obtained by Marshall et al (1986) where a linear portion of the CBT above the shoulder was found to fit the temperature dependence of the dispersion parameter α_c.

The present coplanar TPC results on both low quality As-doped and high quality P-doped a-Si:H samples can be distinguished from previous results (Hvam and Brodski, 1981, and Oheda, 1985) by observation in this work of the dispersive transport at short times which ends with a "plateau" non dispersive region. The drift mobility activation energies E_{f0} (for As-doping) and E_t (for P-doping) on one hand, and the "complete thermalisation times" t_0 (for As-doping) and t_t (for P-doping) on the other hand, are consistent with the multiple trapping equation.2.9.16 giving an "attempt to escape" frequency $\nu \simeq 1\text{-}3.10^{12}\text{sec}^{-1}$ (for As-doping) and $\nu \simeq 1\text{-}2.10^{11}\text{sec}^{-1}$ (for P-doping).

Hvam and Brodsky observed at 300 K, over the time range of the "plateau" region (10^{-7}-10^{-3}sec) studied here, a dispersive region followed by rapid recombination decay without level off in the TPC response. Oheda observed also pre-recombination power-law TPC decays with slopes of up to 0.3 and assigned them to states located 0.2 eV below E_c. In the present results, however, the drift mobility and, as will be seen below, the effects of optical bias and band tail saturation point to a multiple trapping non dispersive recombination free transport in this "plateau" region.

The Arrhenius plots of figure.6.A.3 are used to calculate the room

temperature free electron mobility μ_0 which can be deduced from the extrapolation of the Arrhenius plot at $T^{-1} = 0\ K^{-1}$ that represents the pre-exponential factor μ_{d0} of μ_d . For the P-doped sample, μ_{d0} equals $\mu_0.(N_c/N_t)$ (Eqn.5.A.32), and for the As-doped sample, μ_{d0} equals $\mu_0.(N_c/N_{f0})$ (Eqn.5.A.24). The results are shown in table.6.A.1.

Sample	μ_d (cm^2/V.sec)	μ_{d0} (cm^2/V.s)	$N_c/(N_t$ or $N_{f0})$	μ_0 (cm^2/V.sec)
P-doped sample	0.325	305	30 - 15	10 - 20
As-doped sample As	$5.13.\ 10^{-3}$	736	735	1

Table.6.A.1. Calculated mobilities from the TPC non dispersive region.

Note that, for the high quality P-doped sample, μ_0 is in good agreement with Marshall et al result (1985), but μ_d is three times less because of a larger E_t. The low μ_0 in the low quality As-doped sample may be due to a higher degree of disorder (sect.2.2).

6.A.2.b. Optical bias effect on the short time region

Figure.6.A.4 shows 300 K TPC decays obtained with the LED integrated pulse $N_e = 6.10^{15} cm^{-3}$ under the different steady state conditions (or OB levels) indicated for (a) the P-doped sample and (b) the As-doped sample. While in the P-doped case the effect of OB on the short time region is negligible, it is pronounced in the As-doped case. As explained in section.5.A.2, the reason for this effect is that the steady excitation tends to raise the QFL E_{fn} (by filling the tail states below it) which represents, for the As-doped case, the energy at which non-dispersive multiple trapping transport occurs, whereas this is represented in the P-doped case by E_t which lies well above E_{f0}, thus avoiding such trap filling effects. The rise in the short time TPC with OB was observed earlier by Pandya and Schiff (1983) and interpreted by them as being due to a reduction in deep D^- traps as a result of depopulation of D^0 states, under OB, through the reaction D^0 + hole $\longrightarrow$ D^+ (Pandya et al, 1984).

Figure.6.A.4.
The TPC decay shown for different OB levels at 300K (for the P-doped high quality sample)

(a)

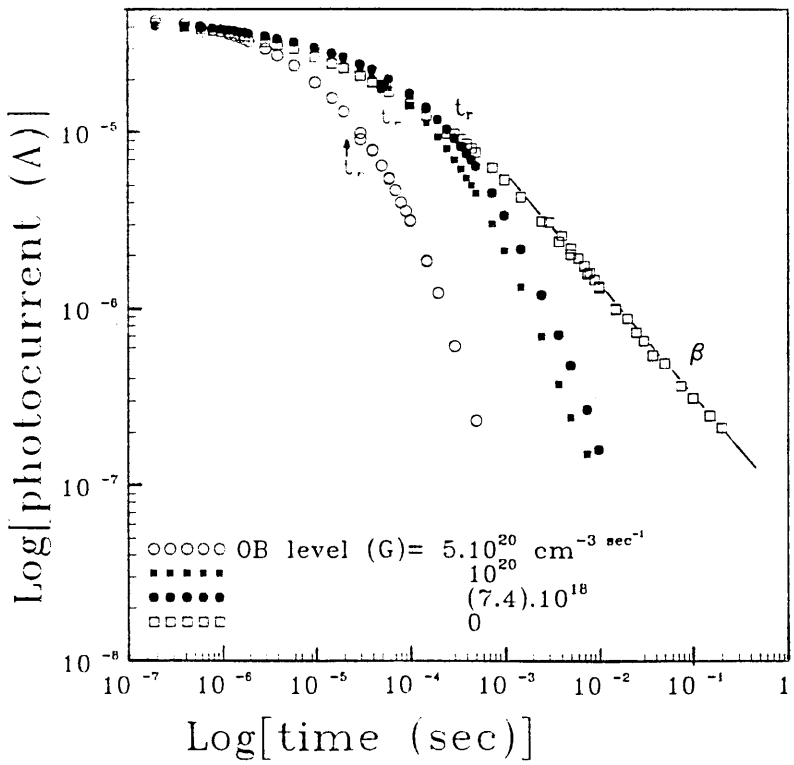

The TPC decay shown for different OB levels at 300K (for the As-doped sample)

(b)

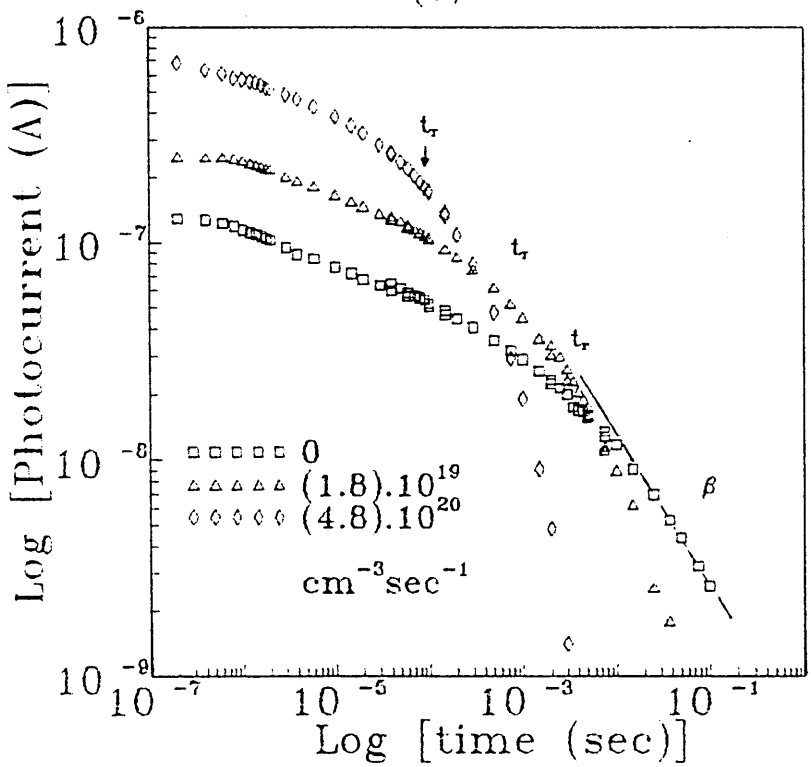

The electron QFL E_{fn} can be held fixed relative to E_{f0} by adjustment of the SSPC bias (Vomvas and Fritzsche, 1987) while measuring the temperature dependence of the non dispersive TPC, (see sect.4.4). The associated Arrhenius plot should present an activation energy equal to the E_{fn} position in the As-doped case. For the P-doped case, this method yields no additional information since the OB does not affect the short time region of the TPC. The experimental results from the As-doped sample are shown in figure.6.A.5 for three controlled E_{fn} positions, $E_{fn}-E_{f0}$= 0.03, 0.06 and 0.12 eV. The measured activation energies for each E_{fn} position are 0.32, 0.26, and 0.18 eV respectively, and the dark current plotted in the same figure shows an activation energy (or E_{f0} position) of 0.36 eV. The energies obtained by adding up the 200 nsec TPC activation energies to the QFL shifts are 0.35, 0.32 and 0.30 eV respectively. This result is readilly explained by the fact that, in the As-doped sample, the electron packet thermalises to the trap QFL E^t_{fn} above E_{fn} and the difference $E^t_{fn}-E_{fn}$ increases with the OB level from 0.01 eV (for E_{fn} shift of 0.03 eV) to 0.06 eV (for E_{fn} shift of 0.12 eV). This method could be used to determine the parameter r and the ratio of free hole to free electron density (p/n) (Eqns.2.9.9 and 2.9.11). Note that in this paragraph the E_{f0} position is deeper than reported in other parts of the text because the measurements were done in a later time after the sample has suffered some light changes.

6.A.2.c Excitation dependence of the short time TPC

Figure.6.A.6 shows the dependence of the non-dispersive TPC on pulsed excitation density measured on the As-doped sample in the absence of OB at a delay time t = 200 nsec for three different temperatures. The calculated curves from Eqns.5.A.12 and 5.A.20 are superimposed on the data showing an excellent fit over three orders of magnitude. The parameters used here are shown in table.6.A.2 with E_{f0}= 0.31 eV (Main et al, 1990).

$G_c(cm^{-3}eV^{-1})$	$T_c(K)$	$N_c(cm^{-3})$	$\mu_0(cm^2.V^{-1}.sec^{-1})$
$1.5.\ 10^{21}$	470	$K.T.G_c$	1

Table.6.A.2. Parameters used for the excitation dependence of the short time TPC in the As-doped sample.

Figure.6.A.5
Arrhenius plots of optically biased TPC at the delay time 200 nsec for three positions of the QFL E_{fn}. The dark current curve is also shown.

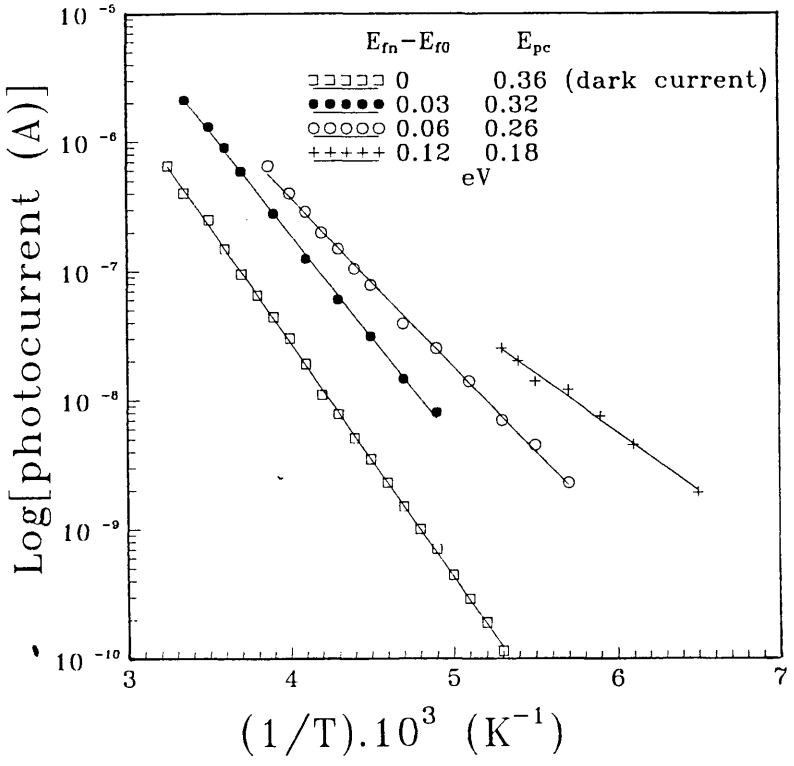

Figure.6.A.6.
The excitation dependence of the short time (200 ns) TPC for the As-doped sample at three different temp--eratures and for the P-doped sample at 200 K The solid curves are calculated for the As-doped case and the dashed line is the best fit to the P-doped case data.

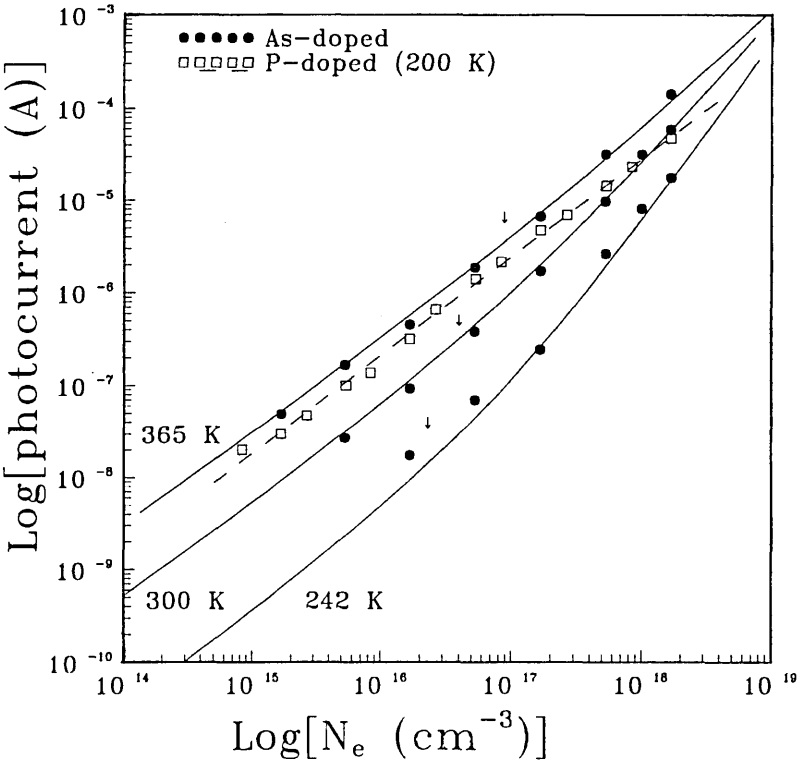

All the features described by the theory (sect.5.A.2) are comfirmed by the data (Main et al, 1990). Namely, the transition from a low excitation linear response to a high excitation superlinear response occuring at the excitation density $N_e = \alpha_c . N_{f0}$ corresponding to E_{f0} as a saturation level (see indication by arrows) and the temperature dependence of the superlinear slope as $1/\alpha_c$.

The excitation dependence of the 200 nsec TPC from the P-doped sample measured at 200 K is included in figure.6.A.6 (open squares). Even at T = 200 K $\ll T_c$, the superlinear response characterisic of the saturation effect is not observed; A linear response is rather seen over the whole excitation range, which is predicted by Eqn.5.A.33 for a sharply varying conduction band tail (see sect.5.A.2).

More information on the saturation effect in the As-doped sample is given in figure.6.A.7 which shows the Arrhenius plots of the 200 nsec TPC for a range of fixed N_e, from the maximum laser pulse generated electron density $N_e = 1.67\ 10^{18}\ cm^{-3}$ to 0.01 % N_e. Again, the data are fitted to the theoretical curves calculated from Eqn.5.A.22, and Eqn.5.A.26. The experimental deviation above the theoretical curves at low temperatures and/or low excitation is due to incomplete thermalisation at the delay time of 200 nsec. The two lowest curves were measured by the LED and the highest of them which was used for the μ_0 determination (sect.6.A.2.a) includes the corrections for the observed complete thermalisation times t_0 (fig.6.A.2) (note that the Laser beam for the four higher curves was covering only $\simeq$ 0.4 of the gap length, and therefore the LED curves should be scaled down by a factor of 0.4 for comparison). Well defined activation energies from the slopes are attributed, according to Eqn.5.A.20, to the saturation energy levels E_{ds} for the appropriate excitation densities N_e. The lowest curve corresponding to $N_e = (1.68).\ 10^{14} cm^{-3} \ll \alpha_c . N_{fn}$ lies well in the linear region with an activation energy of 0.34 eV indicating an observed saturation near E_{f0}. On the other hand, the highest curve ($N_e = 1.68.\ 10^{18} cm^{-3}$) with an activation energy of 0.14 eV indicates saturation occurring at $\simeq$ 0.2 eV above E_{f0}.

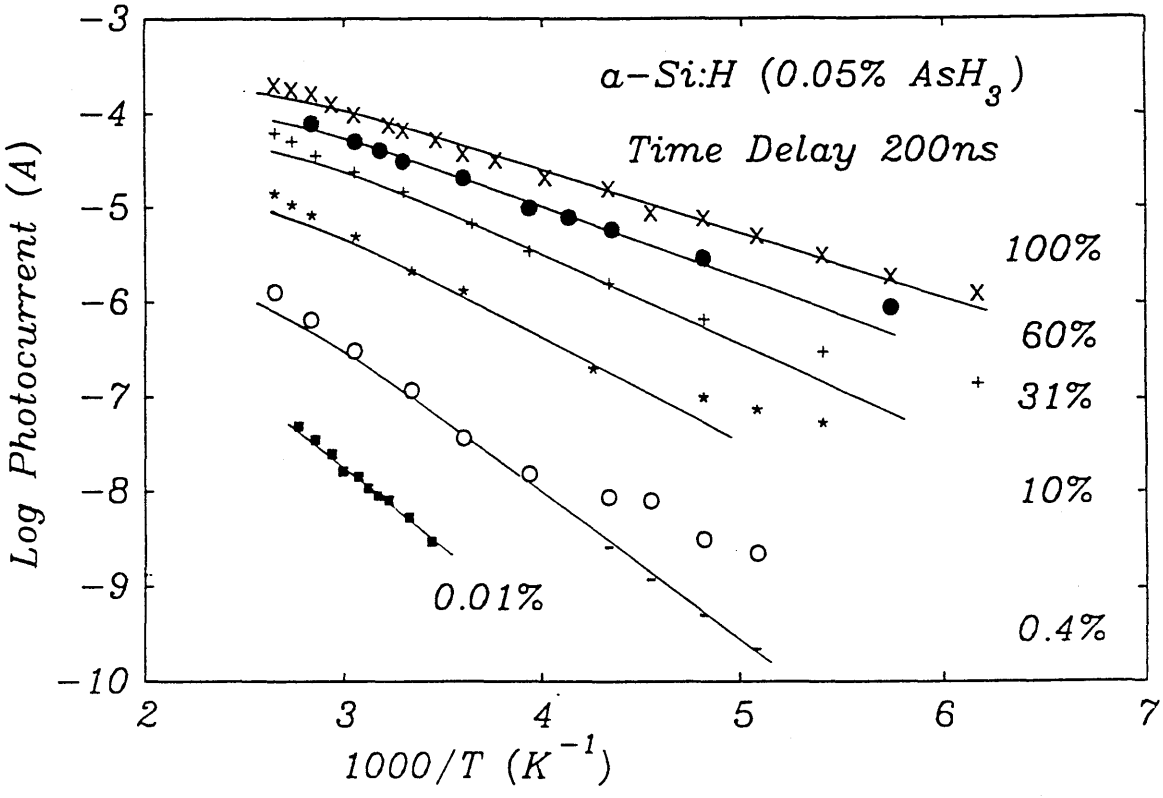

Figure.6.A.7. Arrhenius plots of the 200nsec TPC for a range of fixed excitation densities, from $N_e=(1.67).10^{18}$ cm^{-3} to 0.01% N_e, the solid lines are theoretical. In the 0.4% N_e curve, correction of the low temperature 200nsec TPC was made by taking the TPC at t_0 (see Fig.6.A.2b). Activation energies obtained from the slopes are 0.14, 0.16, 0.19, 0.23, 0.31 and 0.34 eV from top to bottom.

6.A.2.d. Saturation under optical bias

The OB effect on the short time TPC excitation dependence is shown in figure.6.A.8 which contains measurements from Odense University on the 0.01 % As-doped sample (Table.4.2) (see method in sect.4.3.2). Curve fitting to the non biased data was obtained using the parameters used for the 0.05 % As-doped sample (Table.6.A.1) with $E_{f0} = 0.35$ eV, but the fitting to the biased data required knowledge of the E_{fn} position. This was determined by finding first the biased saturation level E_{ds} for the highest excitation $N_e = 4.2.\ 10^{17} cm^{-3}$ from the ratio of the biased to the non biased TPC, and then using Eqn.5.A.27 to calculate E_{fn} (Table.6.A.3).

T (K)	E_{ds} (eV)	E_{fn} (eV)	N_{fn} (cm^{-3})	bias ↓ N_{e0} (cm^{-3})	non bias ↓
300	-0.221	-0.259	$4.63.\ 10^{16}$	$3.\ 10^{16}$	$4.9.\ 10^{15}$
243	-0.207	-0.254	$7.1.\ 10^{16}$	$3.67.\ 10^{16}$	$3.44.\ 10^{15}$
204	-0.200	-0.252	$8.7.\ 10^{16}$	$3.78.\ 10^{16}$	$3.37.\ 10^{15}$

Table.6.A.3. Calculated E_{fn} for a fixed OB level $\simeq$ 8.10^{16} $cm^{-2}sec^{-1}$ at three temperatures, from high pulse excitation $N_e = 4.2.10^{17}$ cm^{-3}.

It should be noted that this method for determining the QFL position E_{fn} shows no significant temperature dependence of E_{fn}. With a fixed high OB level of 25 mW cm^{-2} (equivalent to $\simeq 8.10^{16} cm^{-2}sec^{-1}$), the linear to superlinear transition point shifts to higher N_e (see the arrow indications in the figure and the N_{e0} column in the table). This occurs following the E_{fn} rise and the consequent N_{fn} increase. The experimental deviation at 204 K is thought to arise from incomplete thermalisation at the delay time of measurement (100 nsec).

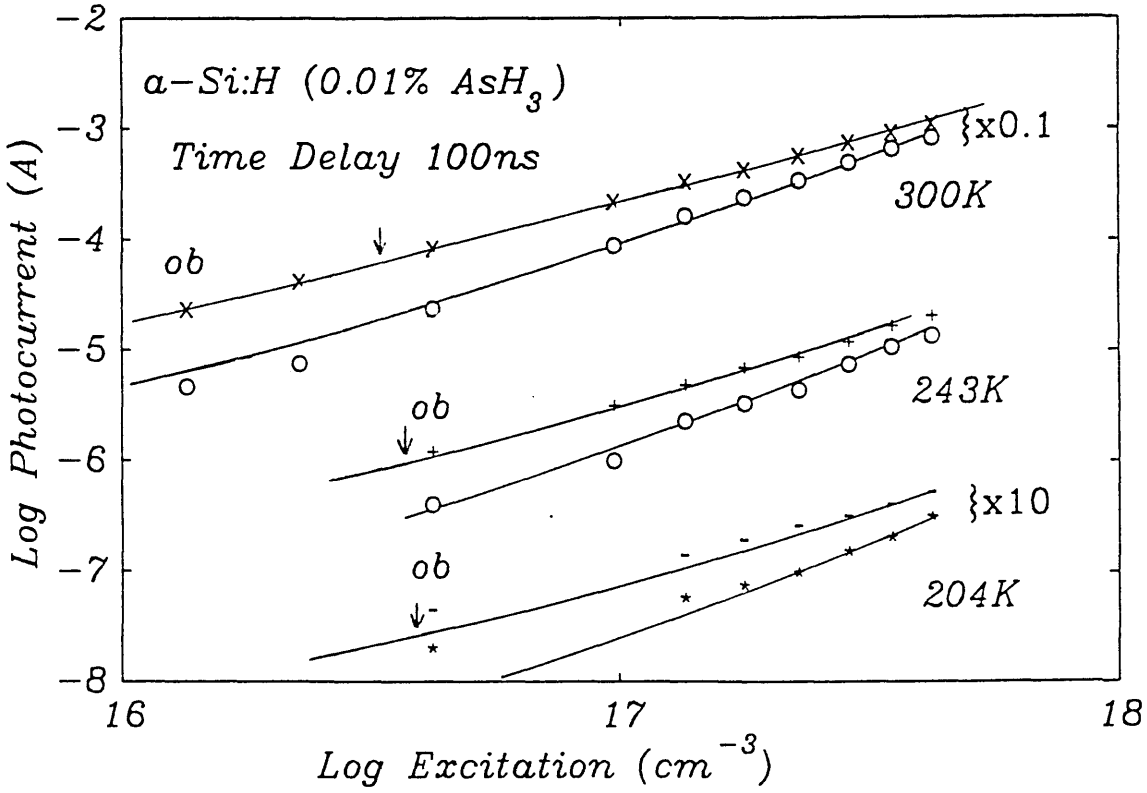

Figure.6.A.8. TPC at 100nsec as a function of excitation density at three temperatures for the 0.01% As-doped sample. The figure includes the effect of 25 mW (ie $\simeq 8.10^{16}$ cm^{-3}) OB, the solid lines are theoretical. The deviation from theory at 204K is due to incomplete thermalisation at 100nsec.

6.A.2.e. The Conduction Band Tail density of states (DOS)

The measured "short time" photocurrent excitation dependence can well be used, with Eqn.5.A.31.b, for the experimental determination of the DOS or an effective DOS (Main et al, 1990) for both sample types. The dark current I_d, or the steady state photocurrent I_{SSPC} under OB, should be measured simultaneously with the TPC to experimentally determine the probe energy using the ratio $R = I_{SSPC} / I_{TPC}$ (Eqn.5.A.29).

For the As-doped sample As, the slope of the superlinear region in figure.6.A.6 gives α_c (Eqn.5.A.28), and the actual DOS $g(E_{ds})$ is deduced for each temperature (Fig.6.A.9). The DOS $g(E_{ds})$ is also obtained from figure.6.A.7 for the set of data points corresponding to 300 K and plotted in the same figure.6.A.9 (open circles).

As for the P-doped sample, the effective DOS N_t at E_t is deduced (Eqn.5.A.35) from the 200 K curve in figure.6.A.6 with $E_t \simeq 0.17$eV (Fig.6.A.3). The DOS $g(E_t)$ assumed to be (1/k.T) times higher than N_t is shown in figure.6.A.9, with the As-doped DOS, for all excitation levels.

Figure.6.A.9 includes also the modelled exponential DOS with T_c=470 K up to E_c for the As-doped case and T_c=270 K below E_t=0.16 eV (see Steady state results below) for the P-doped sample. The P-doped DOS data inverted from the 200 K curve in figure.6.A.6 for the energy E_t lie well around the modelled P-doped DOS.

6.A.3. The long time region of the TPC decay

This region covers the time range beyond the "turnover time" attributed to the hole effective recombination time t_r (sect.5.A.2). A long power-law decay, of index β follows after a slow curvature which marks the transition from the recombination free regime to a regime dominated by recombination (fig.6.A.1).

Figure.6.A.9
The conduction band tail DOS deduced from the excitation dependence of the short time (200 nsec) TPC in figures.6.A.6 and 6.A.7 for the P-doped sample (P) and the As-doped sample (As). The solid lines are the model exponential DOS's.

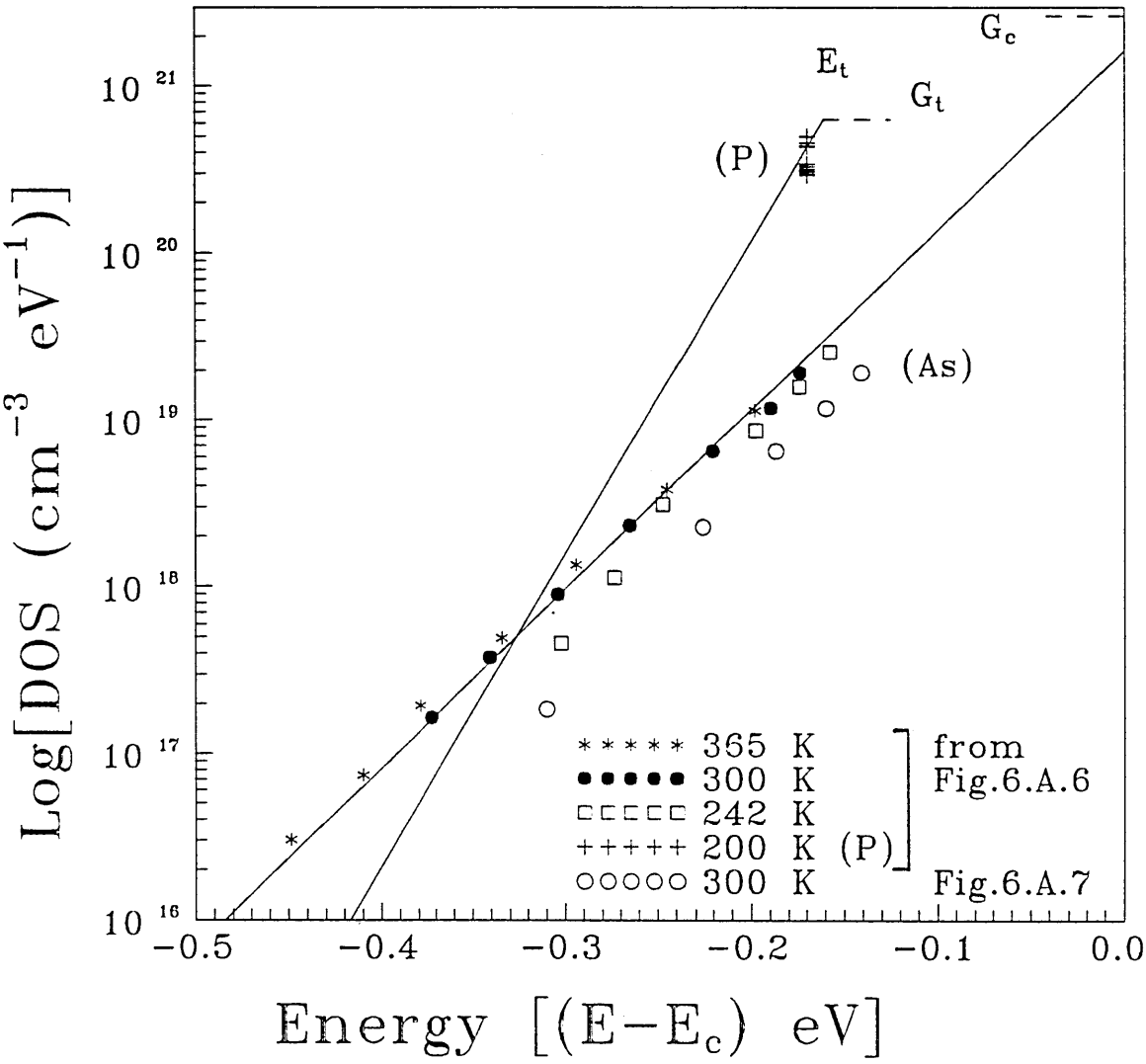

6.A.3.a.In the absence of OB

The power-law index β

As explained in the TPC model (sect.5.A.2), the slow power-law region is thought to reflect a hole recombination limited process. Figure.6.A.10 presents the temperature dependence of the power index β measured as the slope of the TPC in the logarithmic scale (Fig.6.A.1) and plotted as β versus T for both sample types.

The data from the P-doped sample form a linear plot (P) which extrapolates to the axis origin, and whose inverse slope should represent the average characteristic temperature T_v of the valence band tail (Eqn.5.A.47), giving $T_v \simeq 582$ K. A smaller value $T_v = 486$ K was measured by Werner et al (1987) from the TPC method for an undoped sample. And a rather higher value $T_v = 700$ K was obtained by Main et al (1987) for a P-doped sample.

The low quality As-doped sample does not show well defined TPC slope and the average β gives a data scatter when plotted against the temperature (Fig.6.A.12). This leads to the conclusion that the valence band tail (or at least the portion of the VBT located above E_r) is not exponential, provided the recombination mechanism is limited by hole release in this material also.

The effective recombination lifetime t_r

As already mentioned in section.6.A.2, The effective recombination lifetime t_r represented by the "turn over time" is determined by taking the time at which the current falls to 50 % of the extrapolated non dispersive current. This method assumes recombination of half the carrier concentration at t_r.

In figure.6.A.11 are shown Arrhenius plots of t_r for the P-doped (P) and the As-doped (As) samples, and the figure includes also the curves plotted with t_r obtained simply from the intercept of the two TPC regions. According to Eqn.5.A.42, the critical energy level E_r is given by the measured activation energy of t_r, giving $E_r = 0.32$ eV and

Figure.6.A.10
Temperature dependence of the dispersion parameter (β) (or power-law index) for the P-doped sample (P) and the As-doped sample (As).

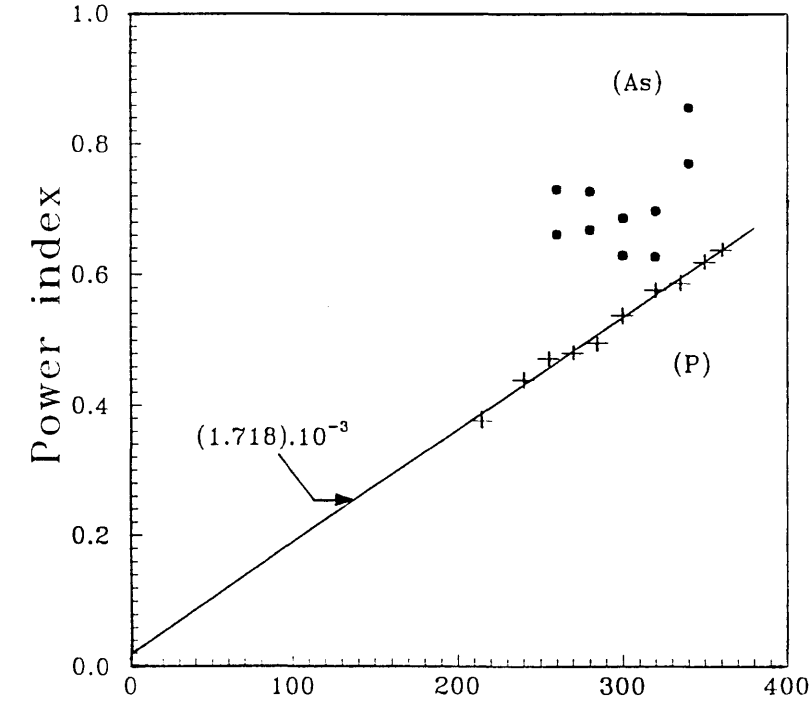

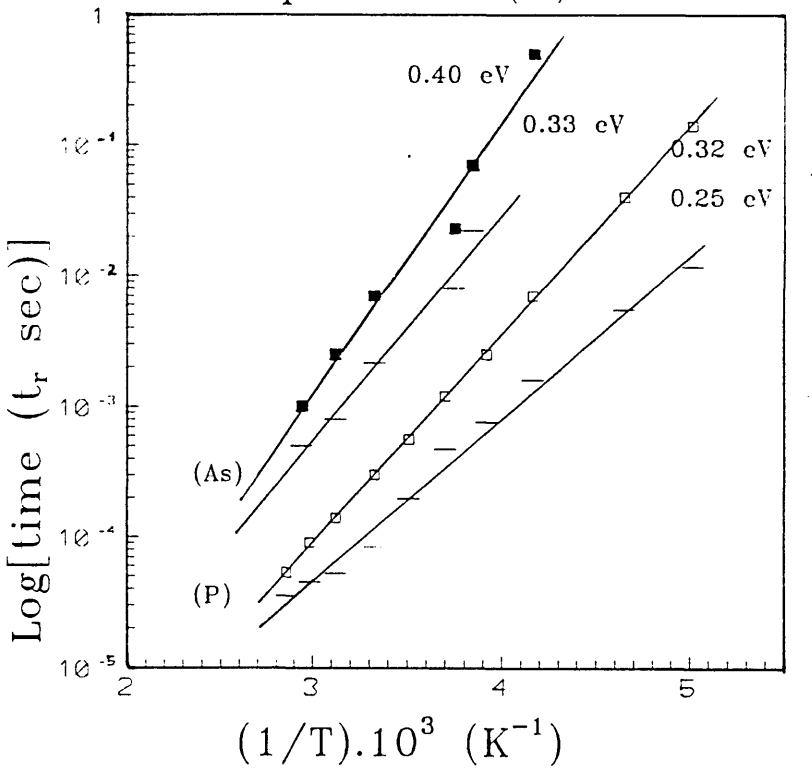

Figure.6.A.11
Arrhenius plots of the effective recombination time t_r determined in two ways: i) taking the average time of intersection of the two TPC regions (horizontal bars) and ii) taking the time at which the current falls to 50 % of the extrapolated region (open and closed squares) for the P-doped sample (P) and the As-doped sample (As). The activation energies are shown

0.40 eV for the P-doped and the As-doped samples respectively. It is clear that such energy depths can not be attributed to the electron thermalisation, since complete electron thermalisation has already been shown to occur at $E_t \simeq 0.17$ eV and at $E_{f0} \simeq 0.32$ eV for the P-doped and the As-doped samples respectively.

Oheda (Oheda, 1987) obtained an activation energy for t_r of 0.18 eV by assigning t_r to the intercept of the two TPC regions, and pointed out the inconsistency between this and the energy of 0.46 eV calculated for 298 K at t_r using the thermalisation Eqn.2.9.16 with $\nu = 10^{12} sec^{-1}$. This point will be discussed further after the discussion of the OB effect on β and t_r.

6.A.3.b. Recombination effects in the presence of OB

The OB effect on the recombination region is well demonstrated in figure.6.A.4 : Accelerating the TPC decay and shortening the effective recombination lifetime t_r, as the bias level increases the TPC decay changes from a power-law to an exponential time dependence for both sample types.

Figure.6.A.12 shows the OB dependence of the measured average t_r for the P-doped sample at a number of indicated temperatures. The OB level is estimated in terms of the steady state generation rate G. The curves obtained are in good agreement with the hole thermalisation theory in section 5.A.2. This theory predicts that t_r remains unchanged by low OB levels since the shift of E_{fp} towards E_r is not large enough to cause a shift of E_r according to the criterion of Eqn.5.A.51. As the OB level increases, E_{fp} shifts closer to E_r which has now to move towards E_v, resulting in the gradual decrease of t_r. At lower temperatures, E_{fp} shifts more for the same OB level, and t_r starts to decrease at lower OB levels. The figure includes the corresponding theoretical curves obtained by solving numerically Eqn.5.A.51 for E_r' at a variable OB level G. Here the QFL E_{fp} is calculated by assuming a constant hole lifetime τ_p in a monomolecular recombination process (cf interpretation of SSPC sect.6.B.1),

$$E_{fp} = E_v - k.T.\log (G.\tau_p/N_v) \qquad (6.A.1)$$

Figure.6.A.12
Dependence of the effective recombination time t_r on the OB level G for the P-doped sample at five temperatures: from top to bottom, 240, 270, 300, 350 and 370 K. (see details in text).

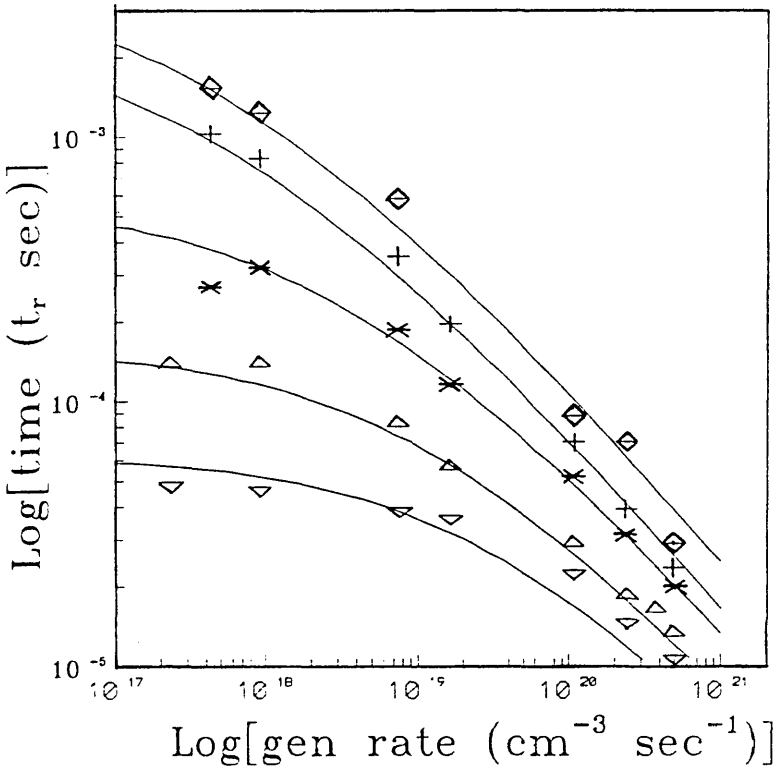

Figure.6.A.13
The OB level (G) dependence of t_r at 270 K for the P-doped sample including the theoretical curves for both t_r and t_p, showing the possibility of E_{fp} to cross the hole recombination energy E_r at high OB levels corresponding to the region where $t_p < t_r$.

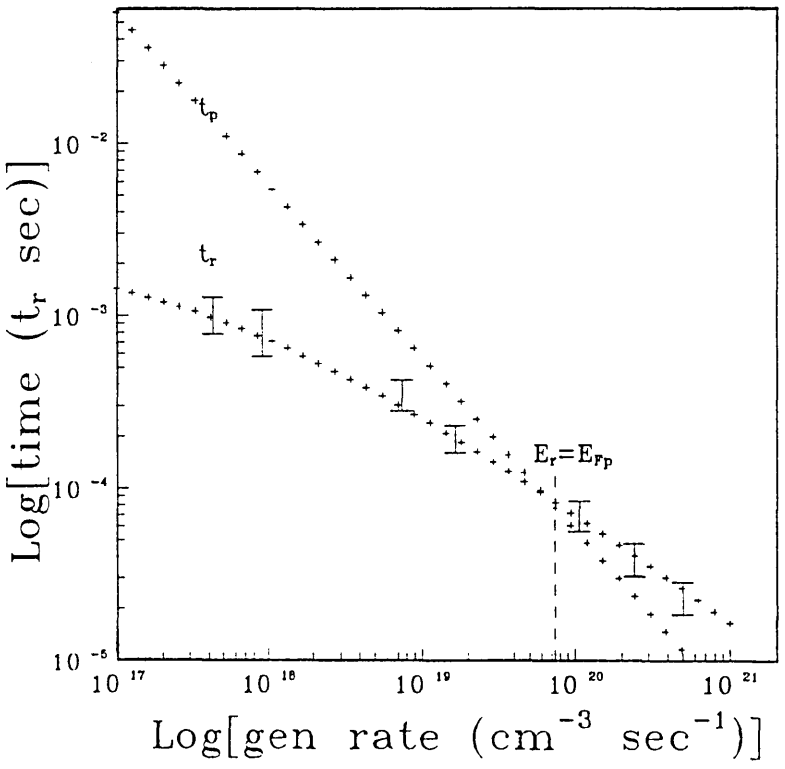

Without invoking the possible temperature and energy dependences of the hole capture coefficient β_p (Okushi et al, 1982, 1983), reasonable fits at various temperatures are obtained for the parameters indicated in table.6.A.4.

T (K)	β_p (cm^3 sec^{-1})	T_v(K)	δE_r / δE_{fp} (eV)
370	$3.\ 10^{-9}$	635	0.521-0.448 0.745-0.452
350	$3.\ 10^{-9}$	635	0.519-0.434 0.705-0.427
300	$2.5.\ 10^{-9}$	595	0.471-0.379 0.604-0.366
270	$3.5.\ 10^{-9}$	570	0.458-0.354 0.544-0.330
240	$2.\ 10^{-9}$	540	0.371-0.312 0.340-0.293

Table.6.A.4. The parameters β_p and T_v used to obtain the curve fitting of figure.6.A.12, the last column contains the intervals δE_r and δE_{fp} of E_r and E_{fp} positions corresponding to the OB range 10^{17}-$10^{21}cm^{-3}sec^{-1}$.

The effective VBT DOS $g'_v(E)$ (Fig.5.A.4) falls sharply above E_{fp}. Its integral above E'_r must then be significant only over a range of a few k.T above E'_r at significant OB levels. Therefore, it appears reasonable that T_v changes from 635 K at deep energy levels above $\simeq$ 0.45 eV to $\simeq$ 540 K for shallow energy levels (close to E_v) below $\simeq$ 0.36 eV with intermediate values of 590 and 570 K (cf.Table.6.A.1). The average value T_v = 582 K measured from the TPC slope β (Fig.6.A.12) lies well in between these two values. This change in T_v is small or may be negligible when compared to the change proposed by Hack et al (1984), occurring at 0.3 eV above E_v, from 1500 to 500 K. The hole "attempt to escape" frequency $\nu = N_v.\beta_p$ = 1.5 to 2.10^{11} sec^{-1} is exactly the same as the electron one (see sect.6.A.2 above) and reasonable, noting that a value of $10^{11}sec^{-1}$ has been reported for electron capture (Tiedje, 1984).

As expected by the theory (sect.5.A.2), it can be shown that at

high OB levels and/or low temperatures, E_r' is located above E_{fp}, and E_{dp} crosses E_{fp} at $t_p = \nu^{-1}.\exp[(E_{fp}-E_v)/k.T]$ before it reaches the recombination level E_r' at t_r. This is shown in figure.6.A.13 for the temperature 270 K, where the t_p versus G curve does indeed cross the t_r versus G curve. The crossing point at this temperature occurs under an OB level $G = 7.10^{19}cm^{-3}sec^{-1}$ for which $t_r = t_p = 8.10^{-5}$sec, ie for which the recombination sets on when E_{dp} reaches $E_r = E_{fp} \simeq 0.38$ eV above E_v.

Finally, returning to the temperature dependency of t_r under no OB, the activation energy 0.32 eV of t_r is inconsistent with the attempt to escape frequency $\nu = 1.5\text{-}2.10^{11}sec^{-1}$ in table.6.A.4; When taken at fixed temperatures, t_r is related, according to equation.5.A.42, to deeper energies (for example at 300 K, $E_r - E_v \simeq 0.46$ eV) as already pointed out by Oheda (1987). Moreover, the maximum energy the hole packet can reach before recombination is 0.52 eV as deduced from the constant t_r region of the 350 or 370 K curve of figure.6.A.12.

A possible explanation which can account for this discrepancy is to assume that, unlike under steady state OB, in the dark case the hole packet thermalises to states located 0.4 to 0.5 eV above E_v known as "safe hole traps" (McMahon et al 1990) from where the holes are released to a certain energy level, of high density of states E_{vt}, around 0.15 eV above E_v, and recombine by tunneling from E_{vt} to D^- DB states (McMahon, 1989). The hole release time from E_r will now be given by

$$t_r = \nu_0^{-1}.\exp[(E_r - E_{vt})/k.T]. \qquad (6.A.2)$$

As the step limiting the recombination is hole release from deep states, t_r is practically the effective recombination lifetime, and $E_r - E_{vt} \simeq 0.32$ eV leads to an attempt to escape frequency $\nu_0 \simeq 8.10^{8}sec^{-1}$ (McMahon, 1990) reduced from ν by the tunneling process.

A temperature dependence of ν could also account for this discrepancy. However, this requires an increase of ν as the temperature decreases, with an activation energy of $\simeq 0.15$ eV, in disagreement with the ICTS measured temperature dependence of ν for electron case (Okushi, 1983) which increases with temperature.

It remains now to explain the low t_r activation energy 0.18 eV measured by Oheda. First, it may be that the association of t_r with 50 % of the extrapolation of the pre-recombination line at t_r is a better method as shown in figure.6.A.11. However, even by using the intercept of the two TPC regions, 0.26 eV measured in this work is higher than Oheda's result. The excitation intensity used by Oheda (a pulse energy of 1 μJ from a Laser light of a photon energy of 2.02 eV onto a 2x5 mm^2 gap area of a 2 μm thick sample) lies above $10^{17} cm^{-3}$, ie in the high excitation range, which may lead to some second order effects. This argument may also account for the feature of the long time TPC decay of Oheda (1987) observed near $\simeq$ 0.1 sec, which is absent in the present results (Fig.6.A.1 (a)).

6.B.The steady state results

The SSPC model described in chapter.5 was meant for high quality n-type a-Si:H characterized by a sharp CBT. Therefore, the curve fitting and explanation apply only to the P-doped samples. The results from the As-doped sample require a rather different interpretion.

6.B.1. The P-doped sample results

The model can explain the SSPC features (Fig.6.B.1) observed at different temperature ranges (a) and the excitation dependence represented by the power index γ as a function of temperature (b). In particular, the small activation energy (0.11-0.13 eV) and power index $\gamma < 0.5$ measured in this work can be explained.

6.B.1.a. Comparison of the results with the model

Experimental Results

Figure.6.B.2 shows (a) the temperature dependence and (b) the excitation dependence of the SSPC. Over the measurement temperature range in (a), a small activation energy ($\simeq$0.13 eV) is found, which decreases gradually with increasing temperature towards the maximum photocurrent, and this feature moves to lower temperatures as the excitation intensity G decreases. Sub-square root dependence on G ($\gamma < 0.4$) is observed in (b) at temperatures lower than $\simeq$ 220 K over a wide range of G (2.10^{17}-4.10^{20}). As the temperature increases above 220 K, the low excitation ($G < 5.10^{18}$) region starts to bend towards super-square root dependence, whereas the portion corresponding to $G > 5.10^{18}$ follows the same dependence as in low temperatures with slightly increasing γ with temperature, but not exceeding 0.4.

It is usefull to refer to the data of Vomvas and Fritcshe (V.F) (Fig.6.B.3) on (a) the temperature and (b) the excitation dependences of SSPC (Vomvas and Fricshe, 1987), since these cover the whole temperature range and thus constitute a good reference to the model. The curve in (a) is divided into three regions: Region.(I) of very

Figure.6.B.1.
The modelled temperature dependence of the SSPC for the generation rate $G=(5.5).10^{18}/cm^3s$ and a quantum efficiency $\eta=1$

(a)

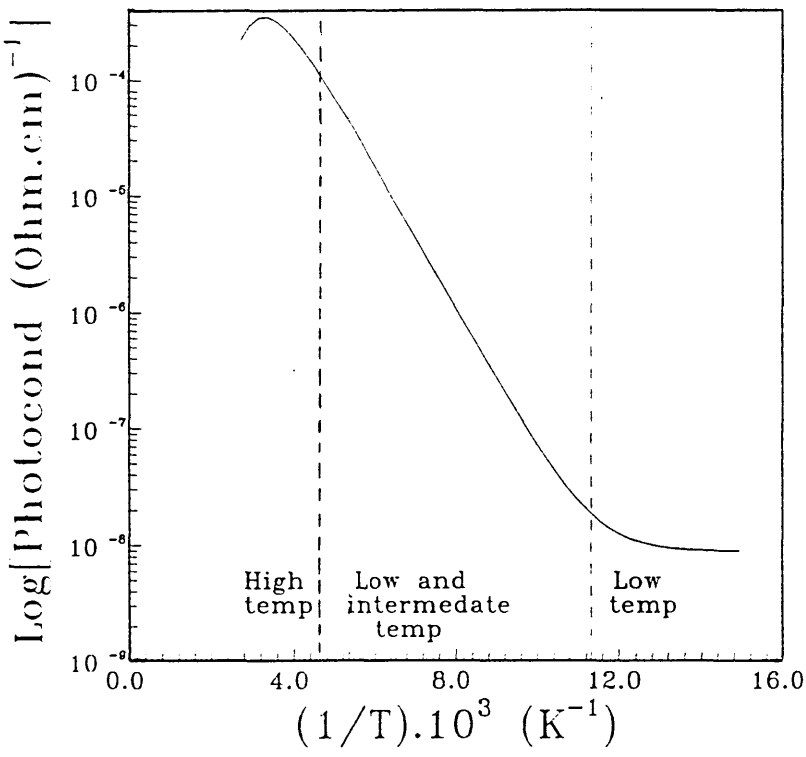

The modelled temperature dependence of the SSPC power index γ for the P-doped sample.

(b)

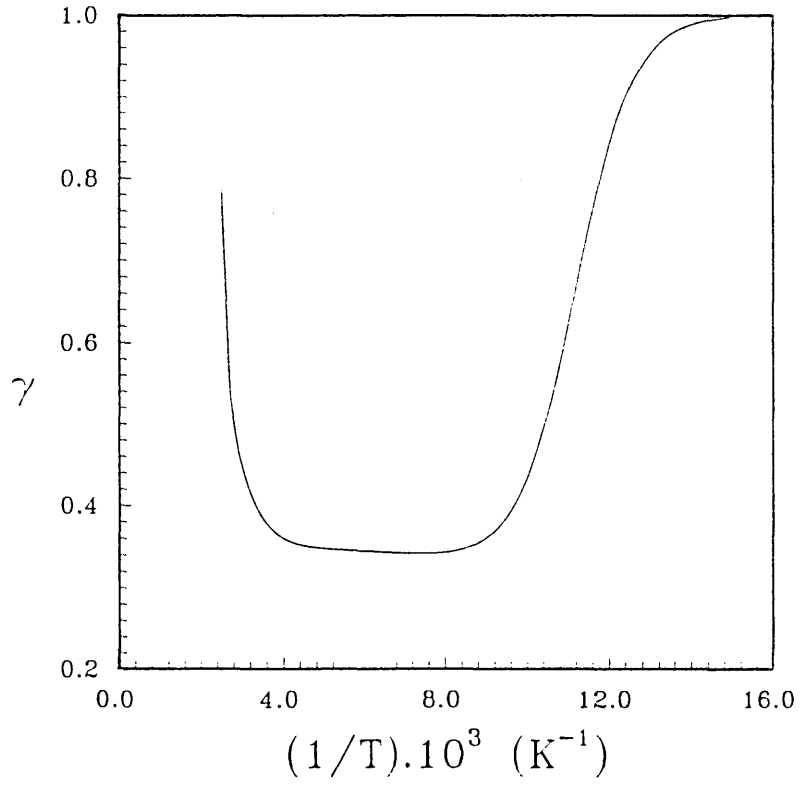

Figure.6.B.2.
Dependence of the SSPC and the dark current on the inverse temperature for the P-doped sample. The model curves are fitted to the data and the activation energies in the activated region of the SSPC curves (E_{pc}) and of the dark current curve (E_d) are indicated. The excitation levels are also shown.

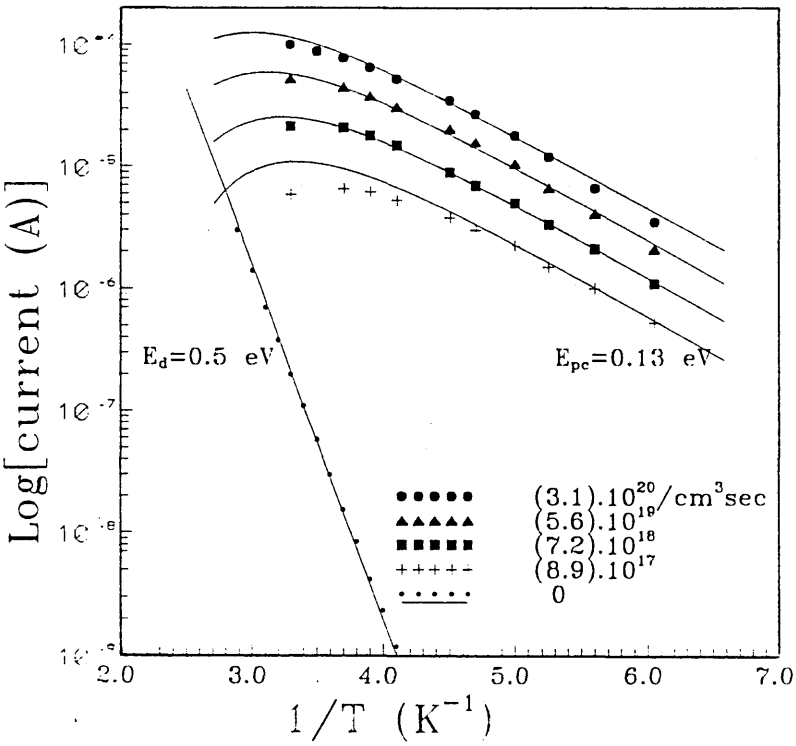

Dependence of the SSPC on the Generation rate at four temperatures for the P-doped sample. The solid lines are the model curves. The power index γ is indicated for each temperature.

(b)

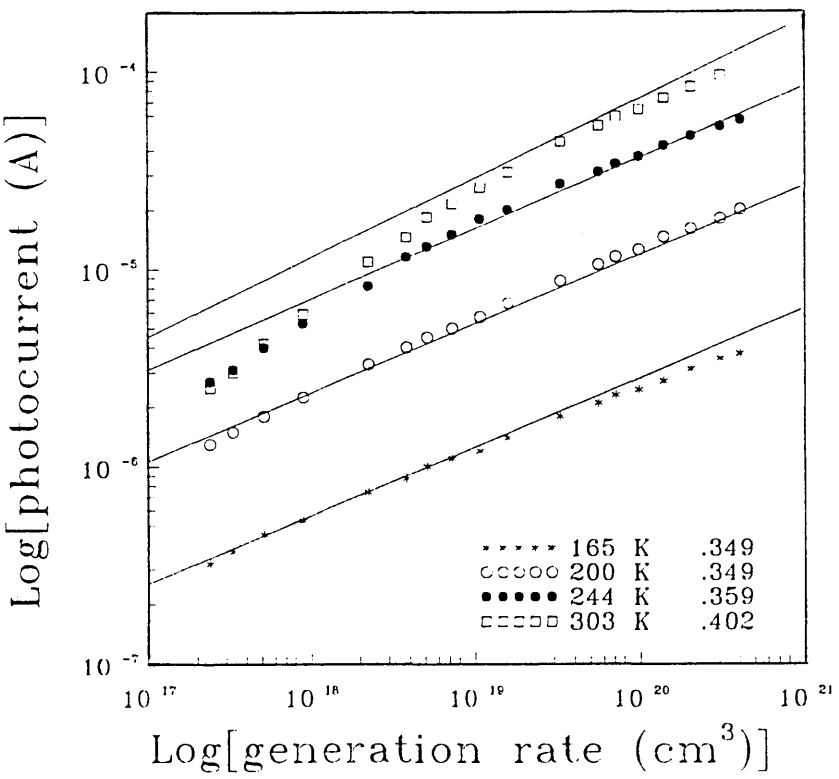

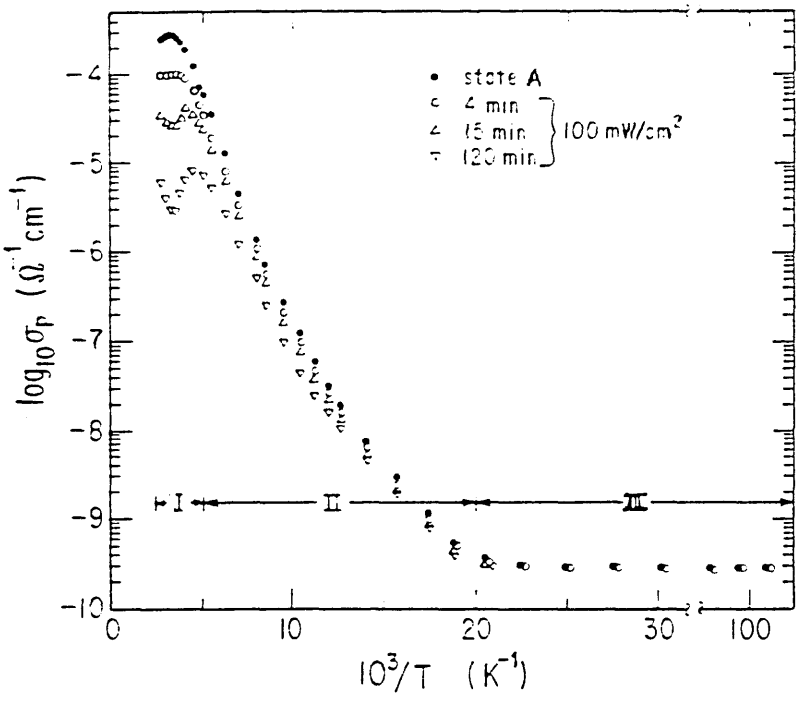

Fig.6.8.3.Photoconductivity measured with $0.1 mW/cm^2$ of n-type a-Si:H
(a) after annealing and after various light exposures.

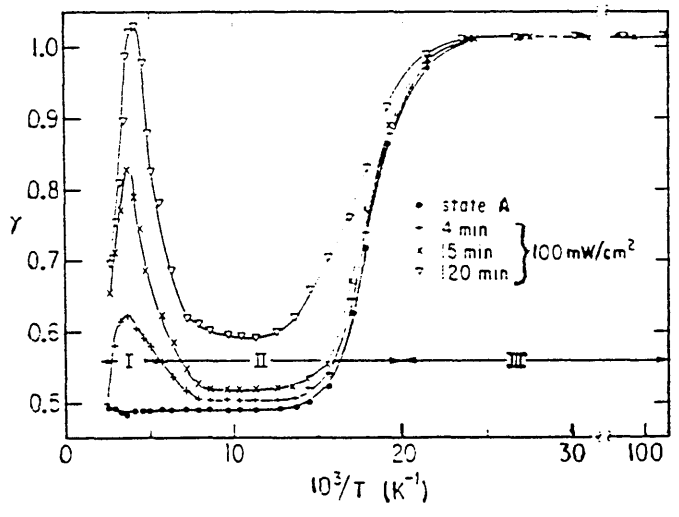

Fig.5.8.3.Change of exponent γ with 1/T
(b) after annealing and after different light exposures.

low temperatures ($10^3/T > 15\ K^{-1}$) showing a constant SSPC, the central activated region.(II) covering the range of low and intermediate temperatures ($15 > 10^3/T > 4.5\ K^{-1}$), and the relatively high temperature region.(III) which includes the SSPC maximum.

Parameters and curve fitting

The parameters used here to fit the experimental results of figure.6.B.2 are those mostly refered to in the literature: For the CBT (figs.5.B.1 and 6.A.9), a similar shape to that proposed by Spear (1988) is used, with about the same $G_c = 2.4.\ 10^{21}\ cm^{-3}eV^{-1}$ and $G_t = 6.\ 10^{20}\ cm^{-3}eV^{-1}$ but with a deeper shoulder at $E_t = 0.16$ eV (Main, 1987) and sharper tail of $T_c = 270$ K. A value of $E_t \simeq 0.17$eV was obtained by TPC as a drift mobility activation energy (cf sect.6.A.1). The VBT used is a broad exponentially varying density without shoulder, characterized by $T_v = 730$ K (Main, 1987) and $G_v = (1.7).10^{21}cm^{-3}eV^{-1}$. The fact that T_v obtained from the TPC measurements (Fig.6.A.10) is smaller than the T_v required here for the SSPC may be assigned to a different energy range (deeper states) probed in the SSPC. For the recombination coefficients associated with DB states, the best fit is obtained using symmetric values for trapped electrons and free holes: $C^+_{nt} = C^-_p = 10^{-9}cm^3sec^{-1}$ (Doghmane and Spear ,1986, obtained $C^-_p = 2.7.10^{-9}cm^3sec^{-1}$ from a double injection experiment); $C^0_{nt} = C^0_p = 10^{-11}cm^3sec^{-1}$ (Cleve and Thomas ,1990, used the same figure for C^0_{nt} in their model). Values of 10^{-9} and 10^{-7} cm^3sec^{-1} are used for the free electron capture coefficients C^0_n (Main, 1987) and C^+_n (Street, 1982 and Main, 1987) by D^0 and D^+ states respectively. The D^+ level is positioned at $E_0 = -1.2$ eV (1.2eV below E_c) (Le Comber and Spear, 1986) and the correlation energy is taken as U = 0.45 eV (Jackson 1982), thus placing the D^- level at 0.75 eV below E_c (Le -Comber and Spear, 1986). The DB density was taken equal to $2.10^{16}cm^{-3}$, which is reasonable for lightly P-doped sample. The free carrier mobilities are $\mu_0 = 10\ cm^2V^{-1}sec^{-1}$ for the electrons (Spear, 1988 and Marshall et al 1985) and $\mu_{0h} = 0.3\ cm^2V^{-1}sec^{-1}$ (Spear, 1988) for the holes.

Tables.6.B.1 summarise these parameters.

Tail states parameters

$G_c(cm^{-3}eV^{-1})$	$G_v(cm^{-3}eV^{-1})$	$G_t(cm^{-3}eV^{-1})$	$E_t(eV)$	$T_c(K)$	$T_v(K)$
$2.4.\ 10^{21}$	$1.7.\ 10^{21}$	$6.\ 10^{20}$	0.16	270	730

Dangling bond parameters

N (cm^{-3})	$C^{+}_{nt} = C^{-}_{p} = C^{0}_{n}$ ($cm^{3}\ sec^{-1}$)	$C^{0}_{nt} = C_{p}$ ($cm^{3}sec^{-1}$)	$C^{+}_{n}(cm^{3}sec^{-1})$	U(eV)	E_0(eV)
2.10^{16}	10^{-9}	10^{-11}	10^{-7}	0.45	1.2 bel E_c

Mobility gap and free carrier mobilities

$E_c - E_v$ (eV)	$\mu_0(cm^2\ V^{-1}\ sec^{-1})$	$\mu_{0h}(cm^2\ V^{-1}\ sec^{-1})$
1.8 eV	10	0.3

Tables.6.B.1.The parameters used in the SSPC model

Both sets of experimental and theoretical curves are shown in fig.6.B.2. As can be seen, there is an excellent agreement between the data curves and the calculated curves in the high G region over the measured temperature range. The disagreement appears relatively at low G and high temperatures. This is because, at temperatures higher than T_c, a considerable part of Δn_t lies above E_{fn}, and the "zero temperature" approximation for tail state charges requires high G so that Δn_t represents most of the charge below E_{fn}.

6.B.1.b. The model physics

The physics of the model can be understood by examining the different charge densities involved in the charge neutrality condition: In figure.6.B.4, are shown (a) the temperature and (b) the excitation dependences of the modelled free and trapped carrier

Figure.6.B.4.
The densities of free and trapped carriers and of the DB states D^-, D^0 and D^+ plotted against the inverse temperature for the P-doped sample (see text for details) $G=10^{20}$ $cm^{-3}sec^{-1}$

(a)

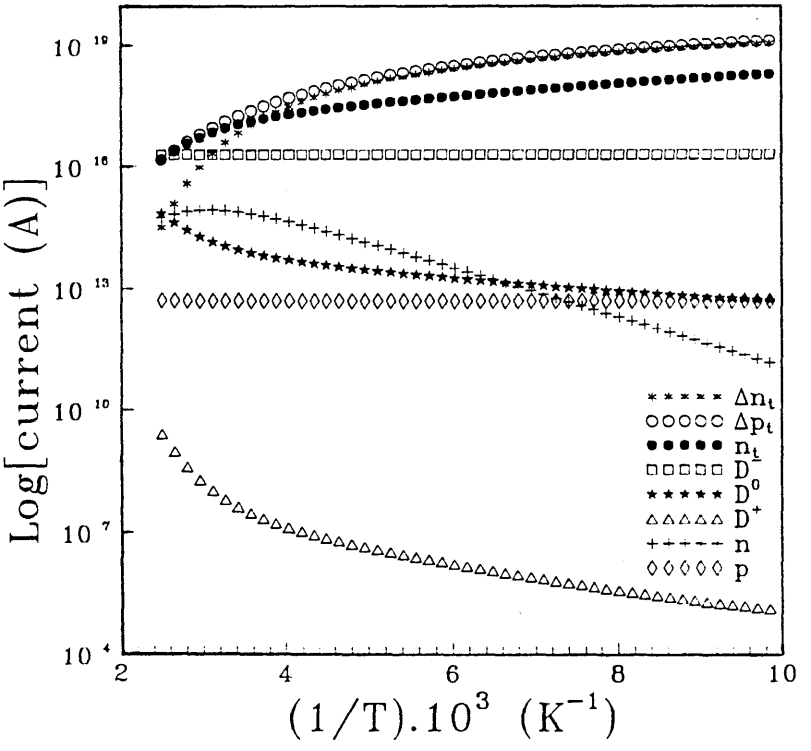

The densities of free and trapped carriers, and of the DB states D^- D^0 and D^+ ploted against the generation rate at 200 K for the P-doped sample.

(b)

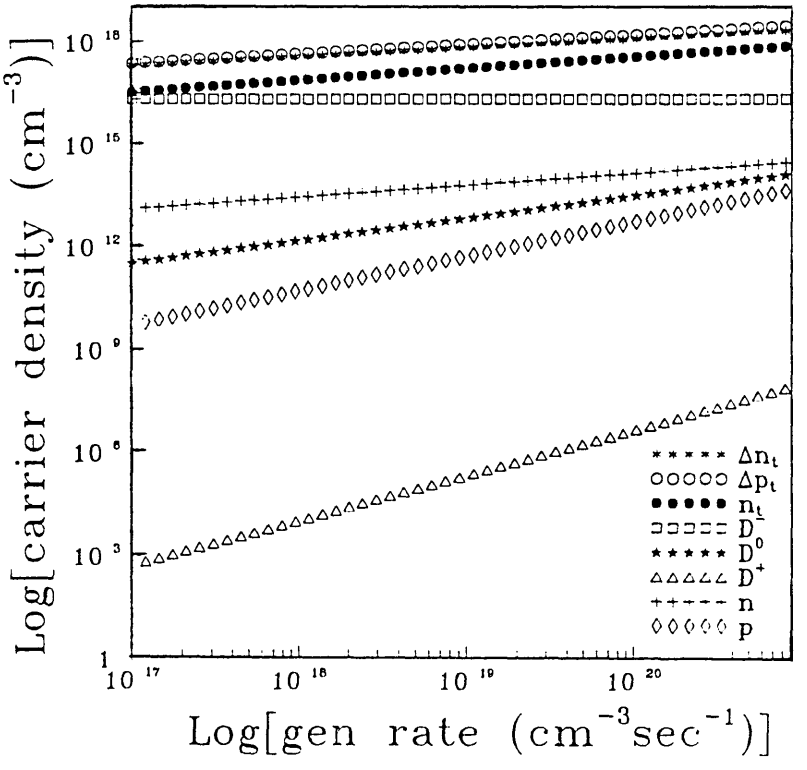

densities and of the DBs occupancies at $G = 1.10^{20}$ cm^{-3} and T = 200 K respectively, where the model curves constitute the best fit to the data.

In Fig.6.A.4.(b), the computed free hole density p increases linearly with G. Fig.6.A.4.(a) shows a constant D^- density over the chosen wide temperature range (100-400 K) with predominancy over D^0 and D^+ states as presumed. As a consequence, the holes recombine via D^- states in a monomolecular process. In this case,

$$p = \tau_p . G \qquad (6.B.1)$$

with $\tau_p = 1/(C_p^-.N.F^-) = 5.10^{-8}$sec, the free hole life time. This has consequences which are explained below.

Low and intermediate temperature region

At low temperatures, below about 220 K for the chosen excitation level ($G = 10^{20} cm^{-3} s^{-1}$), the dominating terms in the charge neutrality are Δn_t and Δp_t with, approximately, equal quantities,

$$\Delta n_t = \Delta p_t \, . \qquad (6.B.2)$$

Replacing by the quantities of Eqns.5.B.8 and inserting Eqn.6.B.1, one obtains for the excess free electron density

$$n - n_0 \simeq N_c . \exp(E_t/k.T) . x^{(T_c/T)} . [G.\tau_p/N_v]^{(T_c/T_v)} \qquad (6.5.3)$$

with x, a constant relating the density of states parameters,

$$x = (T_v/T_c) . (G_v/G_t) \simeq 7.66 \, .$$

Now, Eqns.6.B.3, 6.B.1, and 5.B.9 give the SSPC expression at low and intermediate temperatures,

$$I_{SSPC} = e.\epsilon.A.\ \{\ \mu_0.N_c.\exp\ (E_t/k.T).\ x^{(T_c/T)}.[G.\tau_p/N_v]^{(T_c/T_v)}$$

$$+\ \mu_{0h}.G.\tau_p\ \}\ . \qquad (6.B.4)$$

It is of great interest to notice that this equation also describes all the very low temperature features of the SSPC observed experimentally by V.F (1987) in a pre-annealed n-type a-Si:H (Fig.6.B.3). The SSPC temperature dependence shown in (Fig.6.B.1), modelled for G equivalent to the power 0.1 mW /cm^2 used by V.F, shows a transition to a constant photoconductivity (σ_{pc}) at a very low temperature ($\simeq$ 77 K), in agreement with V.F data. This transition towards a flat region is a consequence of hole conduction since the constant hole term dominates at very low temperatures (Fig.6.B.3.(a)),

$$\sigma_{pc} = \sigma^h_{pc} = e.\mu_{0h}.\tau_p.G\ , \qquad (6.A.5)$$

For the photon energy 1.89 eV and the absorption depth 0.55 μm used in the present work (cf chap.4), the generation rate equivalent to 0.1mW/cm^2 is $G \simeq 5.5.\ 10^{18} cm^{-3} sec^{-1}$, and Eqn.6.B.5 gives $\sigma^h_{pc} \simeq 9.10^{-9}\ \Omega^{-1}.cm^{-1}$, which is thirty times higher than the low temperature V.F experimental σ_{pc}. however, the quantum efficiency η for the electron-hole pair generation measured as a function of temperature (Spear, 1988) drops below 0.1 for temperatures lower than 100 K attaining $\simeq$ 0.05 for $T^{-1} > 15.10^{-3} K^{-1}$, which corrects σ^h_{pc} to $4.5.\ 10^{-10} \Omega^{-1} cm^{-1}$. This figure agrees well with that observed by V.F (Fig.6.B.3 (a)). At the onset of this SSPC region, the power index γ in figure.6.B.3.(b) rises rapidly from less than 0.5 to 1, which is predicted by Eqn.6.B.5, and the modelled temperature dependence of γ (Fig.6.A.1 (b)).

The intermediate temperature activated region is dominated by electron conduction,

$$\sigma^e_{pc} = e.\mu_0.n_0.x^{(T_c/T)}.(G.\tau_p/N_v)^{(T_c/T_v)}\ . \qquad (6.B.6)$$

The activation energy obtained from the derivative of $\log(\sigma^e_{pc})$ with respect to T^{-1}, if N_v is independent of T, is given by

$$E_{pc} = E_t + k.T_c.\log(x) \qquad (6.B.7)$$
$$\simeq -0.11 \text{ eV} ,$$

The assumption of $N_v = k.T.G_v$ adds a small term which brings E_{pc} to the measured activation energy $\simeq$ 0.125 -0.13 eV and the good fit shown in Fig.6.B.2 (a). Eqn.B.6.6 predicts also the sub-square root dependence of the SSPC on G in this activated region, $\gamma = T_c/T_v \simeq 0.35$, in good agreement with the V.F result (Fig.6.B.3.b) and the present result (Figs.6.B.1 and 6.B.2 (b)).

The transition temperature T_0 from the activated to the low temperature constant region is readily obtained from the relation $\sigma^e_{pc} = \sigma^h_{pc}$ and is given by

$$T_0^{-1} = K.\frac{\log\{(\mu_{0h}/\mu_0).(N_v^{\gamma}/N_c).(\eta.G.\tau_p)^{(1-\gamma)}\}}{E_{pc}} \qquad (6.B.8)$$

with the value of η corresponding to low temperature (η =0.05). If $N_c = N_v = 10^{20}cm^{-3}$, T_0^{-1} is evaluated to (13.4) 10^{-3} K^{-1}, which is not far from the observed transition inverse temperature ($\simeq 15.10^{-3}K^{-1}$) . However, a difference in doping level may account for this difference. This is because, increasing the doping level causes structural defects, and thereby modifies the tailing of the bands T_v and T_c (Rehm, 1977 and Furukawa, 1983), it can then result in a decrease of E_{pc} (Rehm, 1977) (Eqn.B.6.7) and an increase of T_0^{-1} as a consequence.

High temperature region

The "high temperature" region is defined as the temperature range above the activated region, beginning where E_{pc} starts to decrease towards the maximum SSPC (above 220 K for the chosen $G=10^{20}cm^{-3}sec^{-1}$). It can be seen in fig.6.B.3.a that this region corresponds to a gradual drop of Δn_t below Δp_t and subsequently below n_t, thus changing the charge neutrality relation from $\Delta n_t = \Delta p_t$ to $n_t = \Delta p_t$; The DB densities are still too small to be considered, even though the drop of n_t is due to an increase in the D^0 density.

Neglecting the rates associated with the DBs in Eqn.5.B.2 and noting that $N_t >> n_t$, a Boltzmann relation between n and n_t is obtained, $n_t = (G_t/G_c).\ \exp(-E_t/k.T).n$, which leads to the charge neutrality relation or the free electron density expression

$$n = k.T_c.G_c.x\ .\ (G.\tau_p/N_v)^{\alpha_v}.\exp(E_t/k.T)\ . \qquad (6.B.9)$$

In this temperature range, $n >> p >> n_0 >> p_0$, and therefore the SSPC can be approximated to

$$I_{SSPC} = e.\epsilon.A.\mu_0.n\ . \qquad (6.B.10)$$

E_{pc} decreases with increasing temperature as

$$E_{pc}(T) = E_t + (K/T_v).\ \log(N_v/G.\tau_p).\ T^2, \quad (E_t<0) \qquad (6.B.11)$$

and the maximum SSPC occurs at T_m where $E_{pc}(T_m)=0$,

$$T_m = [\ (T_v/K).E_t\ /\ \log(G.\tau_p/\ N_v)\ ]^{(1/2)}\ , \qquad (6.B.12)$$

Assuming $N_v = 10^{20} cm^{-3}$, $T_m \simeq$ 284 K is obtained for $G = 10^{20} cm^{-3} sec^{-1}$. This agrees well with the results in figure.6.B.2. It is clear from Eqn.6.B.12 that the maximum SSPC shifts to higher temperatures T_m as G increases. Eqn.6.B.9 predicts also the linear temperature dependence of γ observed by V.F in fig.6.B.3.b (see the modelled γ versus $10^3/T$ in figure.6.B.1.(b)) with $\gamma = T/T_v$.

It appears clear that the model describes, in a self-consistent way, all the features observed for the temperature and excitation dependences of the SSPC in high quality n-type a-Si:H. At very low temperatures (below 80 K), n drops drastically as the CBT traps below E_{fn} ,Δn_t, and around E_t, n_t, become highly populated and the release coeficient from shallaw traps $b_t.\exp(E_t/k.T)$ becomes very small (eg, $\simeq 3.10^{-18}$at 80 K). In such conditions, the conduction could be carried out by the free holes p in the valence band. According to Spear (Spear, 1988), the contribution of the steady state hopping through the tail states ar ound E_t to the photoconductivity σ_{ph} attains 100 %

below 100 K. Spear calculated a σ_{ph} of $10^{-11}\ \Omega^{-1}cm^{-1}$ at 30 K for $E_c - E_{fn} = 0.16eV$, which is more than one order of magnitude less than the experimental σ_{ph} observed in the pre-annealed n-type a-Si:H at this temperature (fig.6.B.3). It is possible that both mechanisms contribute to σ_{ph} in this low temperature range: free hole drift in the VB and electron hopping around E_t. In a recent theory developed by Shklovskii (Shklovskii and Fritzsche, 1989) to explaine the low temperature σ_{pc}, geminate recombination and diffusive hopping of electrons, with defined probability of escape from geminate recombination depending on the electron-hole distance, were considered; The low temperature σ_{pc} is due to the field extraction of the electrons which have reached a distance from their own holes corresponding to equal rates of geminate recombination and diffusive hopping. The calculated σ_{pc} for n-type a-Si:H with $G=10^{20}cm^{-3}sec^{-1}$ was $\simeq 5.10^{-11}\Omega^{-1}cm^{-1}$, in agreement with Spear's calculated value above.

Light soaking effect

Finally, the model predicts also the effect of light soaking on the high temperature SSPC observed in n-type a-Si:H near room temperature, ie the appearance of a minimum in the temperature dependence of the SSPC followed by a sharp rise, (or thermal quenching). The details of this effect are not investigated here, however in figure.6.B.5 are shown $\log(\sigma_{pc})$ versus T^{-1} curves for different values of D^0 and D^- energy levels and DB densities N. Noting that the minimum SSPC appears with increasing N and shifting the D^0 level E_0 upwards, one concludes that light soaking induces more DBs in the D^0 states and thereby modifies the mean energy level positions of the DB states (McMahon, 1990).

Figure.6.B.5.
The modeled temperature dependence of the photocurrent for the indicated energy positions of D^0 and D^- states, and DB densities showing thermal quenching of the photocurrent (for the P-doped sample).

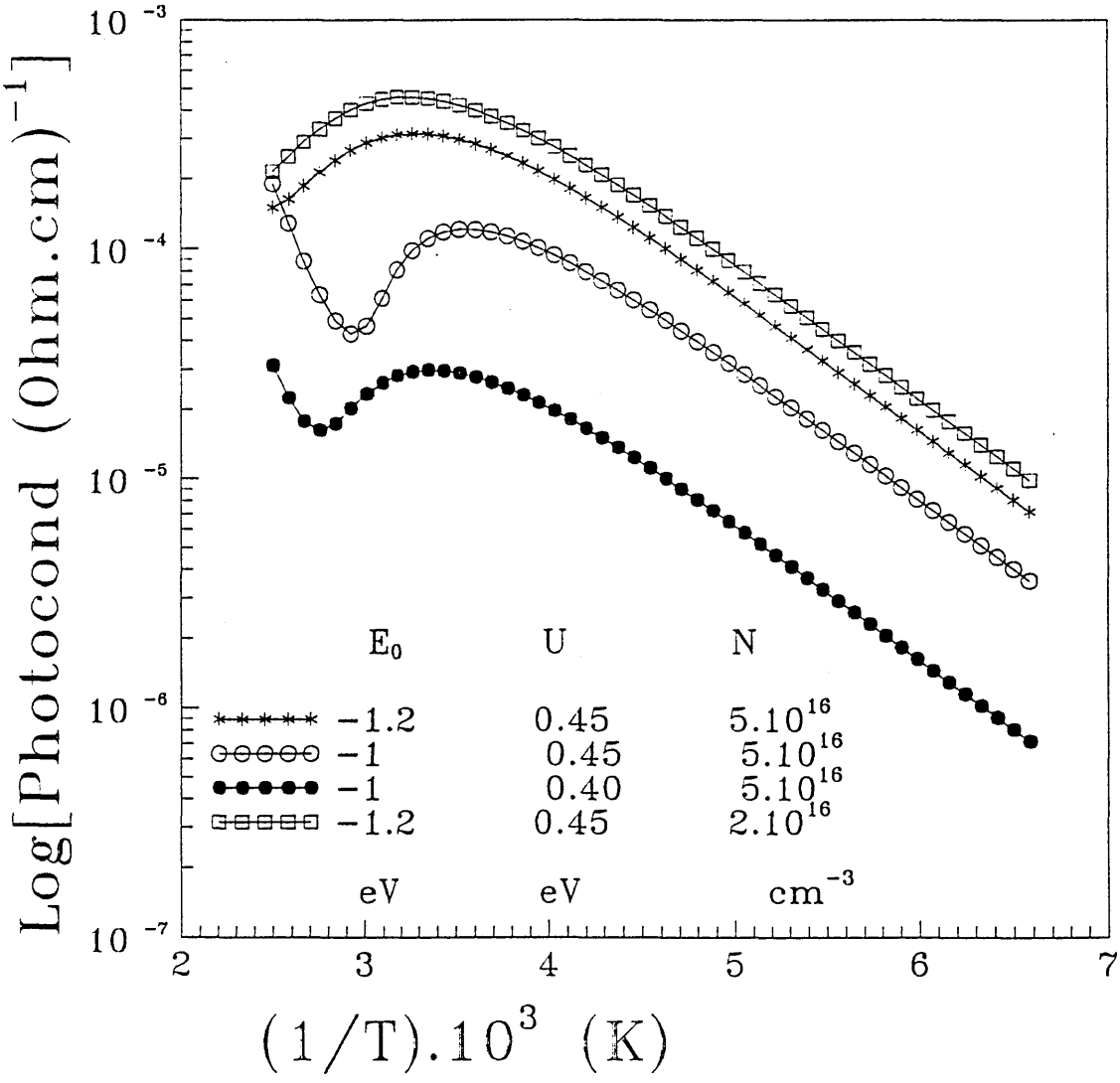

6.B.2.The As-doped sample results

Figure.6.B.6 shows the results of the SSPC excitation dependence from the As-doped sample As plotted in the logarithmic scale for a set of temperaturs covering a wide range (140-330 K). The data follows qualitatively the Rose model (sect.2.9.4): a power-law dependence of I_{SSPC} on G with $0.5<\gamma<1$ decreasing as the temperature increases.

The power index γ is plotted against the temperature in figure.6.B.7 together with the theoretical values obtained from the Rose model (Eqn.2.9.14) using T_c of 470 K as deduced from the TPC data, and a reasonable agreement is observed. There is, however, a deviation of the experimental data towards higher γ at low temperatures, which may due to a significant excess free holes density p appearing in the r expression (cf sects.2.9.3 and 2.9.4).

Figure.6.B.6
Dependence of the photocurrent on the generation rate for the As-doped sample. The power index γ is indicated for each temperature.

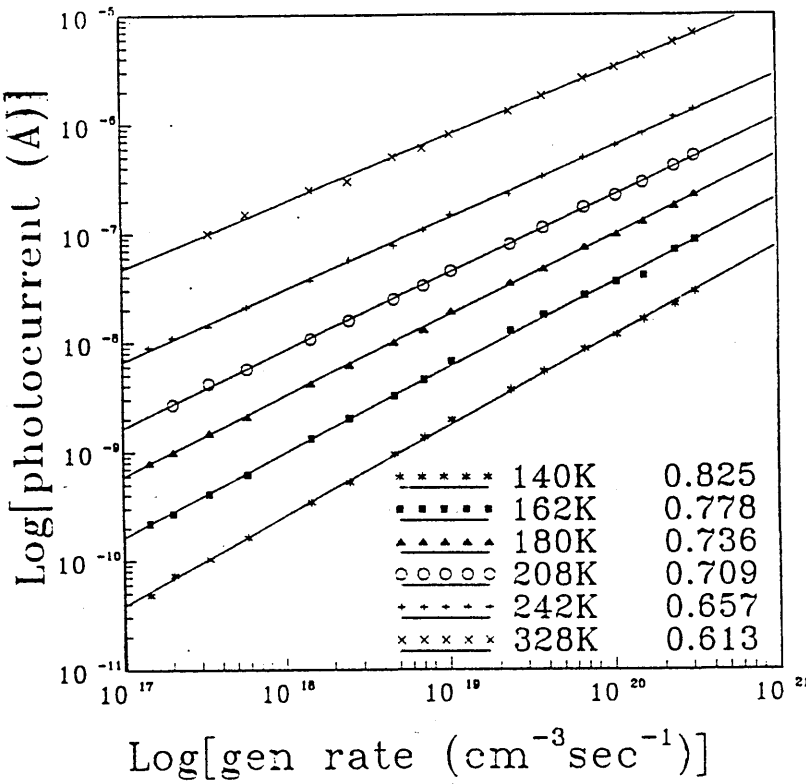

Figure.6.B.7
Comparison between the experimental γ in Fig.6.B.6 and γ obtained from the Rose model using the T_c value 470K obtained from TPC.

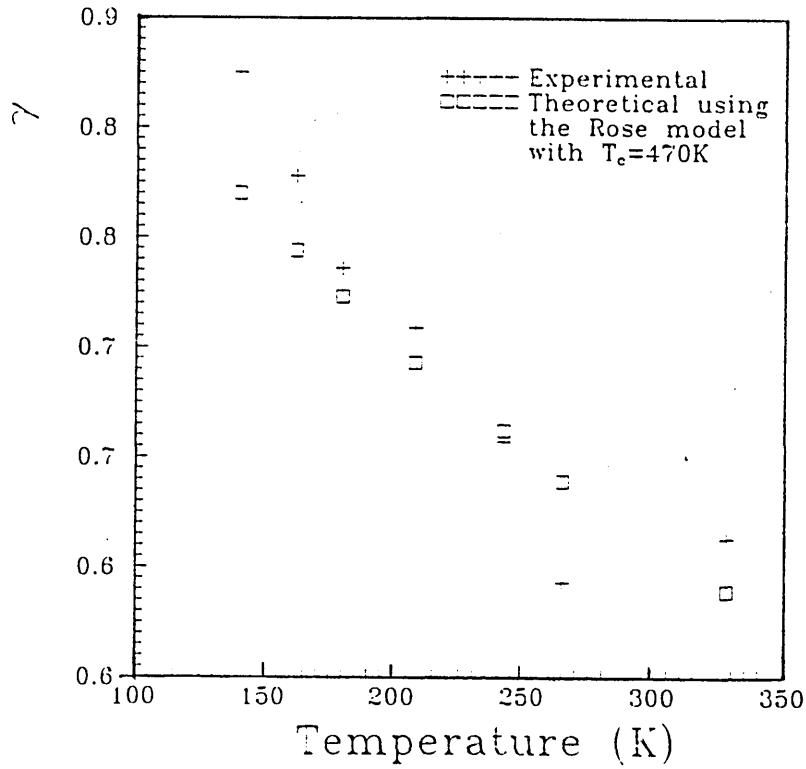

CHAPTER.7.
SUMMARY AND CONCLUSIONS

The study carried out in this project was concentrated on the electrical characterisation of n-type a-Si:H samples produced by the same method (Glow Discharge), but in different conditions and with different doping elements: (a) P-doped, typical of high quality material and (b) As-doped, typical of low quality material. The techniques employed therein were steady state and the transient photoconductivity, applied separately and in combination (optical bias).

A set of physical phenomena relating to carrier dynamics in response to photoexcitation were demonstrated, which can be divided in the following manner,

— Phenomena which occur in the transient regime at short times prior to recombination:

i) Dispersive transport and electron thermalisation in the conduction band tail states.

ii) Saturation of the conduction band tail states with high pulsed electron densities.

iii) Electron trap filling by steady state illumination (Optical bias).

v) Hole thermalisation in the valence band tail occurring simultaneously with the electron thermalisation in the conduction band tail (i).

— Phenomena which occur in the transient regime at long times and in the steady state regime, during the recombination:

i) Electron thermal equilibrium between the extended states and shallow states from which tunneling recombination to nearby dangling bond centres(in the D^0 state) can occur.

ii) Hole release from deep states in the valence band tail and subsequent recombination via the dangling bond (in the D^- state), with the thermal release transition being the rate limiting step in recombination

The model calculations developed on the basis of the above phenomena were in general consistent with most of the experimental

data. In particular, the pre-recombination electron processes in the transient regime, modelled as thermalisation into available "electron-empty" states, led to a clear distinction between the two samples, with respect to the distribution of states in the band tails, *viz*-

(i) a broad and smooth exponential conduction band tail in the As-doped sample, leading to electron thermalisation in which the peak of the excess packet moves down continuously toward the QFL, and in which saturation of the energy levels above the QFL can occur.

(ii) a conduction band tail in the P-doped sample with a sharp drop in density below a relatively shallow 'shoulder'.

In this latter tail form, thermalisation is effectively stopped at the tail shoulder well above the QFL and band saturation is not observed. The trapped electron density peaks around the shoulder energy leading to a good approximation by a discrete level.

The main feature which may distinguish the present study from similar previous work is the coherent model of photoconductivity consistent with both steady state and transient regimes in which the dynamics of both carrier types, majority (or electrons) and minority (or holes), are considered in a single physical model. In this model, the main recombination center is the energy correlated dangling bond (found mostly in the D^- state for the n-type material) and the recombination process is controlled by the minority carriers (holes). Most of the generated carriers are trapped in the localised states which form the band tails and therefore these states control the charge neutrality condition without being involved in recombination.

Future Work.

This model appears to explain reasonably consistently both the SSPC and the TPC responses in the high quality P-doped sample. However, it should be noted that recombination in the As-doped low quality sample can not be fully explained by this model. Rather, the qualitative consistency of the SSPC response with the Rose model points to a possible contribution of the tail states to recombination. This may be a result of the broad high density tails in this material. Further research is then required for such a material as a more detailed study which involves all the gap states in the recombination process.

The model of photoconductivity developed in this work predicts that both steady state and transient photoconductivity should be very sensitive to the position of the Fermi level, since the occupation of the postulated dominant recombination centres will change with the position of E_F. For example, the present model predicts a 'symmetry' of the recombination transitions with respect to the type of doping, arising from the symmetry in the energy levels of the dangling bond states. For example, in Boron-doped a-Si:H the SSPC temperature dependence has a similar trend to the Phosphorus-doped case but with different magnitude and activation energy. The symmetry of the SSPC model suggests that in Boron doped a-Si:H, where D^+ states are dominant and D^- states are in negligible density, the recombination should follows Path.<2>. To avoid speculation, the subject is open for more research including SSPC and TPC measurements on high quality undoped and B-doped a-Si:H in order to generalise the model.

An alternative to the above suggestion is that the model could be tested experimentally, varying the Fermi level position in a suitable field effect structure, and measuring the effect on both SSPC and TPC response. In this way, in a single sample, the dangling bond occupation could be varied, and the effects compared with those predicted by the model. Such an experiment is not without difficulty, since it is known that metastable states can be formed under the influence of applied gate voltages in field effect devices.

The low temperature (< 80 K) SSPC is worth investigation for different types of doping, in order to explore the question of whether the temperature independence of the photoconductivity in this region is due to hole conduction predicted by the model in the case of free hole recombination.

The light soaking effect and thermal quenching near room temperature predicted by the model to arise from an increase in the D^0 density requires also further investigation, both by experiment and computer modelling, since this kind of detailed structure should be a sensitive test of the validity of a given model.

APPENDIX

Derivation of the transient pulsed electron density N_e

The effective (or available) density of states is given by

$$g'(E) = G_c.\exp(E/k.T_c).[1 - (1+r)^{-1}.(1 + \exp\frac{E - E_{fnt}}{K.T})^{-1}] \qquad (A.1)$$

where the term subtracted is the trap occupation function (Eqn.2.9.8) and r is given by Eqn.2.9.9. To simplify the calculation, the trapped electron density per unit energy, using Eqns.5.A.1, A.1 and 5.A.4, can be written as a combination of two terms,

$$\delta n\,(E,T,t) = \delta n_1 + \delta n_2 \qquad (A.2)$$

with

$$\delta n_1 = F(t).G_c.\exp(E/k.T_c).[1 + \exp\frac{E_{fnt} - E}{K.T}]^{-1}.[1 + \exp\frac{E - E_d}{K.T}]^{-1} \qquad (A.3.a)$$

and

$$\delta n_2 = \frac{r}{1+r}.F(t).G_c.\exp(E_{fnt}/k.T).\exp(E/k.T'_c)$$
$$.[1 + \exp\frac{E_{fnt} - E}{K.T}]^{-1}.[1 + \exp\frac{E - E_d}{K.T}]^{-1} \qquad (A.3.b)$$

where $T'_c = T_c.T/(T-T_c)$

The transient pulsed electron density can also be written as a combination of two terms,

$$N_e = N_{e1} + N_{e2} \qquad (A.4)$$

with $N_{e1} = \int_{-\infty}^{+\infty} \delta n_1.dE$ and $N_{e2} = \int_{-\infty}^{+\infty} \delta n_2.dE$

Let a new variable X be

$$X = \exp[(E_{fnt} - E_d)/2.k.T].\exp[(E - E_{fnt})/k.T]$$

N_{e1} and N_{e2} will then have the following expressions:

$$N_{e1} = F(t).G_c.k.T.\exp(E_d/k.T_c).\exp[(E_{fnt}-E_d)/2.k.T_c].$$

$$. \exp[(E_d-E_{fnt})/2.k.T\ ].\ I(T_c) \qquad (A.5.a)$$

and

$$N_{e2} = [r/(1+r)].F(t).G_c.\exp(E_{fnt}/k.T).\exp(E_d/k.T'_c).$$

$$. \exp[(E_{fnt}-E_d)/2.k.T'_c\ ].\exp[(E_d-E_{fnt})/2.k.T\ ].\ I(T'_c) \qquad (A.5.b)$$

where $I(T_c)$ and $I(T'_c)$ are similar standard integrals which differ only by the parameters T_c and T'_c.

$$I(T_c) = \int_0^{+\infty} \frac{X^{\alpha_c}}{1+ \left(\exp\frac{E_{fnt}-E_d}{2.K.T} + \exp\frac{E_d-E_{fnt}}{2.K.T}\right).X + X^2}.dX \qquad (A.6)$$

If $\exp\frac{E_{fnt}-E_d}{2.K.T} = \exp(i.\beta)$, the X factor in the denominator will be equal to $2.\cos\beta$, and $I(T_c)$ will be equal to (Schaum's outline series mathematical handbook, section 15.21)

$$I(T_c) = [\pi/\sin(\pi.\alpha_c)].[\sin(\alpha_c.\beta)/\sin\beta\ ]$$

$$= [\pi/\sin(\pi.\alpha_c)].\ \frac{\exp\frac{E_{fnt}-E_d}{2.K.T_c} - \exp\frac{E_d-E_{fnt}}{2.K.T_c}}{\exp\frac{E_{fnt}-E_d}{2.K.T} - \exp\frac{E_d-E_{fnt}}{2.K.T}} \qquad (A.7)$$

and $I(T'_c)$ is similar except for T'_c and $\alpha'_c = T/T'_c$ instead of T_c and α_c. Inserting (A.7) into (A.5.a) yields the following expression for N_{e1}:

$$N_{e1} = F(t).k.T_c.G_c.[\pi.\alpha_c/\sin(\pi.\alpha_c)].\exp(E_d/k.T_c).$$

$$\cdot\frac{1 - \exp[(E_{fnt}-E_d)/K.T_c]}{1 - \exp[(E_{fnt}-E_d)/K.T\ ]} \qquad (A.8.a)$$

and a similar expression is obtained for N_{e2} after inserting $I(T_c')$ into eq. A.5.b,

$$N_{e2} = [r/(r+1)].F(t).k.T_c'.G_c.[\pi.\alpha_c'/\sin(\pi.\alpha_c')].\exp(E_{fnt}/k.T).$$
$$.\exp(E_d/k.T_c').\ \frac{1 - \exp[(E_{fnt}-E_d)/K.T_c']}{1 - \exp[(E_{fnt}-E_d)/K.T\ ]}$$

which reduces when T_c' and α_c' are replaced by $T_c.T/(T-T_c)$ and $\alpha_c - 1$ to

$$N_{e2} = [r/(r+1)].F(t).[\pi.\alpha_c/\sin(\pi.\alpha_c)].\exp(E_d/k.T_c).$$
$$.\frac{\exp[(E_{fnt}-E_d)/K.T] - \exp[(E_{fnt}-E_d)/K.T_c]}{1 - \exp[(E_{fnt}-E_d)/K.T\ ]} \qquad (A.8.b)$$

The total transient pulsed electron density N_e is then

$$N_e = F(t).k.T_c.G_c.[\pi.\alpha_c/\sin(\pi.\alpha_c)].\ \frac{\exp(E_d/K.T_c)}{1 - \exp[(E_{fnt}-E_d/k.T)]}\ .$$
$$.\{\ [1 - \exp\frac{E_{fnt}-E_d}{k.T_c}\ ] + \frac{r}{1+r}\ .[\ \exp\frac{E_{fnt}-E_d}{k.T} - \exp\frac{E_{fnt}-E_d}{k.T_c}\ ]\ \} \qquad (A.9)$$

REFERENCES

Anderson, D. A and Spear, W. E. (1977), Phil. Mag. 36 695.

Arnoldussen, T.C. and Bube, R. H. (1972), J. Appl. Phys. 43, 1798.

Brodsky, M. H., Title, R. S, Weiser, K and Pettit, G. D. (1970), Phys. Rev. B, 1. 2632.

Brodsky, M.H. and Title, R. S. (1969), Phys. Rev. Lett. 23, 581.

Bube, R, H. and Redfield, D. (1989), J. Appl. Phys. 66, 3074.

Cleve, B. and Thomas, P. (1990), *Proceedings of MRS Spring meeting, San Francisco.*

Cohen, J. D., Harbison, J. P. and Wecht, K. W., (1982), Phys. Rev. Lett. 48, 109.

Cohen, M. H., Fritzsche, H., and Ovshinsky, S. R., (1969), Phys. Rev. Lett. 22, 1065.

Crandall, R. S., (1984), Semiconductors and semimetals, Ed: Pankove, J, I. 21, Part.B, Academic press, Orlando. pp285-288.

Dersch, H., Schweitzer, L. and Stuke, J. (1983), Phys. Rev. B. 28, 4678.

Doghmane, A., and Spear, W. E., (1986), Phil. Mag. B. 53, 463.

Enakshi, B. and Narasimhan, K. L., (1983), Phys. Rev. B. 28, 2287.

Furukawa, S. and Matsumoto, N., (1983), Phys. Rev. B. 27, 4955.

Hack, M. Guha, S. and Shur, M., (1984), Phys. Rev. B. 30, 6991.

Halpern, V. (1986), Phil. Mag. B. 54, 473.

Hindley, N. K. (1970), J. Non-Cryst. Solids. 5, 17.

Hirose, M. (1984). Semiconductors and semimetals. 21.A. Academic press, Orlando. p11.

Hvam, J. M. and Brodsky, M. H., (1980), Phys. Rev. Lett. 46, 371.

Jackson, W. B., (1982), Solid state Comms. 44, 477.

Kagawa, T., Matsumoto, N. and Kumabe, K., (1983), Phys. Rev. B. 28, 4570.

Knights, J. C., Biegelsen, D.K. and Solomon, I., (1977), Solid State Comms. 22, 133.

Kristensen, I. K. and Hvam, J. M., (1985), J. Non-Cryst. Solids. 77 & 78, 611.

Kristensen, I. K. and Hvam, J. M., (1984), Solid State Comms. 50, 845.

Kristensen, I. K. and Hvam, J. M., (1988), Solid State Comms. 65, 415.

LeComber, P. G, (1990), J. Non-Cryst. Solids. 115, 1-13

LeComber, P. G. and Spear, W. E., (1986), Phil. Mag. B. 53, L1.

LeComber, P. G. and Spear, W. E., (1986), Phil. Mag. B. 53, NO. 1, L1.

LeComber, P. G., Loveland, R.G., Spear, W. E. and Vaughan, R. A., (1974), Proc. 5th Int. Conf. Amorphous and liquid semiconductors. Eds: Stuke, J. and Brenig, W., p245.

Main, C. and Owen, A. E., (1973), Electronic and structural properties of amorphous semiconductors, Eds: Le Comber, P. G and Mort, J. Academic press, London. p527.

Main, C., Berkin, J. and Merazga, A., (1991), To be published by World Scientific Press, Singapore, in New Physical Problems in Electronic Materials.

Main, C., Berkin, J., Russell, R., Merazga, A. and Marshall, J. M. (1987), J. Non-Cryst. Solids. **97** & **98**, 779.

Main, C., Merazga, A., Kristensen, I. K. and Berkin, J., (1990), Solid State Comms. **74**, 667.

Main, C., Russell, R., Berkin, J. and Marshall, J. M., (1987), Phil. Mag. Lett. **55**, 189.

Marshall, J. M., LeComber, P. G. and Spear, W. E., (1985), Solid State Comms. **54**, 11.

Marshall, J. M., Street, R. A. and Thompson, M. J., (1986), Phil. Mag. B. **54**, 51.

McKelvey, J. P. (1966), Solid state and Semiconductor Physics, Harper, New York. p208.

McKelvey, J. P. *ibid.*, p231.

McMahon, T. J. and Crandall, R. S., (1989), Phys. Rev. B. **39**, 1766.

McMahon, T. J. and Crandall, R. S., (1990), Phil. Mag. B. **61**, 425.

Mott, N. F. and Davis, E. A., (1979), Electronic processes in Non-crystalline materials, Eds: Marshall, W and Wilkinson, D, H, Clarendon press, Oxford. p248.

Mott, N. F., (1969), Phil. Mag. **19**, 835.

Mott, N. F. and Davis, E. A., (1979), Electronic processes in non-crystalline solids. Eds: Marshall, W and Wilkinson, D. H., Clarendon Press, Oxford. p32.

Nagels, P., (1985), Topics in Applied Physics. **36**, Springer-Verlag, p120.

Oheda, H., (1985), Phil. Mag. B. **52**, 857.

Oheda, H., (1987), J. Appl. Phys. **62**, 3803.

Okamoto, H., Kida, H. and Hamakawa, Y., (1984), Phil. Mag. B. **49**, 231.

Okushi, H., Takahama, T., Tokumaru, Y., Yamasaki, S., Oheda, H. and Tanaka, K., (1983), Phys. Rev. B. **27**, 5184.

Okushi, H., Tokumaru, Y., Yamasaki, S., Oheda, H. and Tanaka, K., (1982), Phys. Rev. B. **25**, 4313.

Orenstein, J., Kastner, M. A. and Vaninov,V., (1982), Phil. Mag. B. **46**, 23.

Pandia, R., Schiff, E. A. and Conrad, K. A., (1984), J. Non-Cryst. Solids. **66**, 193.

Pandya, R. and Schiff, E. A., (1983), J. Non-Cryst. Solids. **59** & **60**, 297.

Pandya, R. and Schiff, E. A., (1985), Phil. Mag. B. **52**, 1075.

Pandya, R., Schiff, E. A. and Conrad, K. A., (1984), J. Non - Cryst. Solids. **66**, 193.

Rehm, W., Fischer, R., Stuke, J. and Wagner, H., (1977), Phys. Stat. Sol. (b). **79**, 539.

Rose, A., (1963) Concepts in Photoconductivity and Allied Problems, Interscience, New York. p38.

Schiff, E. A., (1981), Phys. Rev. B. **24**, 6189.

Shklovskii, B. I., Fritzsche, H. and Baranovskii, S. D., (1989), J. Non-Cryst. Solids. **114**, 325.

Shockley, W. and Read Jr., W. T., (1952), Phys. Rev. **87**, 835.

Simmons, J. G. and Taylor, G. W., (1974), J. Phys. C: Solid State Phys., **7**, 3067

Simmons, J. G. and Taylor, G. W. (1971), Phys. Rev. B. **4**, 502.

Simmons, J. G. and Taylor, G. W. (1973), J. Phys. C: Solid State Phys. **6**, 3706.

Spear, W. E. and Cloude, C., (1987), Phil. Mag. Lett. **55**, 271.

Spear, W. E. and LeComber, P. G., (1975), Solid state Comms. **17**, 1193.

Spear, W. E. and LeComber, P. G., (1983), Topics on applied physics, Springer. **55**, 63.

Spear, W. E. and LeComber, P, G., (1976), Phil. Mag. **33**, 935.

Spear, W. E., Steemers, H. L., Le Comber, P. G. and Gibson, R. A., (1984), Phil. Mag. B. **50**, L33.

Spear, W.E. and LeComber, P. G., (1976), Phil. Mag. **33**, 935.

Spear, W. E., Loveland, R. and Al-Sharbaty, A., (1974), J. Non-Cryst. Solids. **15**, 410.

Spiegel, M. R, Mathematical Handbook. Schaum's outline series, No. 15.21.

Staebler, D. L and Wronski, C. R, (1977), Appl. Phys. Lett, **31**, 292.

Street, R. A., (1982), Phil. Mag. B. **46**, 273.

Street, R. A. and Biegelsen, D, K., (1980), J. Non-Cryst. Solids. 35 & 36, 651.

Street, R. A., (1982), Phys. Rev. Lett. 49, 1187.

Street, R. A., Biegelsen, D. K. and Weisfield, R. L, (1984), Phys. Rev. B, 30, 5861.

Taylor, G. W. and Simmons, J. G., (1974), J. Phys. C: Solid State Phys. 7, 3067.

Thomas, P. A., Brodsky, M. H., Kaplan, D. and Lepine, D., (1978), Phys. Rev. B. 18, 3059.

Tiedje, T., (1984), Semiconductors and semimetals, Eds. Pankove, J, I, Academic press. 21, part.C, 212-220.

Tiedje, T., (1984), *ibid.*, p227.

Tiedje, T. and Rose, A., (1980), Solid state comm. 37, 49.

Vaillant, F., Jousse, D. and Bruyere, J-C., (1988), Phil. Mag. B. 57, 649.

Vanier, P. E., Delahoy, A. E. and Griffith, R. W., (1981), in Tetrahedrally bonded Amorphous Semiconductors, ed R. A. Street, D.K. Beigelson and J. C. Knights, (AIP, New York), p227.

Vomvas, A. and Fritzsche, H., (1987), J. Non-Cryst. Solids. 97 & 98, 823.

Weiser, K., Fisher, R. and Brodsky, M. H., (1970), Proceedings of the Tenth International Semiconductor Conference, Cambridge, Mass, p667.

Werner, A. and Kunst, M., (1987), Phys. Rev. B. 36, 7567.

Wronski, C. R. and Daniel, R. E., (1981), Phys. Rev. B. 23, 794.

Yoffa, E. I. and Adler, D., (1975), Phys. Rev. B. 12, 2260.

Zeldov, E. and Weiser, K., (1984), Phys. Rev. Lett. 53, 1012.